SOLAR RADIO SPIKE BURSTS

A

DISSERTATION

Presented to the Faculty of the

University of Alaska in Partial Fulfillment

of the Requirements

For the Degree of

DOCTOR OF PHILOSOPHY

by

Guy L. Tarnstrom, B.A.

College, Alaska

May 1971

SOLAR RADIO SPIKE BURSTS

APPROVED:

R Parthasarathy

Jerry Tarbox

Daniel W. Swift

Kenneth W. Ehby
Chairman

Roger Sheridan
Department Head

APPROVED: C. Rollett Date May 17, 1971
Dean of the College of Mathematics,
Physical Sciences and Engineering

E. Case
Vice President for Research and Advanced Study

ABSTRACT

Spectral observations of meter wavelength solar radio emission with $\lesssim$ 0.01 second time-resolution show three types of spike bursts: fast drift spike bursts, with $\dot{f} \geq 100$ MHz/sec; medium drift spike bursts, with $\dot{f} < 100$ MHz/sec; and simple spike bursts, of $\sim$ 1 MHz bandwidth and no apparent frequency drift. All types of spike bursts tend to occur in regular sequences of similar bursts. Rare, extensive sequences of quasiperiodic fast drift spike bursts are observed. Fine structure of type III burst events reveal occasional spike burst-type III burst associations which appear to fall into three classes. Type III bursts are observed with duration $\sim$0.1 second approaching the range of spike burst durations ($\lesssim$ 0.1 second). Large-frequency-range spike bursts resemble such short-duration type III bursts, suggesting a morphological continuity between spike bursts and type III bursts. A plasma hypothesis interpretation of spike bursts requires spike burst exciters of spatial extent less than $\sim 10^3 - 10^4$ km, density $\sim$ 1-10 electrons/cm^3, and coronal temperature $\sim 10^6$°K. It is suggested that the spatial extent of a given exciter determines whether a spike burst or a type III burst is produced. Unusual meter wavelength fine structure observed includes spike burst and type I burst chains with a sharp high-frequency cut-off, complex patterns of parallel drifting bands, and ionospheric scintillation of noise storm continuum. Several examples are given.

ACKNOWLEDGEMENTS

This work was supported in part by NSF Grants No. GP-169, GP-4633, GA-900, and GA-19475 and by a NASA Traineeship.

This project was conceived by Dr. Leif Owren. The original design and construction of the high-time-resolution swept-frequency receiver was the work of Mr. G. LaPoint. Later, Principal Investigators, Mr. E. J. Gauss and Dr. K. W. Philip, developed the radio spectrograph to its present state with the assistance of Mr. William Nickparenko and Mr. R. Domke, Dr. Philip made major scientific, technical, and administrative contributions to the project.

Prompt and effective maintenance of the equipment at its remote location was accomplished by Mr. R. Domke, who saved the project a considerable amount of time and trouble.

Mechanical problems of the project and the maintenance problems of the site (the Chena Valley Radio Facility), including the 1967 flood, were ably handled by Mr. J. C. Carver.

Considerable assistance was given the author with operating and maintaining the system, and recording data, by Mr. J. N. Davies.

The author enjoyed many informative conversations with Dr. K. W. Philip on an unending variety of subjects.

The completion of this dissertation was made possible only by the patience, industry, and encouragement of many people. Notable among them are Mr. M. Alexander and Mr. F. Daniels and the staff of Photographic Services, and Mrs. Meg McCoy and the staff of the Steno Center. Special thanks are due to Mr. Alexander, who made the tremendous number of tedious and demanding prints of the data in an unbelievably short time.

Foremost, I wish to thank Dianne, my wife, for encouragement and patience during the course of this study and for the last-minute assistance which brought it to a timely conclusion.

TABLE OF CONTENTS

	Page
ABSTRACT	3
ACKNOWLEDGEMENTS	4
TABLE OF CONTENTS	6
LIST OF ILLUSTRATIONS	8
LIST OF TABLES	14
INTRODUCTION	15
CHAPTER 1 SPIKE BURSTS	17
A. Dynamic Spectra	
B. Spike Burst Observations	
CHAPTER 2 SIMILAR BURSTS	29
A. Type III Bursts	
B. Type I Bursts and Related Bursts	
1. Noise Storms: Observations	
2. Type I Bursts	
3. Similar Bursts	
i. Meter Wavelengths	
ii. Dekameter Wavelengths	
iii. Decimeter Wavelengths	
4. Interpretation	
C. Application to Spike Bursts	
CHAPTER 3 INSTRUMENTATION	64
A. Recording	
B. Data	
CHAPTER 4 SPIKE BURST MORPHOLOGY	81
A. Burst Classification	
B. Groups of Spike Bursts	

		Page
CHAPTER 5	SPIKE BURSTS - TYPE III BURST ASSOCIATION	91
	A. Observations	
	B. Plasma Hypothesis Interpretation of Spike Bursts	
CHAPTER 6	PARALLEL DRIFTING BANDS	138
CHAPTER 7	UNUSUAL FINE STRUCTURE	155
	A. Unusual Spike Bursts	
	B. Unusual Chains of Spike Bursts and Type I Bursts	
CHAPTER 8	SUMMARY	171
LIST OF SYMBOLS		176
BIBLIOGRAPHY		179

LIST OF ILLUSTRATIONS

Figure I.1 Burst parameters.

Figure I.2 Examples of dynamic spectra illustrating the five principal spectral types recorded at metre wavelengths. The inset represents an idealized sketch of the complete flare-associated radio event (from Wild, et al., 1963).

Figure I.3A. a) Spike burst. b) Ordinary type I burst (from Eckhoff, 1966).

Figure I.3B Dynamic spectrum showing both spike bursts and ordinary type I bursts (from Eckhoff, 1966).

Figure I.4. Spike bursts during the type IV event, 4-I-1960. a) course of the type IV event. b) pulsations. c) spike bursts during the type IV event (from deGroot, 1963)

Figure I.5. Spike bursts and pulsations during the type IV event of 8-22-58 (from deGroot, 1966).

Figure I.6. Single-frequency observations of spike bursts (after Dröge, 1967).

Figure 2.1. Groups of type III bursts, showing variations in the duration, frequency range, and frequency-drift rate (from Hughes and Harkness, 1963).

Figure 2.2 Distribution of the frequency ranges of type III bursts (from Malville, 1962).

Figure 2.3. a) Distribution of starting frequencies of type III bursts (from Malville, 1962). b) Variation of monthly averages of frequencies of type III bursts (from Malville, 1967).

Figure 2.4. a) Frequency-drift rate of type III bursts as a function of frequency (from Hughes and Harkness, 1963). b) Average frequency drift rates for type III bursts (from Hartz, 1969).

Figure 2.5. Average duration of type III bursts as a function of frequency (after Hughes and Harkness, 1963).

Figure 2.6. Source positions of eight type III bursts associated with limb flares (optical positions shown as circles). The circular arcs show the levels of the fundamental (F) and second harmonics (S) of the plasma frequency, assuming the Baumbach-Allen corona. (from Kundu, 1965).

Figure 2.7. The electron densities deduced from different radio observations compared with those of the Baumbach-Allen model and coronal streamer model of Newkirk (from Kundu, 1965).

Figure 2.8. Burst duration as a function of frequency for T equal to (a) 10^6 °K, (b) 2×10^6 °K, (c) 4×10^6 °K, and (d) 6×10^6 °K (from Elgarøy and Rødberg, 1964).

Figure 2.9. Deduced temperatures for the source regions of the type III bursts; These regions are located in terms of their plasma frequency, left ordinates, and their infered solar distances, right ordinates (from Hartz, 1969).

Figure 2.10. Elgarøy's 1961 examples of type I bursts. Photographs of CRT screen and corresponding contour diagrams (from deGroot, 1966).

Figure 2.11. Observed bandwidth of type I bursts. The hatched areas indicate the intervals within which most bandwidths occur (after Elgarøy and Eckhoff, 1966).

Figure 2.12. Average burst duration on different frequencies. The upper and the lower limits of the duration are indicated (from Elgarøy and Eckhoff, 1966).

Figure 2.13. Distribution of frequency-time slopes for (a) type II bursts, (b) split pair bursts, (c) drift pair bursts, (d) fast drift storm bursts, (e) type III bursts, and (f) chains of split pair bursts (from Ellis, 1969).

Figure 3.1. Diagram of a radiospectrograph (from Wild, et al., 1954).

Figure 3.2. HTR -SPECTROMETER-1967 (from Philip; 1968a).

Figure 3.3 Nonlinearity of frequency scale; 1 MHz markers (a), 5 MHz markers (b), 10 MHz markers (c).

Figure 3.4. Variations of gain with frequency; prepared from densitometer trace along frequency axis; antenna temperature = 3000°K

Figure 3.5. a) Effect of band B gain-variation on type III burst. b) equal-intensity contours prepared from densitometer traces.

Figure 3.6. Interference: a) moiré pattern produced by modulation of carrier on band A, with spurious responses on bands B and C. b) moiré pattern produced by periodic interference (eg., ignition). c) lightning. d) noisy or diode switch. e) moiré pattern produced by 60-cycle hum.

Figure 3.7. Scintillation. a) 8-16-68, 1606-1619 UT. (LS film). b) 8-16-68, 1606:18 UT. c) 8-16-68, 1606:45 UT. d) 8-16-68, 1619:26 UT.

Figure 3.8. Sketches showing idealized examples of the principal types of dynamic spectra of radio-star scintillation observed (from Wild and Roberts, 1956).

Figure 4.1. fd-spike bursts: a) 6-20-68, 2231:09 UT. b) 6-20-68, 1920:08 UT. c) 6-20-68, 1840:30 UT. d) 7-24-67, 2332:00 UT. e) 7-24-67, 2356:24 UT.

Figure 4.2. md-spike bursts: a) 7-18-68, 0037:25 UT. b) 6-20-68, 1846:48 UT. c) 6-24-68, 0305:41 UT. d) 8-17-68, 0033:20 UT. e) 7-24-67m 1432:29 UT.

Figure 4.3. s-spike bursts: a) 7-24-67, 2201:37 UT. b) 7-14-68, 1651:25 UT. c) 6-13-68, 0318:55 UT. d) 7-11-68, 1644:18 UT. e) 7-17-68, 2101:43 UT.

Figure 4.4(a-c) Spike burst grouping: a) spray, 6-24-68, 1909:12 UT. b) spray, 6-30-68, 1812:22 UT. c) storm, 7-24-67, 1625:45 UT.

Figure 4.4(d-f) Spike burst grouping: d) spike burst background, 6-13-68, 0249:34 UT. e) quasiperiodic spike bursts, 6-3-68, 2355:05 UT. f) quasiperiodic spike bursts. 6-7-68, 1719:26 UT.

Figure 5.1(a-b) Type III bursts: a) 8-2-67, 0240:51 UT. b) 8-12-68, 2049:00 UT.

Figure 5.1c. Type III bursts: c) 8-13-68, 1826:50 UT.

Figure 5.2. Spike burst-type III burst associations (from Philip, 1969). a) 6-7-68. b) 6-22-68A. c) 6-22-68B. d) 7-14-68A. e) 7-14-68B. f) 7-16-68. g) 7-17-68.

Figure 5.3a. Spike burst-type III burst association, 9 July 1968: i) 0316-0322 UT. ii) 0318:11 UT.

Figure 5.3b. Spike burst-type III burst association, 18 July 1968: i) 2344-2350 UT. ii) 2347:50 UT.

Figure 5.3c Spike burst-type III burst association, 26 September 1968: i) 0026-0032 UT. (LS film) ii) 0026:47 UT iii) 0028:18 UT.

Figure 5.4 Possible spike burst-type III association (from deGroot, 1966).

Figure 5.5. deGroot's "bright spots" and type III bursts, 12-30-68, 1424 UT. (from deGroot, 1970).

Figure 5.6 Positive drift fd-spike bursts during type III event 9 July 1968, 0250 UT. a) 0248-0254 UT. (LS film) b) 0250:20 UT.

Figure 5.7. Spike bursts occuring during type III burst events: a-i) 7-26-67, 0748-0750 UT. (LS film). a-ii) 0749:14 UT. b-i) 7-9-67, 1649-1651 UT. (LS film). b-ii) 1649:27 UT. b-iii) 1649:35 UT. b-iv) 1650:02 UT.

Figure 5.8. Spike bursts concurrent with type III bursts (from deGroot, 1966).

Figure 5.9a. fd-spike bursts following type III bursts, 17 October 1968. i) 2151-2157 UT. (LS film) ii) 2152:49 UT. iii) 2155:01 UT.

Figure 5.9a. fd-spike bursts following type III bursts, 27 July 1967. i) 2035-2037 UT. (LS film). ii) 2036:35 UT.

Figure 5.10(a-d) Short-duration type III bursts: a) 6-21-68, 1659:35 UT. b) 6-22-68, 0236:59 UT. c) 6-20-67, 1540:12 UT. d) 7-9-67, 1338:18 UT.

Figure 5.10e. Short-duration type III bursts, 25 June 1967. i) wide band dynamic spectrum, 1754 - 1800 UT. (courtesy A. Maxwell). ii) 1754 - 1800 UT. (LS film). iii) 1757:00 UT. (width of sprocket hole represents 0.25 seconds along time axis).

Figure 5.10f. Short-duration type III bursts, 25 August 1967. i) wide band dynamic spectrum, 1953-2016 UT. (courtesy A. Maxwell); see format, fig. 5.10e. ii) 2001-2007 UT. (LS film). iii) 2003:31 UT. (interval between frequency calibrations is 1.0 second). iv) 2005:23 UT. v) 2005:43 UT.

Figure 5.11a. Large-frequency-range fd-spike bursts during type III burst event, 27 July 1967. i) Wide band dynamic spectrum 2004-2022 UT. (courtesy A. Maxwell); see format, fig. 5.10 e. ii) 2012:58 UT. iii) 2013:28 UT. iv) 2013:54 UT. v) 2015:29 UT.

Figure 5.11b. Short-duration type III bursts, 27 June 1968. i) wide-band dynamic spectrum, 0024-0031 UT. (courtesy A. Maxwell); see format, fig. 5.10e. ii) 0024-0031 UT. (LS film). iii) 0026:48 UT. iv) 0026:58 UT.

Figure 5.12. Duration of Type III bursts as a function of frequency after Elgarøy and Rødberg, 1964, and Hughes and Harkness, 1963. The lines give collisional damping times as a function of plasma frequency for various temperatures.

Figure 5.13. Duration of type III bursts as a function of frequency Solid line: average measured duration of 90 type III bursts; Dashed line: exciter pulse duration and theoretical damping time (from Hughes and Harkness, 1963).

Fiugre 5.14. Radial and transverse dimensions of the fast-drift burst exciter are shown by the solid and dashed lines, respectively (from Hughes and Harkness, 1963).

Figure 5.15. Average velocity dispersion inferred from fig. 5.14 (from Smith, 1970).

Figure 5.16. Position and vertical extent of exciter with vertical speed V_s, total speed dispersion ΔV_s.

Figure 6.1. PDB Events (from Philip, 1968) a) 6-3-68, b) 6-7-68a, c) 6-7-68b, d) 6-9-68, e) 6-9-68, e) 6-9-68 cont., f) 6-9-68 cont.

Figure 6.2. PDB Event, 24 October 1967: a) 2131-2137 UT. b) 2133:42 UT.

Figure 6.3. PDB Event 4 November 1957 (from Boischot, et al., 1960).

Figure 6.4. PDB Event, 18 August 1959 (from Elgarøy, 1961).

Figure 6.5. Histories of PCDB events. a) 8-18-59. b) 10-24-67. c) 6-3-68. d) 6-7-68A. e) 6-7-68B.

Figure 6.6. Histories of PCDB events. a) 11-4-57. b) 8-18-59. c) 6-9-68A. d) 6-9-68B.

Figure 6.7. Illustrating the origin of synchrotron radiation. E(t) represents the electric field at a stationary observer in the orbital plane of an electron gyrating at velocity βc. The emission spectrum P(f) is the Fourier transform of E(t). (from Wild, et al., 1963).

Figure 7.1. Unusual spike bursts: a) 7-14-68, 1416-1422 UT. (LS film). b) 7-14-68, 1419:03 UT.

Figure 7.2. srt-spike bursts: a) 9-26-68, 0026-0032 UT. (LS film) b) 9-26-68, 0028:02 UT.

Figure 7.3. a) unusual burst. 7-11-68, 1748:47 UT. b) same burst exposed to show spike burst-like feature in center.

Figure 7.4. sls-chains: a) 6-25-67, 1348:11 UT. b) 7-24-67, 1926:10 UT. c) 6-25-67, 2149:55 UT. d) 9-27-68, 2339:42 UT. e) 8-16-68, 2325:41 UT.

Figure 7.5. f-chains: a) 7-22-67, 0048:32 UT. b) 7-12-68, 1856:27 UT. c) 7-25-67, 1802:41 UT. d) 7-24-67, 2116:55 UT. e) 5-23-68, 0349:11 UT.

Figure 7.6(a-d). hco-chains: a) 8-16-68, 0230:24 UT. b) 8-16-68, 1635:24 UT. c) 6-23-68, 1956:32 UT. d) 8-16-68, 1635:32 UT.

Figure 7.6e. hco-chains: 10-19-68, 0052:45 UT.

Figure 7.7. Combination of drifting spike bursts and s-spike burst (a), type I(s) bursts (b and c). a) 10-18-68, 0028:51 UT. b) 8-17-68, 1803:51 UT. c) 8-17-68, 0422:55 UT.

Figure 7.8. Persistent bursts (PB). a) 7-13-68, 0359:15 UT. b) 6-22-68, 0429:54 UT. c) 7-12-68, 0051:11 UT.

Figure 7.9. Rope-like Parallel Structure (PS): a) 8-1-67, 2130:21 UT. b) 8-2-68, 0236:10 UT.

LIST OF TABLES

Table 2.1. Observed distribution of type I bursts of types I(s), I(d), I(r), and I(f); after Elgarøy (1961).

Table 4.1. Number of s-, md-, and fd- spike burst events catalogued in each receiver band.

INTRODUCTION

Of the various manifestations of solar activity, the flare appears to produce the most notable effects on the earth and pose the greatest threat to communication and space exploration. Magnetic storms, aurorae, communication disturbances, and cosmic rays have all been associated with the occurrence of major flares.

Optical studies of flares are largely limited to the lowest, densest portions of the solar atmosphere. The turbulent and ordered motions of the high-energy charged particles released in a flare produce radio frequency emissions in the fully-ionized, less-dense, higher regions of the solar atmosphere. Thus, spectral observations at radio frequencies aid the study of the corpuscular emissions of a flare and the structure of the solar corona above the flare.

Accepted interpretations of the radio aspects of a flare are at best tentative. As these interpretations improve, the understanding of the flare phenomenon and its corpuscular emission will improve.

The most common radio aspect of a flare is the type III burst, which appears to indicate the ejection of 10-100 kev electrons into the interplanetary medium. The observations taken with the meter wavelength, high-time-resolution (HTR) Radiospectrograph of the Chena Valley Radio Facility of the Geophysical Institute indicate a close association between these major flare-initiated bursts and the shortest-lived solar radio bursts yet observed, spike (or flash) bursts.

Spike bursts have previously been shown to occur during type IV bursts and noise storms. Type IV bursts are major radio events which occur after proton flares. Noise storms are long lasting radio

events of uncertain flare association. Observations of the HTR Radiospectrograph show some spike bursts to occur in flare-associated quasi-periodic sequences, followed by complex patterns of parallel-drifting narrowband emission.

Each of these varied associations may serve to mutually restrict the possible interpretations of both burst types involved.

In an attempt to improve the understanding of both spike bursts and type III bursts, this study discusses the association between spike bursts and type III bursts as it was observed with the HTR Radiospectrograph.

A short morphology of spike bursts is presented as well as several examples of unusual spectral fine-structure observed with the HTR Radiospectrograph.

CHAPTER I. SPIKE BURSTS

A. Dynamic Spectra

Meter-wavelength solar radio emission has been morphologically divided into types according to the dynamic spectra of the emissions. A dynamic spectrum is a plot of the radio-frequency spectrum of the emission as a function of time. By convention, dynamic spectra are presented as in figure I.2. with time increasing to the right, frequency increasing in the downward direction, and intensity increasing out of the page. Intensity is indicated either by film density (figure I.2.) or contours of equal film density or rf-intensity (figure I.1.).

Burst parameters of interest to us in the following discussion are defined in figure I.1., which represents the dynamic spectrum of a frequency-drifting burst of limited duration and bandwidth. Intensity is indicated by contours of equal intensity. If the contour used to measure a given parameter represents one-half the maximum intensity of the burst, one obtains the half-power value of the parameter. Sometimes the one-quarter and e^{-1} intensity levels are used, as is the level at which the burst is just discernable from the background continuum. We will denote values obtained from half-intensity and zero-intensity levels by HP (half-power) and B (background) thus b_f(HP), d_o (B). Mean values will be indicated by a bar thus: $\overline{b_o}$(B), $\overline{d_f}$.

Unfortunately, in the literature one may find the words "bandwidth" and "duration" used for b_o and d_o as well as for b_f and d_f. For $\dot{f} = o$, $b_o = b_f$ and $d_f = d_o$. However, for $\dot{f} \neq o$, b_f and d_f can

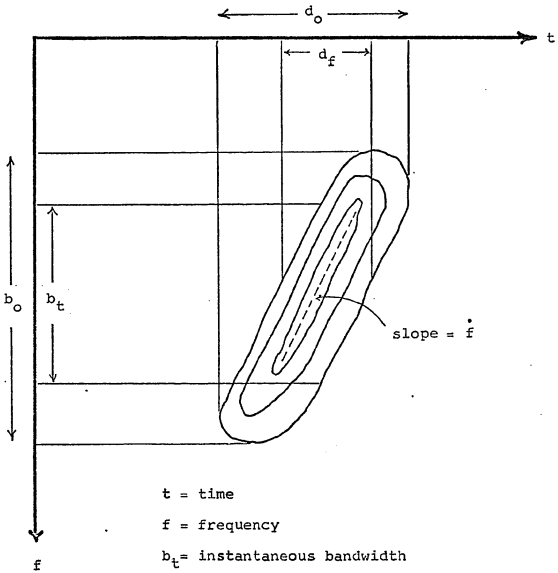

t = time

f = frequency

b_t = instantaneous bandwidth

b_o = frequency range

d_f = duration at one frequency

d_o = lifetime

$\dot{f}$ = frequency drift

Fig. 1.1 Burst Parameters

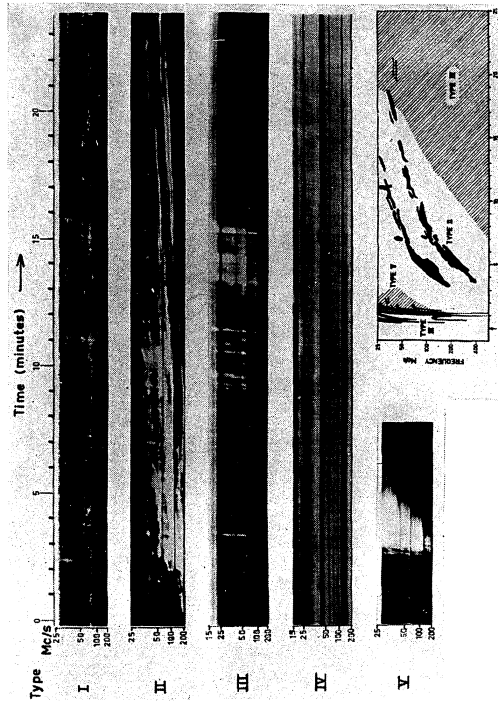

Fig. 1.2. Examples of dynamic spectra illustrating the five principal spectral types recorded at metre wavelengths. The inset represents an idealized sketch of the complete flare-associated radio event (from Wild, et al.,1963).

differ considerably from b_o and d_o; the two sets of parameters reflect information of different natures on the burst mechanisms involved. Given a drifting source, b_f and d_f are a property of the emission mechanism, b_o is a consequence of the length of time the source continues emitting, d_o. When "bandwidth" and "duration" are clearly defined, the appropriate symbols will be used below; otherwise the symbols b and d will be used.

Frequency drift, $\dot{f}$, is sometimes measured from the leading or trailing edge of the burst, instead of from the ridge of maximum intensity as illustrated. By convention, negative frequency drift ($\dot{f}<0$) is referred to as "direct drift"; positive frequency drift is referred to as "reverse drift".

Figure I.2., after Wild, et al.(1963), gives examples of dynamic spectra illustrating the five principal spectral types recorded at meter wavelengths,with the usual low to moderate time-resolution. The inset represents an idealized sketch of the complete radio event associated with a flare. The complete event, however, is only rarely observed.

B. Spike Burst Observations

In 1962, Ø. Elgarøy and T. deGroot independently announced the discovery of meter wavelength bursts of extremely short duration, which they named "flash bursts" and "spike bursts", respectively. In the ensuing literature on such bursts, both names were used. The terminology used by the authors will be retained in the following review of that literature, though no morphological distinction appears to have been intended in the papers. For general use in this study, we have chosen the name "spike burst", in keeping with the majority of the literature. We use "spike burst" as a generic name for all

bursts with $d_f \leq 0.1$ second.

Observing with swept-frequency techniques on about 210 MHz, Elgarøy (1962, 1963) reported very brief flashes of solar radio emission during a noise storm. The bursts were of shorter duration than type I bursts of the kind previously observed in that frequency range. On one occasion $\overline{d}_o(B)$ values of 0.19 and 0.50 second were obtained for flash bursts and type I bursts, respectively. Values down to 0.06 second, close to the instrumental limit of time resolution, were recorded for $d_o(B)$. The bursts occurred singly, in groups of two or three, or in clusters lasting from 0.5 to 1 minute. Their bandwidths were the same or slightly larger than those of normal type I bursts and they exhibited both senses of drift. Figure 1.3. (Eckhoff, 1966) compares flash bursts with normal type I bursts.

Observing with multiple-frequency techniques on about 330 MHz, de Groot (1962, 1963) reported bursts with $d \leq 0.1$ second which are distinct in character from even the short type I bursts that have d ranging downward to 0.1 second. The bursts often occurred in groups and were always strongly polarized. The bursts usually occurred during periods of increased activity, mainly in the type IV stage of a complete solar radio event. Figure 1.4., from de Groot (1963), shows a pulsating background observed during the early part of a type IV event and spike bursts during the later part of the event. Figure 1.5., from de Groot (1963), shows the same behavior during another

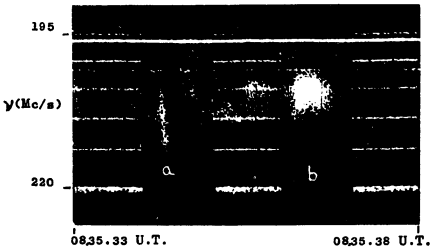

Fig. 1.3A. a) Spike burst. b) Ordinary type I burst (from Eckhoff, 1966).

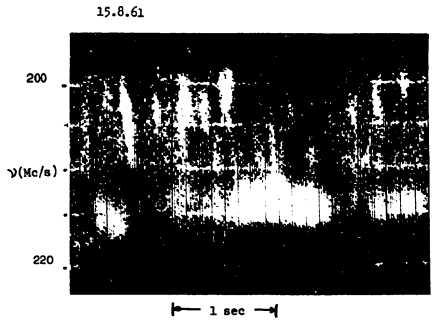

Fig. 1.3B. Dynamic spectrum showing both spike bursts and ordinary type I bursts (from Eckhoff, 1966).

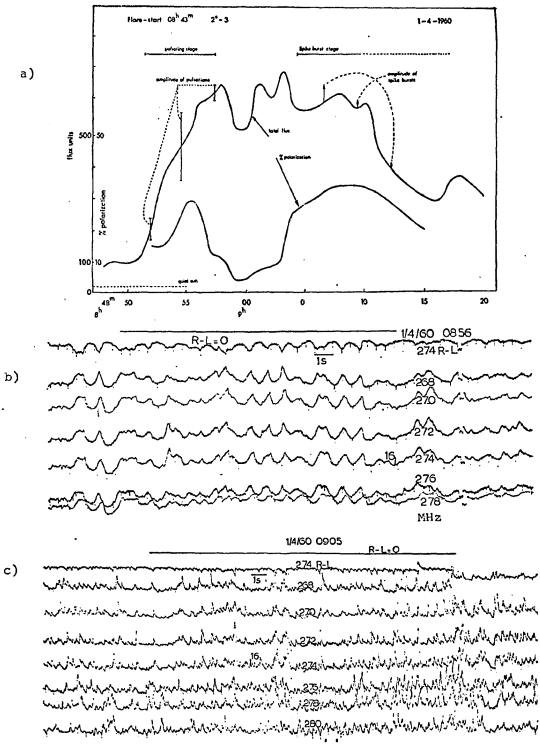

Fig. 1.4. Spike bursts during the type IV event, 4-1-1960. a) course of the type IV event. b) pulsations. c) spike bursts during the type IV event.(from de Groot, 1963)

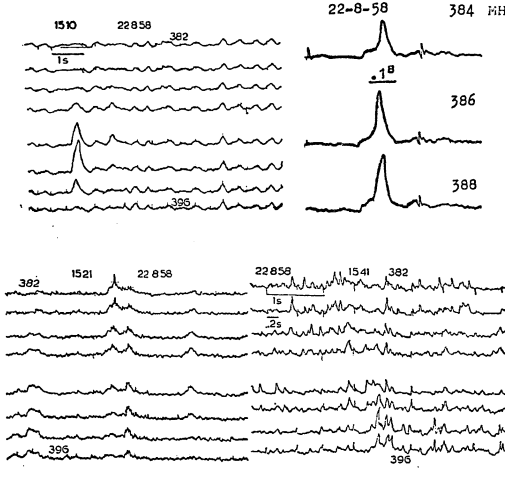

Fig. 1.5. Spike bursts and pulsations during the type IV event of 8-22-58 (from deGroot, 1966).

type IV event.

In 1965, Elgarøy (1965; Elgarøy and Eckhoff, 1966) reported an unusual event during which $\bar{d}$ decreased within a few minutes to about 50% of the normal value for type I bursts. For a few minutes d values remained with a narrow spread around 0.15 second or less. Longer duration bursts then reappeared, the short duration bursts disappeared, and $\bar{d}$ increased to normal for type I bursts. That is, type I bursts appeared to evolve continuously into flash bursts, then back into type I bursts, suggesting that flash bursts may be due to a perturbation of the type I burst source.

In 1966, Elgarøy summarized flash burst properties:

1. $f > \pm$ 100 MHz/sec ;
2. 0.10 sec. $< d_o <$ 0.20 sec. (a few bursts: 0.05 sec. $< d_o <$ 0.10 sec.);
3. $d_f \sim$ 0.10 sec ;
4. b up to 13 MHz.

In 1967, Malville reported the results of single-frequency observations of over 400 spike bursts on 345 and 230 MHz. The mean, half-power decay times at the two frequencies were 0.055 and 0.085 second, respectively. The mean half-power duration was 0.094 second at 345 MHz. The bursts were all observed during a type IV event. The equipment used had an effective time constant of < 0.01 second.

In 1967, Dröge reported single-frequency observations made on 107, 240, 460 and 1420 MHz with a time resolution of 0.005 second. On 240 MHz Dröge observed solar radio bursts with $d_f(HP) \sim$ 0.07 second (range 0.1 - 0.05 second) which he identified as spike bursts.

Bursts of such duration had actually been reported by Dröge and Riemann in 1961. The spike bursts always occurred during a type IV event. Burst intensities reached 50 x 10^{-21} w/m^2Hz, and appeared to depend, up to a limit, on the strength of the type IV continuum. Spike burst activity usually lasted only a few minutes. Though the bursts, in general , followed one another irregularly and had simple, uniform profiles, they were at times very closely grouped, often overlapping and producing very complex profiles.

On 460 MHz Dröge observed bursts with $\overline{d}_f$(HP) $\sim$ 0.03 second (range 0.05 - 0.01 second), which, aside from their shorter duration, were essentially the same as the above 240 MHz bursts. They occur more frequently and are easier to recognize, owing to the absence of interfering type I and type IV bursts and type I continuum at 460 MHz. Figure 1.6. (from Dröge, 1967) shows examples of spike bursts from Dröge's 240 and 460 MHz observations and similar bursts recorded on 1420 MHz having $\sim$ 0.003 second duration.

In 1968, Philip reported three events in which a quasi-periodic succession of flash bursts had been observed. The quasi-periodic flash bursts had b > 15 MHz, $d_f \sim 0.05$ second, and recurrence rates of 5 - 8/sec. All events lasted 4 seconds or more, and then broke up into normal flash bursts with b $\sim$ 5 MHz and essentially random recurrence. One event occurred 40 minutes after a 1 B flare; two occurred 50 and 75 minutes after a 1 N flare. All three events were followed by complex narrow-band drifting bursts. Examples of these observations will be given in chapters 4. and 6.

In 1969, Philip reported four occasions on which spike bursts of

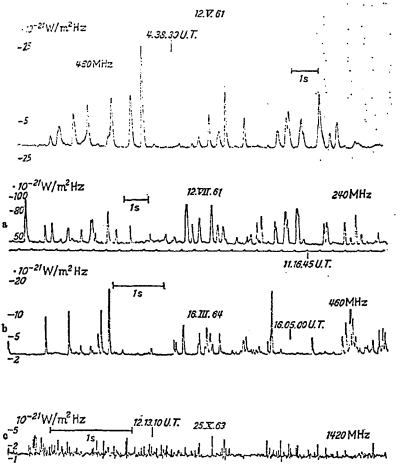

Fig. 1.6. Single-frequency observations of spike bursts (after Dröge, 1967).

$d_f \sim 0.05 - 0.15$ second were observed to occur over a 20 MHz channel centered at 250 MHz, simultaneously with type III or III-like activity on two lower-frequency channels centered at 183 and 140 MHz. The spike bursts were clearly associated with the type III bursts, occurring within a sharply defined time interval which matched the period that would have shown type III activity had the starting frequencies of the type III bursts been high enough to register on the upper channel. Many of the spike bursts had drift rates (direct or reverse drift) within the range 15-35 MHz/sec, and the majority were quite limited in instantaneous bandwidth ($b_f \sim 1$-3 MHz). The type III activity, on the other hand, showed no unusual fine structure. Examples of these observations will be given in chapter 5.

Recently, Markeev and Chernov (1971) reported similar bursts, in the range 190-220 MHz, with $d_f \sim 0.1$ second, $b_f \sim 1$-1.5 MHz, $b_o \sim 6$ - 30 MHz, $\dot{f} \sim 20$-40 MHz/sec, and $\sim 100\%$ right-circular polarization.

We will use "spike burst" as a generic name for all bursts with $d_f \lesssim 0.1$ second. However, the possibility exists that deGroot's "spike bursts", with their definitive periodicity and association with type IV sources (deGroot, 1970, 1963), may be a subdivision of all bursts with $d_f \lesssim 0.1$ second. In the present study an insufficient number of type IV events were observed to examine this question.

CHAPTER 2. SIMILAR BURSTS

In this chapter we shall review spectral characteristics of bursts of types I and III and similar decimetric and dekametric bursts. All these bursts bear some resemblance to spike bursts, by virtue of having short-duration and narrow-bandwidth and/or having high frequency drift rate. The "plasma hypothesis" is described in connection with type III burst observations. Plasma hypothesis and cyclotron emission models for type I bursts are described. Applications of type I and type III burst models to spike bursts are then reviewed.

A. Type III Bursts

One of the most dramatic features of meter wavelength solar radio emission is the type III burst. These bursts are characterized by their high negative drift rate ($\dot{f} < 0$) and large frequency range. The examples of type III bursts given in figure 2.1., from Hughes and Harkness (1963), show variations in duration, frequency range, and drift rate. Other wide-band records of type III bursts are shown in figures 5.10.e.-5.10.g., 5.11.a., 5.11.b.

The observed distribution of frequency ranges of type III bursts is given in figure 2.2 from Malville (1962). Distributions of starting frequencies for type III bursts are given in figures 2.3.a. (from Malville, 1962) and 2.3.b (from Malville, 1967). Figure 2.3.b. shows a possible trend of decreasing starting frequencies with decreasing general level of solar activity. Type III bursts have been observed, by means of satellites, to extend to frequencies of less than 1 MHz (Slysh,

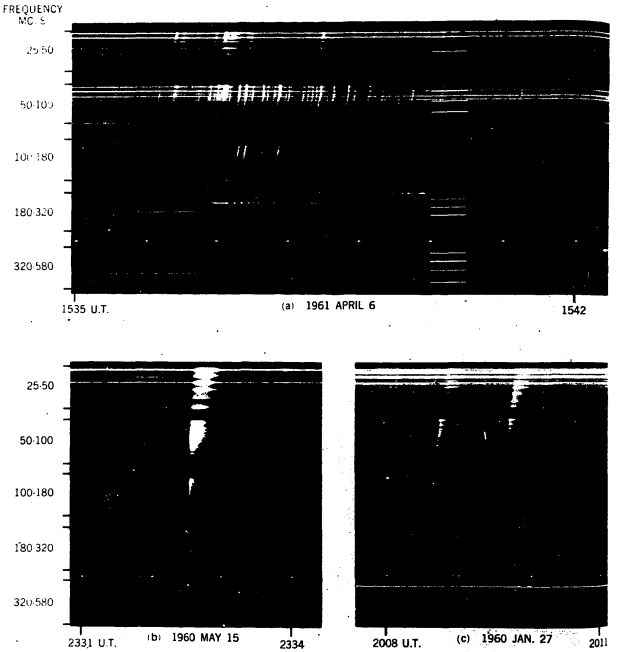

Fig. 2.1. Groups of type III bursts, showing variations in the duration, frequency range, and frequency-drift rate (from Hughes and Harkness, 1963).

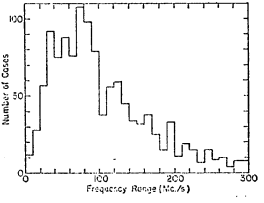

Fig. 2.2. Distribution of the frequency ranges of type III bursts. (from Malville, 1962).

a)

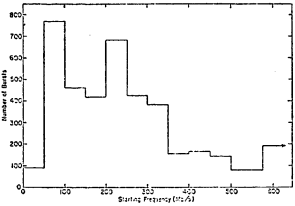

b)

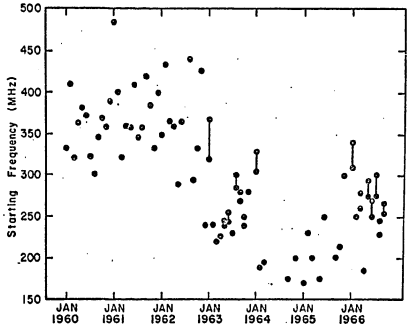

Fig. 2.3. a)Distribution of starting frequencies of type III bursts (from Malville,1962). b) Variation of monthly averages of frequencies of type III bursts (from Malville, 1967).

1967; Hartz, 1969; Alexander, Malitson and Stone, 1969; Fainberg and Stone, 1970a, 1970b).

The high negative drift rate characteristic of type III bursts is seen to decrease with decreasing frequency as shown in figures 2.4.a., from Hughes and Harkness (1963), and 2.4.b., from Hartz (1969). Maxwell, et al. (1960) report mean values of -700 MHz/sec. at 550 MHz, -500 MHz/sec. at 425 MHz, -150 MHz/sec. at 200 MHz, and -75 MHz/sec. at 125 MHz. Elgarøy and Rødberg (1964) report a mean value of -60 MHz/sec. at 200 MHz, with a range of -20 to -150 MHz/sec.

The duration at one frequency, d_f, of type III bursts is seen to increase with decreasing frequency (figure 2.5., after Hughes and Harkness, 1963). Maxwell, et al. (1960), give average durations of 1.4 seconds at 50 MHz, 1.6 seconds at 425 MHz, 3.2 seconds at 200 MHz, and 4.0 seconds at 125 MHz. Elgarøy and Rødberg (1964) give an average half-power duration of 0.5 seconds at 215 MHz. The measurements of Hughes and Harkness (1963) and Maxwell, et al. (1960) give the total length of time the bursts were discernable from the background.

The instantaneous bandwidth, b_f, of type III bursts is essentially difficult to measure. Wide-band swept-frequency radiospectrographs have insufficient time-resolution; high-time-resolution swept-frequency radiospectrographs lack sufficient bandwidth. The development of wide-band multi-frequency techniques (de Groot and Van Nieuwkoop, 1968; de Groot, 1970) provides an answer to this problem. An estimate of $\sim$30 MHz is given by Elgarøy and Rødberg (1964) for the instantaneous bandwidth of type III bursts.

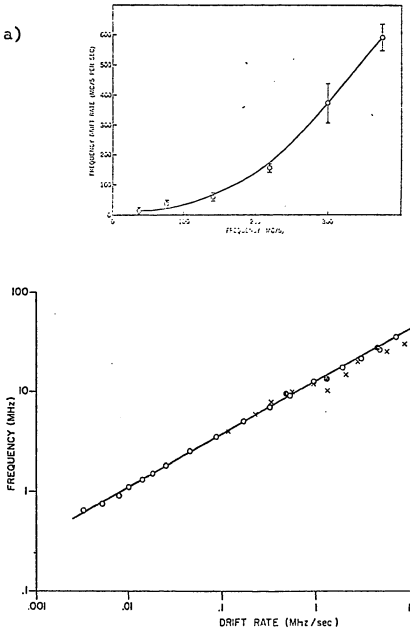

Fig. 2.4. a) Frequency-drift rate of type III bursts as a function of frequency (from Hughes and Harkness, 1963). b) Average frequency drift rates for type III bursts (from Hartz,1969).

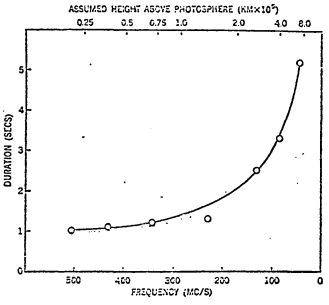

Fig. 2.5. Average duration of type III bursts as a function of frequency (after Hughes and Harkness, 1963).

Payne-Scott, Yabsley, and Bolton (1947) suggested that the slow negative drift of a type II burst was due to upward motion through the corona, of some physical agency. This interpretation of frequency drift was based on Martyn's (1947) suggestion that the radiation observed at any one frequency originates near the level in the corona where the electron density reduces the refractive index to zero. Ignoring the coronal magnetic field, we expect em-waves of frequency f to originate at the level in the corona where $f \approx f_o$, where f_o is the electron plasma frequency,

$$f_o = \sqrt{\frac{e^2 N_e}{\pi m_e}}$$

where N_e is the number of electrons/cm^3, e is the electronic charge, and m_e is the electronic mass.

Wild (1950) noted that the sharp cut-off observed on the low-frequency edge of type II bursts could be due to the inability of em-waves to propagate at frequencies less than f_o. The spectrum due to macroscopic disturbances in such a medium would consequently exhibit a complete cut-off in the range of frequencies $< f_o$. In a non-uniform medium such as the corona, a cut-off will occur if the disturbance is bounded. The cut-off, or critical, frequency is the value of f_o determined by N_e at the boundary of the disturbance. If we assume N_e to decrease continuously outwards in the corona, the critical frequency will be determined by N_e at the outermost boundary of the disturbance.

Further support for the "critical frequency hypothesis" was found in the observation of harmonics in type II bursts (Wild, Murray, and Rowe, 1953). Comparison of the frequency profiles of the fundamental

and harmonic bursts indicated that the low-frequency skirt of the fundamental had been cut off and, consequently, the ratio between frequencies corresponding to peaks lay mainly in the range 1.90-1.99 and in no case exceeded 2.0.

The existence of harmonics in type II bursts and of a narrow-band peak of high-intensity commonly observed near the cut-off frequency is suggestive of some kind of resonance taking place near the f_o level, as discussed theoretically by Martyn (1947) and Jaeger and Westfold (1949). Wild, Murray, and Rowe (1954) concluded that the emission observed was due to charge oscillation at the plasma frequency. Thus, the "critical frequency hypothesis" (that type II burst emission originated near the critical frequency, f_o, level of the corona) was extended to become the "plasma hypothesis", namely, that the emission mechanism of type II bursts involves charge oscillations at the electron plasma frequency, f_o.

Wild, Roberts, and Murray (1954) found that the same behaviour was observed in harmonics of type III bursts as had been observed in harmonics of type II bursts, namely, cutting off of the low frequency skirt of the fundamental burst and a frequency ratio of less than 2.0. It was this result which originally justified the application of the plasma hypothesis to type III bursts. Attributing the observed frequency drift to upward motion of a disturbance through the Baumbach-Allen corona, speeds of 0.1-0.3 c were determined for the disturbance, where c is the speed of light.

The plasma hypothesis predicts that when a type III source is ejected outwards from near the limb of the sun (edge of the visible

disc), the radio source should appear beyond the limb and its angular displacement from the limb should increase as frequency decreases. This behaviour was indeed observed, providing the most direct verification of the plasma hypothesis, with a swept-frequency interferometer (Wild, Sheridan, and Trent, 1959; Wild, Sheridan, and Neylan, 1959). Figure 2.6. (after Kundu, 1965; Wild, Sheridan, and Neylan, 1959) shows the positions, at four frequencies, of eight type III bursts associated with flares occuring at the limb. The distribution of disturbance (or "exciter") speeds determined in this study was 0.2-0.8 c, with an average of 0.45 c. With velocities comparable to c, it was pointed out that account must be taken of the finite difference in times taken by signals at two frequencies to propagate from their points of origin to the observer. The correction depends on the angle, θ, between the path of the exciter and the sun-earth line, and is given approximately by (de Groot, 1966):

$$\dot{f}_o = \dot{f}_r(1 - \beta\cos\theta)^{-1}$$

where $\dot{f}_o$ is the observed $\dot{f}$, $\dot{f}_r$ is the frequency drift rate of the emitting source, and βc is the speed of the exciter. The heights shown in figure 2.6. are above the plasma frequency levels determined from the Baumbach-Allen corona and agree better with a Newkirk model for coronal streamers (figure 2.7., from Kundu, 1965).

The decrease of $\dot{f}$ with decreasing frequency may be attributed largely to the decrease of $|\nabla N_e|$ with height in the corona. Fainberg and Stone (1970b) find exciter speeds of 0.3-0.4 c, with little deceleration over distances of at least 1 A.U.

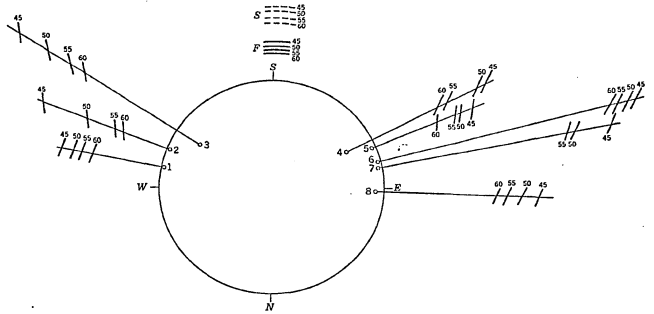

Fig. 2.6. Source positions of eight type III bursts associated with limb flares (optical positions shown as circles). The circular arcs show the levels of the fundamental (F) and second harmonics (S) of the plasma frequency, assuming the Baumbach-Allen corona. (from Kundu, 1965; after Wild, Sheridan, and Neylan, 1959).

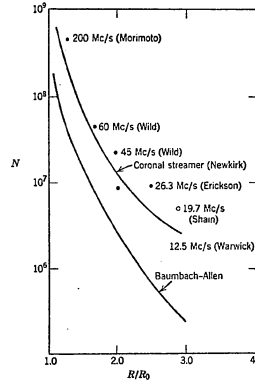

Fig. 2.7. The electron densities deduced from different radio observations compared with those of the Baumbach-Allen model and coronal streamer model of Newkirk (from Kundu, 1965).

The increase of d_f with decreasing frequency may be largely attributed to the decrease of N_e with height above the photosphere. Bohm and Gross (1949) show that plasma frequency oscillations should decay in approximately the inverse of the electron-ion collision frequency ν_{coll}. From Jaeger and Westfold's (1949) equation for ν_{coll}, we have the decay time, t_D, given by

$$t_D \simeq \nu_{coll}^{-1} \simeq \frac{T^{3/2}}{42N_e}$$

where T is the electron kinetic temperature. In terms of plasma frequency, we have (Kundu, 1965)

$$t_D \simeq \frac{1.92\times10^3\ T^{3/2}(10^6\,^\circ K)}{f^2\ (MHz)} \quad \text{sec}$$

Assuming that the exciter passes through the region responsible for emission at the frequency, f_o, in much less time than the total duration of the burst at f_o, we may set $d_f \sim t_D$, obtaining the temperatures shown in figure 2.8. (Elgarøy and Rødberg, 1964) for the various plasma frequency levels. Hughes and Harkness (1963) and Elgarøy and Rødberg (1964) conclude that a significant portion of d_f is excitation time, due to passage of an exciter with large spatial extent through the region responsible for emission at the frequency in question. The approach of Hughes and Harkness (1963) will be discussed in section 5.B. Duration values may be contaminated by the overlapping of type III bursts, and of type III bursts and type V bursts (continuum emission, lasting ~1 minute, following some type III bursts).

Elgarøy and Eckhoff (1966) suggest that Landau damping may significantly affect the duration of short duration bursts. Malville (1962)

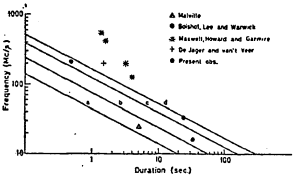

Fig. 2.8. Burst duration as a function of frequency for T equal to (a) 10^6 °K, (b) 2 x 10^6 °K, (c) 4 x 10^6 °K, and (d) 6 x 10^6 ° K (from Elgarøy and Rødberg, 1964).

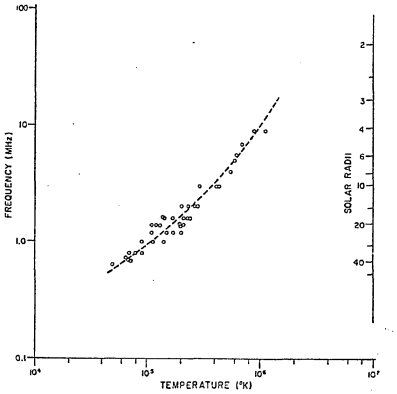

Fig. 2.9. Deduced temperatures for the source regions of the type III bursts; These regions are located in terms of their plasma frequency, left ordinates, and their infered solar distances, right ordinates (from Hartz, 1969).

shows that Landau damping narrows the bandwidth of plasma oscillations but does not affect burst duration. Hartz (1969), arguing against the effect of exciter dispersion and type V burst contamination, determines the temperature profile for the outer corona given in figure 2.9. It should be noted that Hartz used the rate at which the burst emission decayed rather than the total duration of the bursts.

Thus, experimental evidence supports the hypothesis that type III burst emission is due to electron plasma frequency oscillation in the active region corona (N_e about ten times that of the quiet corona) initiated by a disturbance ("exciter") moving outwards through the corona at speeds of $\sim 1/3$ c. The exact nature of the emission mechanism involved and the nature of the exciter have not been established with certainty. It is generally believed that the exciter is a stream of electrons, though proton models have been proposed (eg., Smith, 1970b). The apparent exciter speed indicates the electrons have energies of ~10-100 kev. Anderson and Lin (1966) and Lin (1968) have detected, by satellite, bursts of $\geq$ 40 kev electrons at the time of type III bursts.

The exciter is believed to generate plasma waves by the two-stream instability (Ginzberg and Zheleznyakov, 1958, 1961; Kaplan and Tsytovich, 1968).

Ginzberg and Zheleznyakov (1958) proposed that the plasma waves were converted into em-waves by scattering off the thermal density fluctuations of the ambient plasma. The frequency spectrum of such fluctuations shows a large maximum about $f_1 \sim 0$ and weak side bands at $f_2 \sim f_o$. It was proposed that em-waves at the fundamental were produced

by scattering of the plasma waves off the fluctuations of the peak at $f_l \sim 0$, producing em-waves at $f_o + f_l \sim f_o$, and that emission at the second harmonic was due to scattering of the $f_2 \sim f_o$ peaks, producing em-waves at $f_o + f_2 \sim 2f_o$. A similar analysis is given in Yip (1970a, 1970b).

Estimating the efficiency with which plasma waves could be produced and transformed into em-waves, Ginzberg and Zheleznyakov (1958) estimated stream densities, N_s, of $\sim 10^6$ electrons/cm^3. Quasilinear analysis of the two-stream instability indicated that streams of such high density ($N_s \sim 10^{-2} N_e$) would undergo plateau formation very rapidly, becoming unable to produce plasma waves by the two-stream instability after traveling only a few kilometers. This problem has led to the proposal of several nonlinear plasma effects which might be able to stabilize the stream against plateau formation (Sturrock, 1964; Kaplan and Tsytovich, 1968; Smith, 1970a, 1970b; Melrose, 1970a, 1970b).

Whereas the stream is capable of producing plasma waves by non-coherent Čerenkov emission, Ginzberg and Zheleznyakov (1961) have shown that a coherent mechanism is required. A recent analysis of the type III burst mechanism and of plateau formation by Zheleznyakov and Zaitsev (1970a, 1970b), which will be discussed in section 5.B, indicates that nonlinear plasma effects may be unnecessary. In particular this study notes that the density fluctuations at the peaks $f_2 \sim f_o$ are greatly enhanced by the presence of plasma waves. The efficiency of transformation of plasma waves into em-waves is considerably increased and the necessary stream density, N_s, is reduced to $N_s \sim 1\text{-}10$ electrons/cm^3.

B. Type I Bursts and Related Bursts

1. Noise Storms: Observations

Noise storms consist of an enhanced background continuum and superimposed bursts of short duration and narrow bandwidth, called type I bursts. The noise storm is the most commonly observed kind of solar radio emission at meter wavelengths. The following includes a summary of general noise storm characteristics taken largely from Kundu (1965), a summary of type I burst characteristics, and a discussion of various kinds of bursts which resemble type I bursts.

Noise storms may last for anywhere from a few hours to a few days. Noise storms generally occur within the frequency range 100-350 MHz, but have been observed to occur on frequencies as high as 500 MHz and as low as about 10 MHz, the lower limit of observation imposed by the ionosphere. The bandwidth of the background continuum usually extends over a frequency range of about 100 MHz and rarely shows any steep variations of intensity with frequency or time. The continuum often shows a maximum in the frequency range 150-250 MHz. The maximum may sometimes drift gradually into another range in the course of the day.

During periods of high solar activity the number of type III bursts increases, their upper (starting) frequency decreases, and noise storm activity appears below 100 MHz. The upper frequencies of type III bursts are found generally to fall in the range of concurrent noise storms.

Noise storm radiation originates from small regions located high in the corona, which appear to be closely associated with sunspots. Storm centers have apparent diameters of a few minutes of arc; type I bursts

appear somewhat smaller. The apparent diameters of both storm and burst decrease with an increase in observing frequency. Type I bursts appear to come from within the region emitting the continuum.

Storm centers are observed at heights of a few tenths of a solar radius above the photosphere. The apparent height increases toward the limb and decreases with an increase in observing frequency. Observed heights suggest noise storms occur at or near the critical frequency level for a coronal region with ten times the electron density of the Baumbach-Allen model for the quiet corona. Storm centers tend to be above major sun spots, but in many cases they are displaced from the radius passing from the center of the sun through the sunspot.

The intensity of noise storm radiation varies greatly, from barely discernable from the quiet (thermal) sun (about $10 \times 10^{-22} wm^{-2} Hz^{-1}$ at 200 MHz) to 10^{2} -10^{3} times the quiet sun intensity.

Noise storm radiation is highly directive. Most noise storms are observed near the center of the disc; slightly more are observed on the west side of the disc than on the east side (the sides to the observer's west or east, respectively). The intensity of a moderate noise storm is reduced by half in moving from the center of the disc to 40° from the center. Strong noise storms are much more directive.

Both continuum and bursts are highly circularly polarized, both in the same sense and to about the same degree. The sense of polarization is related to the magnetic polarity of the spot (usually the leading largest spot of a group) associated with the noise storm. A right-handed circularly polarized wave is emitted if the spot is a south

(negative) magnetic pole, and vice-versa. If the magnetic field in the high corona, at the place where emergent polarization is determined, is due simply to this spot, then the radiation is the ordinary magneto-ionic component. Infrequently, storms are observed which are of mixed polarization or are unpolarized. Storms of mixed polarization may be due to more than one storm being observed at one time. Unpolarized storms tend to occur more often near the limb rather than near the center of the disc.

2. Type I bursts

Wild and McCready (1950), in their classification of meter wavelength solar radio bursts, labeled noise storm associated bursts as "type I bursts" and described them as non-drifting bursts of narrow bandwidth and short duration.

High-time-resolution observations by Elgarøy (1961, 1965), showed that type I bursts had durations and bandwidths of a few tenths of a second and a few MHz respectively, and often exhibited frequency drift. Most type I bursts could be sub-classified by their frequency drift into (figure 2.10., from de Groot, 1966; after Elgarøy, 1961):

1. Non-drifting, stable bursts, type I (s);
2. Slow drift bursts, type I (d) and I (r), of direct and reverse drift, respectively, at rates below 10 MHz/sec; and
3. Fast drift bursts, type I (f), or direct, type I (fd), or reverse, type I (fr), drift at rates above 10 MHz/sec.

Table 2.1 after Elgarøy (1961), shows observed distributions of type I bursts which fit in the above scheme.

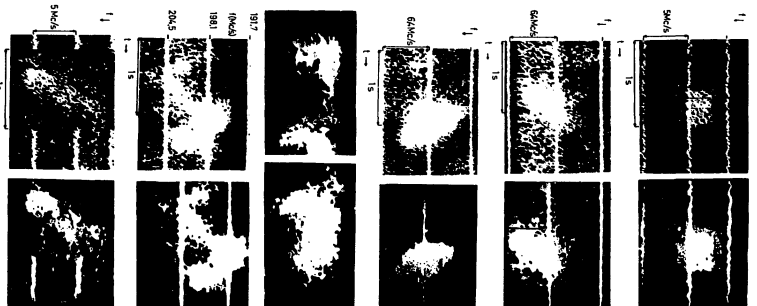

Fig. 2.10. Elgarøy's 1961 examples of type I bursts. Photographs of CRT screen and corresponding contour diagrams (from deGroot, 1966).

Table 2.1

Date (1959)	I(s)	I(d)	I(r)	I(fd)	I(fr)	I(d+fd)	I(r+fr)	number of bursts
13 Aug	49	14	17	7	13	21	30	159
10 Sept	71	11	13	2	3	13	16	174
11 Sept	77	-	-	-	-	12	11	310

Elgarøy (1961) originally included three other categories: I (c), curved burst, irregular frequency drift; I (o), burst with oscillating center frequency; and I (x), dubious cases, not possible to classify. Types I (o) and (x) may be due to the overlapping of simpler bursts (Elgarøy 1965). Type I (c) bursts resemble u-bursts, which appear to be a variant of type III bursts. Type I (c) bursts may be similar variants of bursts of type I (f) or I (d, r).

Elgarøy (1965) notes that the distinction between bursts of types I (f) and (d, r) may be artificial, i.e., a continuous distribution of drift rates may exist. In the same paper he notes that type I (f) bursts tend to have a somewhat shorter duration and larger bandwidth than other type I bursts.

Perhaps it should be suggested here that spike bursts might be an extension of this trend. Spike bursts have higher drift rates, shorter durations, and larger bandwidths than type I (f) bursts.

Elgarøy and Eckhoff (1966) present a summary of burst properties in the range 100-400 MHz. Figures 2.11. and 2.12. taken from that paper, give b_f(HP) and d_f(HP), means and ranges of observed values, from the work of several authors. Flash bursts appear to have been included among the bursts summarized.

Frequency dependence is suggested by Figures 2.11. and 2.12, though it may be due to the variety of observers and techniques involved. Individual authors (see, e.g., Wild, 1951; Vitkevich and Gorelova, 1961; and de Groot, 1960) report no conclusive frequency dependence. In 1967, Elgarøy reported frequency dependence in bursts recorded during a single

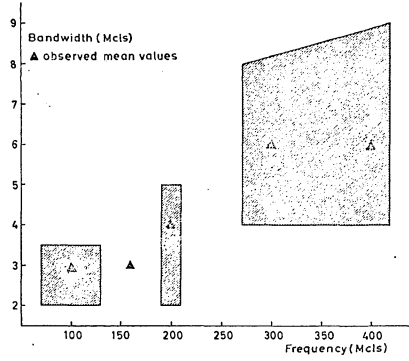

Fig. 2.11. Observed bandwidth of type I bursts. The hatched areas indicate the intervals within which most bandwidths occur (after Elgarøy and Eckhoff, 1966).

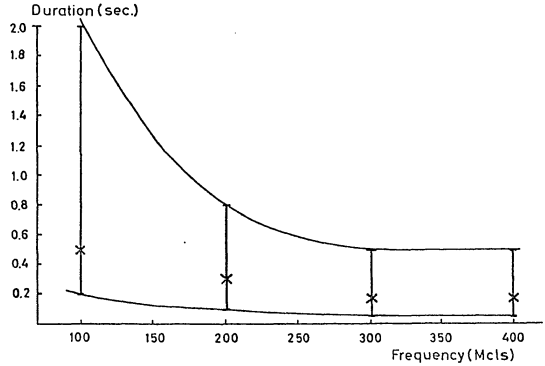

Fig. 2.12. Average burst duration on different frequencies. The upper and the lower limits of the duration are indicated (from Elgarøy and Eckhoff, 1966).

noise storm and attributed previous difficulties to inclusion of bursts from several noise storms.

3. Similar Bursts

i. Meter Wavelengths

It is necessary to consider whether type I (f) bursts are actually type I bursts. Elgarøy's high-time-resolution observations were made during noise storms. This sampling problem leaves the possibility that a particular class of burst may be as common outside of noise storm periods as during them. No polarization measurements were made to guarantee that all bursts considered had the high circular polarization characteristic of type I bursts. Furthermore, there exist two classes of meter wavelength activity which are not associated with noise storms, but do resemble type I (f) bursts:

1. The "herring-bone" structure in type II bursts, described by Roberts (1959); and
2. Type III bursts.

The herring-bone structure is formed by a rapid succession of broadband, short duration elements with fast drift of both direct and reverse senses. It appears to diverge from a narrow-band feature with direct drift at a rate typical of type II bursts. The herring-bone form may be less clearly developed, and the drifting elements may extend over only 5 or 10 MHz. The drift rates of the individual elements can be greater than those commonly seen for type III bursts, and d_f often less than 1 second.

Vestiges of herring-bone structure can be seen in perhaps 20% of all type II events.

Elgarøy (1961) considers it unlikely that type I (f) bursts are part of a herring-bone pattern because, if that were the case, one should expect several bursts of the same type in rapid succession, or some faint evidence of a simultaneous type II burst. Neither phenomenon was observed. On the contrary, type I (f) bursts occur in noise storms, and are preceded and followed by other classes of type I bursts.

Stewart (1966) reports that the fast-drift bursts of the herring-bone structure are at times found to be strongly circularly polarized. Thus we are unfortunately left with circularly polarized, short-duration, fast-drift bursts of limited frequency range which, as far as we know without high-resolution studies, differ from type I (f) bursts only by being associated with a type II burst instead of a noise storm continuum.

Whether type I (f) bursts constitute a variant of type III bursts is somewhat less clear. The ranges of observed values of $d_f(HP)$ overlap for type I bursts (Elgarøy and Hauge, 1958; Elgarøy, 1961) and type III bursts (Elgarøy and Rødberg, 1964; Elgarøy, 1965) on 200 MHz. Similar $\dot{f}$ are observed in bursts of type I (f) and III. For type III bursts, b_o values as low as 30 MHz have been observed by Malville (1962). Type I bursts with $b \sim 30$ MHz have been mentioned by Maxwell et al. (1958), Vitkevich and Kameneva (1958), Vitkevich et al. (1960), and Malville (1962).

High-resolution studies make no mention of type I bursts with $b_f \sim 30$ MHz. Perhaps drifting type I bursts could have $b_o \sim 30$ MHz.

Unfortunately, high-resolution studies have not discussed b_o values, perhaps because technical reasons have limited continuous observing ranges, e.g., to 20 MHz in Elgarøy's early observations.

It was hoped by Elgarøy (1961) that polarization measurements of type I (f) bursts would show them to be type I bursts (strongly circularly polarized) rather than type III bursts (weakly circularly or linearly polarized). Unfortunately, Rao (1965), from observations at 40 and 60 MHz, reports an inverse relationship between d_f(HP) and degree of circular polarization for type III bursts, such that bursts of (short) duration comparable with type I bursts have (strong) circular polarization comparable with type I bursts.

Differentiating between type I (f) and type III bursts is complicated by the close association often exhibited by type I and type III bursts. Type I bursts are occasionally seen to correspond in frequency and time with the start of a type III burst (Hanasz, 1966; Malville, 1962; Philip, 1969) or occur during a type III burst as fine structure in the burst (Roberts, 1958; Ellis and McCulloch, 1967, 1969). Malville (1962) comments that the primary difference between type I bursts and type III bursts may be in the growth rates of the associated plasma instabilities, but cautions that noise storm features such as enhanced background continuum or reverse drift bursts are not easily explained in terms of a type III mechanism. Kai's (1970) observation that type III sources avoid the precise locations of type I sources suggests environment may decide which type of burst is emitted by a given disturbance.

ii. Dekameter Wavelengths

On the chance that meter wavelength observations might record a burst straying in from another frequency range, we should acquaint ourselves with typical dekameter and decimeter wavelength bursts. The bursts we have discussed above are characteristic of frequencies from about 100 MHz through about 400 MHz. Normally restricted to frequencies below about 50 MHz are three types of (dekametric) bursts described by Roberts (1958), Ellis (1969), Ellis and McCulloch (1967), and Warwick and Dulk (1969). All three types are short-duration, narrow-band-width bursts associated with noise storms, thus qualifying as type I bursts. However, in the opinion of Warwick (1965) and Warwick and Dulk (1969), dekametric continuum events with bursts, though closely associated with noise storms, are distinct from noise storms, owing to the predominance of type III bursts over type I bursts. Therefore, these dekametric burst types may be of a different origin than the meter wavelength noise storm (type I) bursts. However, Boischot et al. (1970) interpret metric and dekametric noise storms as concurrent manifestations of the same disturbance. The different spectra of the bursts in the two ranges may be due to the transition of the corona at about the 40 MHz plasma frequency height. At this height the corotation of the corona with the sun ceases and the solar wind enters the interplanetary regime. The dekametric burst types are, with properties taken largely from Ellis's (1969) and Ellis and McCulloch's (1967) high-resolution observations:

1. Fast drift storm bursts: $|\dot{f}|$ = 1.9 MHz/sec., predominantly direct drift; b_f = 0.03 MHz; d_f = 0.6 sec.; identified with

Elgarøy's type I (fd); no circular polarization observed;

2. Split pair bursts: frequency split bursts with 0.1 MHz splitting at 25 MHz, 1.0 MHz at 60 MHz; $\dot{f}$ = 0.08 MHz/sec; b_t = 0.05 MHz for a single component; d_f = 1.4 sec; chains of split pair bursts were observed, the chain resembling a type III burst with fine structure; and
3. Drift pair bursts: time split bursts with mean time difference 1.2 sec; $\dot{f}$ = 1.2 MHz/sec; b_t = 0.45 MHz for a single component. Roberts (1958) finds 1/4 sec < d_f < 1 sec for a single component; instantaneous frequency separation is 4-10 MHz; bursts occasionally occur within a type III burst, and evidently form part of the fine structure of a type III burst.

Though other drift pair burst properties are quite similar in the two studies, Roberts (1958) reports a predominance of reverse drift, naming the bursts "reverse pairs", while Ellis (1969) reports a predominance of direct drift.

Note that the drift pair bursts reported by Ellis and Roberts are from different solar cycles. Though the change of predominant drift sense may be due to limited samples, it would be curious if it were due to the reversal of the general magnetic field of the sun between solar cycles.

As in Wild and McCready's (1950) and Elgarøy's (1961) classification schemes, the various bursts observed at dekametric wavelengths may be distinguished by their drift rates, as exhibited in Figure 2.13, due to Ellis (1969).

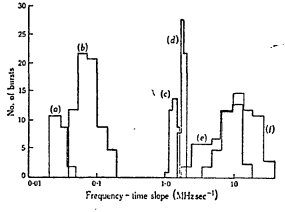

Fig. 2.13. Distribution of frequency-time slopes for (a) type II bursts, (b) split pair bursts, (c) drift pair bursts, (d) fast drift storm bursts, (e) type III bursts, and (f) chains of split pair bursts (from Ellis, 1969).

Note that for Ellis's fast drift storm bursts we have $\dot{f} \sim (f/20)$/sec, which falls between Elgarøy's types I (d) and I (fd). Note also that split pair bursts observed with lower frequency resolution would resemble type I (s) bursts, as do some of Ellis's photographic prints of split pair bursts. His photographic prints of drifting chains of split pair bursts resemble records of type I (f) bursts. High-frequency-resolution observations are needed at higher frequencies to examine possible continuity between dekameter and meter wavelength burst types.

iii. Decimeter Wavelengths

Characteristic of frequencies from about 300 - 3000 MHz are two general classifications of decimetric bursts described by Kundu (1965): the "generalized class of fast drift bursts" and "continuum events".

Within the generalized class of fast drift bursts are "type III-like bursts" and "decimeter-type bursts". The type III-like bursts have drift rates from 100 MHz/sec to > 2000 MHz/sec, predominantly direct, bursts with higher drift rates tending to shorter durations. Observed d_f range from 0.3 to 2 seconds (0.2 second time resolution). Some b_o values exceeded the 450 MHz observing range.

The decimeter-type bursts exhibited $d_f \geq 0.2$ seconds (time resolution) and $\dot{f} \geq 2000$ MHz/sec (observational limit on measuring drift rate). Both senses of drift were observed for bursts with measurable $\dot{f}$. The decimeter-type bursts occur typically in the range of 400-800 MHz, usually having their lowest frequency in the range 400-550 MHz. They are related to, but distinct from type III bursts which typically extend down through the meter wavelength region. The decimeter-type

bursts exhibit more reverse drift, lower ratio between starting and ending frequencies, and less burst continuity than type III bursts.

Decimetric continuum events sometimes exhibit fine structure which falls into three categories:

1. Sequences of intense short duration bursts of very high drift rate and large frequency range;
2. "Sprays"; and
3. "Intermediate drift bursts".

Sprays consist of several fast drift bursts of b $\sim$ 10 to 20 MHz, d $\sim$ a fraction of a second. The entire spray phenomenon lasts only one or two minutes.

The spray phenomenon, observed in the decimetric continuum, is similar to type I bursts in the noise storm continuum. Sprays have been observed in the 100-580 MHz range (Kundu and Spenser, 1963).

The intermediate drift bursts are of $d_f \sim 0.2 - 0.6$ seconds; direct drift, $\dot{f} \sim 10 - 50$ MHz/sec (and up to 150 MHz/sec); $b_f \sim 10$ MHz, $b_o \sim 50 - 150$ MHz (extremes: 20 MHz > 300 MHz). The bursts have been observed throughout the range 500 - 1000 MHz. Even on frequencies of about 300 MHz or lower such intermediate drift bursts have been observed. It appears that such bursts occuring at the lower frequencies always occur in a strong continuum and tend to have lower drift rates.

The intermediate drift bursts occur in groups of 10 - 30, sometimes exhibiting both drift senses, with the spacing between successive bursts ranging from a small fraction of a second to many seconds. The bursts in a group are often remarkably similar, and sometimes the bursts are fairly periodic.

4. Interpretation

Takakura (1963) has proposed a plasma hypothesis interpretation of type I bursts. Since type I bursts are of short duration and limited bandwidth, the excitation of plasma waves must be short-lived. Takakura proposes that electron streams are produced in the corona by the collision of two packets of Alfvén waves. The streams decay, in the observed duration of type I bursts, by the deflection of the stream particles through 90° in the time

$$t_D \simeq 2.0 \times 10^{-3} \frac{m_e^2 v_o^2}{e^4 N_e}$$

for the corona, where V_o is the speed of the stream, (cgs units are used). We require that $V_o > 2V_T$, where V_T is the electron thermal speed. Values of V_o corresponding to typical type I burst durations, are $\sim 2.9\ V_T$ at 200 MHz, $\sim 2.2\ V_T$ at 80 MHz. ($V_T \sim 5.5 \times 10^3$ km/sec for electrons at 10^6°K). Magnetic fields necessary for the acceleration of thermal electrons to these values are estimated to be $\sim$ 50 gauss at the radio source for 200 MHz, $\sim$ 15 gauss at 80 MHz. In order that the type I bursts are completely polarized in the ordinary sense, the magnetic fields at the radio sources are required by Takakura to be > 29 gauss for 200 MHz, > 12 gauss for 80 MHz.

The strong circular polarization of type I bursts has often led to the proposal of cyclotron emission mechanisms (see Kundu, 1965). Two major difficulties are faced by cyclotron emission mechanisms: in the corona one expects cyclotron emission to be generated beneath the critical frequency (f_o) level and, hence, to be unable to escape from the corona;

and cyclotron emission would produce em-waves of extraordinary sense, rather than ordinary sense of polarization, as observed. Recent attempts to provide sufficient flux from cyclotron emission (by amplification of the resulting em-waves) and transformation to ordinary polarization (by mode coupling) have been made by Fund and Yip (1966a, 1966b) and Molliwo (1970), respectively. Yip (1970) has found, however, that mildly relativistic electron streams (required by the Fung and Yip model) are more prone to the excitation of plasma waves than the generation of low harmonic normal cyclotron radiation.

Plasma hypothesis interpretations for drift pairs have been proposed by Roberts (1958) and Zheleznyakov (1965); for decimeter fast drift bursts by Young, et al. (1961) and Zaitsev (1967); and herring-bone structure by Wild (1969).

C. Applications to Spike Bursts

Elgarøy and Eckhoff (1966) apply Takakura's (1963) type I burst model to spike bursts, equating burst duration to deflection time. To explain spike burst durations they require a reduction of $\sim$ 20% in the stream velocities necessary to explain type I burst durations. Such a decrease of stream velocities could be due to a decrease of local magnetic field if Takakura's acceleration mechanism is involved. This interpretation is supported by observations of an event in which normal type I bursts appeared to evolve continuously into spike bursts and then back into type I bursts.

Malville, et al. (1967), found the distribution of stream speeds necessary to explain their observed distribution of 345 MHz spike burst

durations assuming the duration was determined by stream deflection. The resulting stream speed distribution was very narrow, $\sim 1.1 - 2.1 \times 10^9$ km/sec, though it should be noted that their observations were limited to 46 minutes during one type IV event. Assuming next that the observed distribution of decay times at 345 MHz and 230 MHz were due to collisional damping of plasma waves, temperatures of $\sim 2.9 \times 10^6$°K (345 MHz) and $\sim 2.4 \times 10^6$°K (230 MHz) were determined. The distribution of calculated temperatures agreed favorably with optical measurements. Malville, et al., note that if collisional damping determines the decay rate, the particle velocity cannot be as low as those suggested by Takakura's theory. At velocities so close to the electron thermal velocity, Landau damping procedes very rapidly. Only at velocities above $\sim 4 \times 10^9$cm/sec is the Landau damping time longer than the observed decay time of 5×10^{-2} second. On the other hand, if the observed cut-off of type III burst velocities near 0.2 c is set by the mean free path of electron streams in the corona, the particle streams responsible for spike bursts cannot have velocities $> 6 \times 10^9$cm/sec and still produce narrow-band phenomena.

If spike bursts were due to amplification of cyclotron radiation, Malville, et al., conclude the amplification would take place in a stream of $\sim 1.6 \times 10^9$cm/sec imposed between the observer and a source of emission of longer duration.

CHAPTER 3. INSTRUMENTATION

A. Recording

The observations described in this study were recorded in the spring, summer, and fall of 1967 and 1968 with the meter wavelength, swept-frequency, high-time-resolution (HTR) Radiospectrograph of the Chena Valley Radio Facility (CVRF) of the Geophysical Institute.

The operation of a swept-frequency radiospectrograph is portrayed in figure 3.1 (from Wild, et al., 1954, in Tandberg-Hansen, 1967) and is described by Wild, et al. (1954) and Thompson (1961a). A tunable receiver is swept through a given frequency range, registering the spectrum of the receiver input as an intensity-modulated oscilloscope trace. An image of the oscilloscope trace is focused onto film as a line perpendicular to the direction of motion of the film. As the receiver sweep repeats at a fixed rate and the film moves continuously at a fixed rate, the spectrum of the input is recorded as a function of time, namely, the "dynamic spectrum" of the input is recorded on the film.

Figure 3.2. (after Philip, 1968b) is a block diagram of the HTR Radiospectrograph.

The CVRF 61' dish was used as antenna with a tapered helix feed built for operation from 100-400 MHz. The dish has an optimum beam width of 7-4° over the frequency range used in these observations, ∿ 140-250 MHz. Observed quiet sun flux, to be discussed later, indicated that the dish-feed combination had an aperture-efficiency of ∿ 25%.

During spring and summer, the dish can track the sun in hour

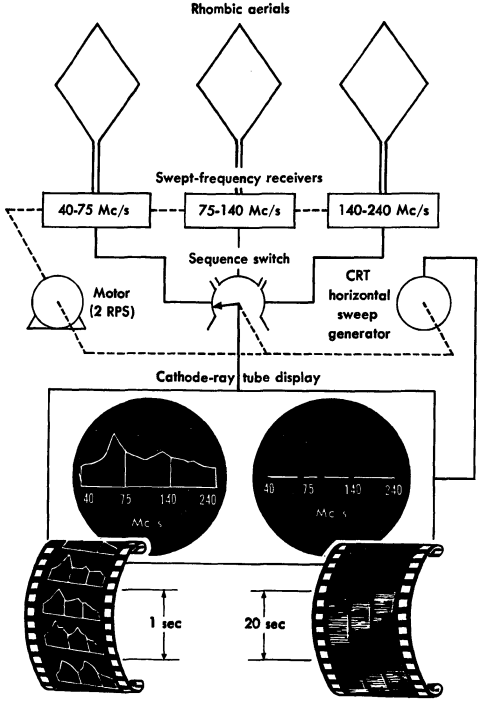

Fig. 3.1. Diagram of a radiospectrograph (from Wild, et al.,1954).

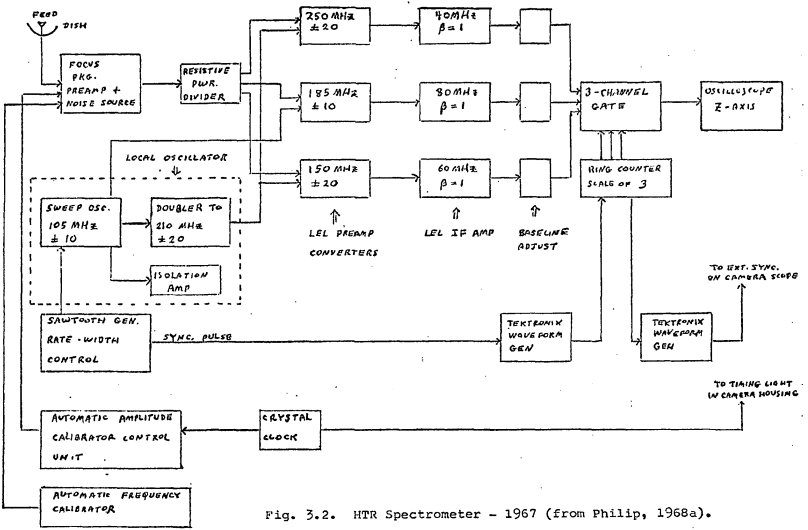

Fig. 3.2. HTR Spectrometer - 1967 (from Philip, 1968a).

angle at a preset declination. While observations were being made during this period, the dish tracked continuously, was automatically recycled at midnight, and was corrected in both declination and hour angle approximately daily. During fall, the dish could track the sun only in the azimuth-elevation mode. In fall, the dish was operated only when an observer was present; azimuth and elevation were corrected approximately hourly, using a calculated track of the sun. In all observations, tracking corrections were intended to keep the sun within 1° of the center of the beam. Wind-load, flexibility, and lack of balance of the mount may have caused additional tracking error of 1-2°.

The frequent, often very brief, power failures that plagued the CVRF were monitored by a latching relay. Various pieces of equipment were reset and any necessary tracking corrections were made after each power failure.

Three swept-frequency receivers were used, covering the bands 255-235 MHz (band A), 190-180 MHz (band B), and 155-135 MHz (band C). Shifts of a few MHz, up or down, were made in these bands in the course of this study. The receivers were swept synchronously with the same local oscillator, at a sweep (recurrence) rate of ∿ 290 Hz for 1967 observations and ∿ 580 Hz for 1968 observations. A ring-counter stepped through the three receiver outputs, displaying them in order ABC in one intensity modulated oscilloscope trace. A portion of band C was sacrificed to allow time for the return sweep of the data oscilloscope. By this means the sweep (recurrence) rates of the recorded data were one-third of the receiver sweep (recurrence) rates, or ∿ 95 Hz for 1967, ∿ 190 Hz for 1968. The proper triggering of the data oscilloscope (at these rates) was determined by simultaneously monitoring the data oscillo-

scope horizontal sweep (sawtooth) and an amplitude-modulated representation of the data signal on a dual-channel oscilloscope. Several equipment malfunctions were quickly detected by this means. The monitor also indicated the level and nature of solar activity to the observer.

During periods of high solar activity the high-speed (HS) camera was operated by the observer. The HS camera recorded the data oscilloscope on 16 mm film with continuous film transport at 30.6 cm/min. A second 16 mm camera, the low speed (LS) camera, with continuous film transport at 36.4 cm/hr, recorded the data oscilloscope trace at all times. To assure proper exposure of the film, the intensity of the data oscilloscope trace was frequently measured by temporarily placing a photocell directly in front of the trace and the trace intensity corrected, if necessary. The last foot of each roll of film exposed was immediately developed as a check on the proper operation of the entire system.

As we were able to resolve (by microscope) the individual data oscilloscope traces in the film record, our time-resolution was ~ 0.01 second and ~ 0.005 second for 1967 and 1968, respectively.

Our frequency resolution was the bandwidth of the i.f. sections of the receivers, 1 MHz.

A receiver sampling a bandwidth β of noise for a time interval τ has an approximate minimum detectable relative noise fluctuation (intensity-resolution) of

$$\frac{\Delta T}{T} = \frac{1}{\sqrt{\beta\tau}} ,$$

where T is antenna temperature. To be detectable, a change in T must be greater than ΔT, the fluctuations encountered in measuring T. The above values of receiver band-widths, sweep-rates, and frequency ranges, yield values of $\Delta T/T$ ranging from $\sim$ 0.05 (band B, 1967) to $\sim$ 0.1 (bands A and C, 1968), or from $\sim$ 0.2 db to $\sim$ 0.4 db. The noise level of the system was not measured; the effective antenna temperature of both the system and the sky was much less than the antenna temperature of the quiet sun.

The intensity of the signal was calibrated by occasionally switching from the feed to a type 5722 noise diode and running an automatic sequence of servo-controlled plate currents through the diode. The sequence was performed in $\sim$ 13 seconds for a HS calibration or $\sim$ 50 seconds for a LS calibration. The LS calibration could not be initiated while the HS camera was operating. The resulting film density steps correspond to antenna temperatures of approximately 1600°K, 3000°K, 5700°K, 11200°K, 22100°K (Kraus, 1966). Comparison of the observed quiet sun value (1600-3000°K) with 200 MHz flux measurements given in AFCRL Geophysics and Space Data Bulletin indicate an aperture efficiency of $\sim$ 25%. Assuming 25% aperture efficiency, the calibration steps correspond to flux values of approximately 4, 7, 13, 26, and 52 in units of 10^{-22} watts m^{-2} Hz^{-1}. Climatic temperature variations of the focus package, housing the noise diode, should produce variations in the above values of about $\pm$ 10% over an observing season, about $\pm$ 5% over the course of a day. It is uncertain how much the temperature, hence the output, of the noise diode was increased by heat from its own filament in its small compartment in the focus package during either of the calibration sequences. Uncertainty in aperture efficience would produce only a systematic error in the above flux equiv-

alents of the calibration steps.

The effective dynamic range was limited, by the characteristics of the phosphor on the cathode ray tube used in the data oscilloscope, to about 15 dB above the quiet sun during normal operation. For strong solar activity the signal was attenuated by a step attenuator placed between the preamp and the receivers. As the noise diode and feed preceded the preamp, this measure did not affect the intensity calibration.

The low aperture-efficiency determined above may be due to defocusing of the feed and incomplete illumination of the dish by the feed. The feed was intentionally defocused, presumably to improve frequency-response. The large-diameter, 100 MHz, end of the feed is situated at the focus of the dish, placing the 400 MHz end $\sim 5'$ inside the focus. The system is farther out of focus as the frequency increases above 100 MHz. Thus the aperture-efficiency decreases as frequency increases above 100 MHz. The beamwidth of the tapered-helix feed is unknown, but very likely less than the $>120°$ necessary to illuminate the entire dish.

After 29 July 1967, frequency calibration of the signal was achieved by automatically switching from the feed to a 5 MHz marker source for at least one data oscilloscope sweep every two seconds. Before this date, a signal generator was fed directly into the receivers to mark certain frequencies at the beginning and end of each roll of film.

Time was indicated on the film by placing a very small lamp adjacent to the data oscilloscope trace. The lamp was pulsed by the

Serial Coded Decimal Time (SCDT) signals provided by the Geophysical Institute. The lamp was controlled by a Sprengnether oven-controlled, crystal clock, modified to provide minute and hour pulses whenever the SCDT system was not operating or when only LS data was being taken.

B. Data

The resulting data format is shown in figures 5.2 & 6.1. We will now discuss various effects which may interfere with the interpretation of the data.

The most obvious effects are the frequency-nonlinearity across each band and the gain variation across all three bands. Figure 3.3. is a print of a recording of 1, 5, and 10 MHz markers. Note the compressed frequency scale toward the high-frequency edge of each band. This nonlinearity is due to the response of the local oscillator (l.o.) to the (Varactor) voltage sawtooth controlling the frequency of the l.o., i.e., causing it to sweep through a given frequency range. Namely, the l.o. did not have a linear response to its controlling voltage. This effect was reduced somewhat by curving the varactor sawtooth.

The character of the gain variation across all three bands is shown in figure 3.4, which is prepared from a microdensitometer trace made along the frequency axis (i.e., across the film) during a calibration step. The largest grain variation is across band B. The band B gain variation produces the curious effect shown in figure 3.5.a., in which a type III burst appears to start at the low-frequency edge of band B before starting at the high-frequency edge. This effect has been largely

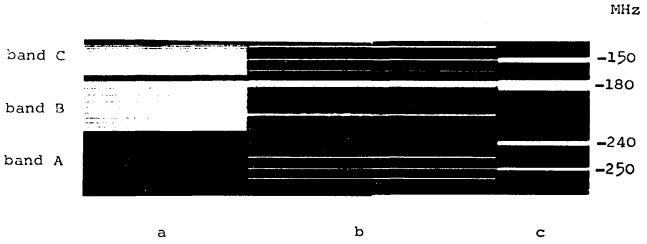

Fig. 3.2. Nonlinearity of frequency scale; 1 MHz markers (a), 5 MHz markers (b), 10 MHz markers (c).

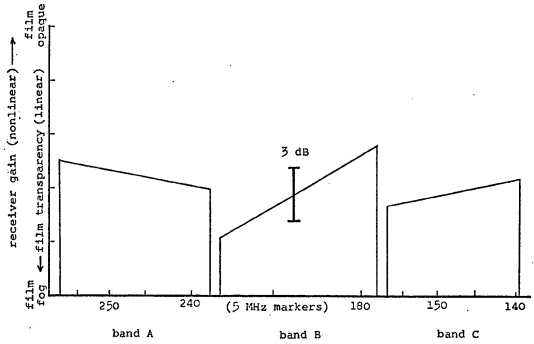

Fig. 3.4. Variation of gain with frequency; prepared from densitometer trace along frequency axis; antenna temperature = 3000°K.

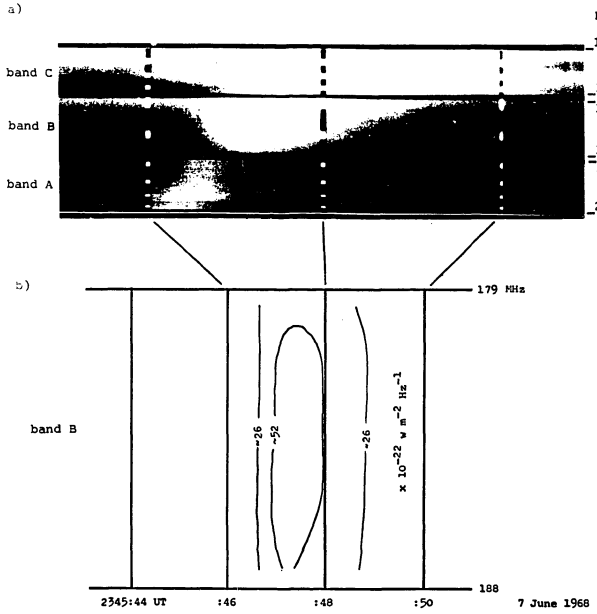

Fig. 3.5. a) Effect of band B gain-variation on type III burst. b) Equal-intensity contours prepared from densitometer traces.

corrected in figure 3.5.b. by drawing contours of equal signal intensity, obtained by comparing microdensitometer traces of the burst with traces of the calibration steps made at the same frequency.

A further problem with the film is the appearance of the return sweep of a band. The return portion of the Varactor sawtooth caused the l.o., hence, all bands, to sweep backwards through their normal frequency ranges. If displayed on the film, this return sweep would appear as a miniature mirror-image of each band along its low-frequency edge. The ring-counter normally switched away from each band before the return sweep occurred. This effect, an example of which is shown in band B in figure 5.7.b.iii., was observed very rarely.

Another instrumental effect appearing in the data, also occuring only rarely, is the appearance of spurious responses on bands A and B to a strong signal on band C. This effect appears to be due to the following mechanism. As a strong signal is being swept through on band C, the i.f. of that band is briefly enhanced and harmonics of the i.f. may be produced. A strong signal at $\sim$ 140 MHz in band C would produce harmonics of the 60 MHz band C i.f. at the same time that the receiving frequencies of the other bands are being swept through 180 MHz and 240 MHz. There is very little isolation between the input stages of the three receivers. Bands A and B appear to be receiving harmonics of the band C i.f. Though the observed effect is easily reproduced with a signal generator, it appears to occur in the data very rarely, only when very strong, carriers existed at $\sim$ 140 MHz. A different type of spurious response is shown in figure 3.6.a. The 142 MHz carrier in band C exhibits a faint superimposed

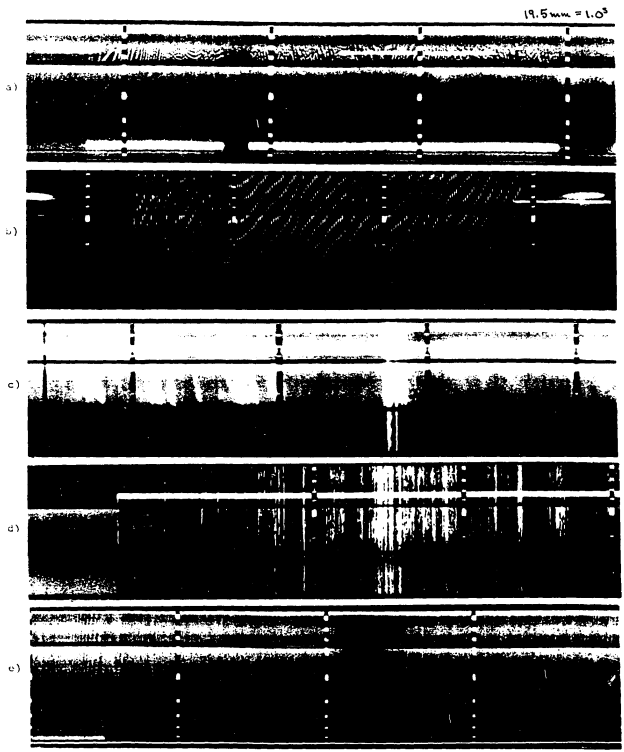

Fig. 3.6. Interference: a) moiré pattern produced by modulation of carrier on band A, with spurious responces on band B and C. b) moiré pattern produced by periodic interference(eg., ignition). c) lightning. d) noisy connector or diode switch. e) moiré pattern produced by 60-cycle hum.

moiré pattern, presumably due to its own modulation. The intermittent 250 MHz carrier in band A exhibits a pronounced moiré pattern (in absorption) with simultaneous identical moiré patterns (in emission) on bands B and C. This interference may be due to the 108 MHz frequency difference of the two carriers (which must both be present) which is equal to the frequency of the local oscillator at the time (in the l.o. sweep) that the band A carrier and the band B and C moiré patterns are being recorded.

Man-made r.f. interference ranged from the ever present carrier signals, to ignition noise (figure 3.6.b.), and an occasional bad connector (figure 3.6.d.). Natural r.f. interference was produced by lightning (figure 3.6.c.).

Upon increasing the data oscilloscope sweep rate to $\sim$ 180 Hz for 1968 observations, 60-cycle-hum was found to produce moiré patterns in the film background (figure 3.6.e.). This effect was countered by introducing out-of-phase hum in the data oscilloscope.

Film speed variations simulated the occurrence of very short duration bursts on the film (figure 5.9.b.iii. & 5.10.d.). Film speed variations may be identified by their simultaneous occurrence on all bands. The film speed was determined by a synchronous motor. Small-scale ($\sim$ 0.01 sec.) film-speed variations were produced by fluctuations in the take-up tension. Of the several attempts to keep the take-up tension constant, the most successful involved driving the take-up reel, with a second synchronous motor, through a teflon-to-steel slip-clutch.

The most dramatic effect interfering with observations of the sun was ionospheric scintillation (figure 3.7.). Such activity was identified as ionospheric scintillation because:

1) it resembles the radio-star scintillation dynamic spectra reported by Wild and Roberts (1956; figure 3.8;
2) sources of solar radio emission have angular dimensions of $\sim$ 1-3' arc, comparable with radio stars (see, for example, Daigne, 1968; Le Squeren - Malinge, 1963; Gnezdilov, 1970);
3) it occurred predominantly at $\leq$ 0600 or $\geq$ 1800 local time, hence, at elevations $\leq \sim 20°$, and during periods of enhanced solar activity - both features are charactistic of radio star scintillation; and
4) it resembles solar radio emission spectral structure attributed to ionospheric scintillation by Rabben, 1962.

Its interpretation as the passage of the sun through lobes of a Lloyd's-mirror ground effect is precluded by the following:

1) the lobe separation for the dish-image system is $\sim 3°$;
2) the rate of change of elevation of the sun at $\sim$0600 or 1800 local time was $\sim$ 6' per minute (July);
3) the period of the observed background pulsations ranged from < 1 second to $\sim$ 2 minutes; and
4) the effect was not observed with the quiet sun, even though the fringe separation is greater than the diameter of the quiet sun.

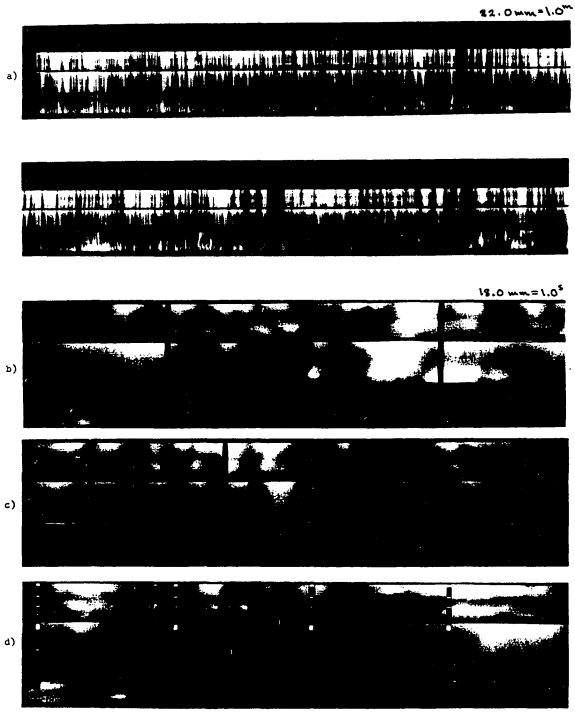

Fig. 3.7. Scintillation. a) 8-16-68, 1606-1619 UT. (LS film). b) 8-16-68, 1606:18 UT. c) 8-16-68, 1606:45 UT. d) 8-16-68, 1619:26 UT.

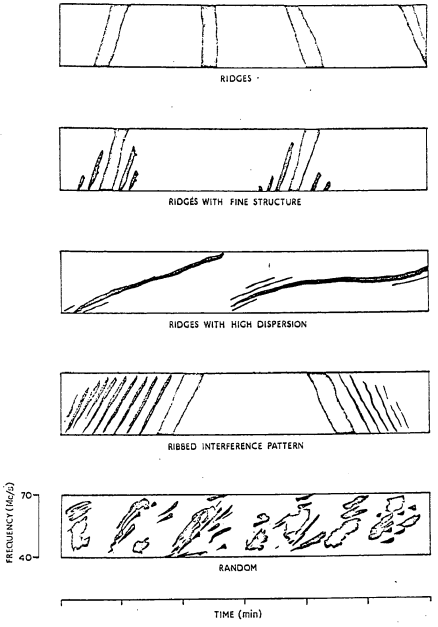

Fig. 3.8. Sketches showing idealized examples of the principal types of dynamic spectra of radio-star scintillation observed (from Wild and Roberts, 1956).

CHAPTER 4. SPIKE BURST MORPHOLOGY

We are interested in developing a scheme for classifying spike bursts. As seen in Chapter I, there is variety in the bursts referred to as spike or flash bursts. As a working definition, which encompasses the variety of bursts described in Chapter I, we require simply that $d_f \lesssim 0.1$ second. The following classification scheme was developed from those bursts observed with the HTR Radiospectrograph which thus qualified as spike bursts.

A. Burst Classification

The dynamic spectra of short duration, limited frequency range bursts may be specified by the set of parameters

$$(d_o, b_o, d_f, b_+, \dot{f})$$

defined in figure I.1. We specify that spike bursts have $d_f \lesssim 0.1$ second, and assume no natural divisions of spike bursts according to values of d_f. We note that, of the parameters d_o, b_o, $\dot{f}$, one may be eliminated by the approximate relation

$$b_o = \dot{f}\, d_o$$

leaving the choices

$$(d_o, b_+, \dot{f}), (b_o, b_+, \dot{f}), (b_o, b_+, d_o).$$

We prefer the second alternative because b_o is more readily determined than d_o, and because $\dot{f}$ can be determined for a burst which is only partially observed. For most bursts of high $\dot{f}$, b_+ is very difficult to determine; omitting b_+, we are left with the parameters

$$(b_o, \dot{f})$$

with which to differentiate between two given spike bursts. We shall base our classification scheme on $\dot{f}$, as employed in the schemes of

Wild (1950) for all meter wavelength bursts, and Elgarøy (1961) for type I bursts. We divide spike bursts into

1) fast drift (fd-) spike bursts, with $|\dot{f}| \geq 100$ MHz/sec;

2) medium drift (md-) spike bursts, with $|\dot{f}| < 100$ MHz/sec; and

3) simple (s-) spike bursts, with $d_f \lesssim 0.1$ second, $b_o \sim b_f \sim 1$ MHz (limit of frequency resolution), and no detectable drift.

Several examples of fd- spike bursts are shown in figure 4.1. This classification includes the spike (flash) bursts of Philip (1968), Elgarøy, Eckhoff, and de Groot (see Chapter 1). The observed range of b_o extends from the minimum necessary to detect frequency drift ($\sim$3 MHz) to the maximum measurable in any one band of the observing range ($\sim$20 MHz). Spike bursts extending from one band to another are extremely rare. Most of the "large b_o" spike bursts observed are shown in figures 5.11a, 5.11b, 7.1, and 7.2. Contributing to the small number of large b_o spike bursts observed may be the tendency of spike bursts to occur at the higher frequencies monitored (see Table 4.1) and the greater gap between bands A and B ($\sim$50 MHz) than between bands B and C ($\sim$20 MHz).

Several examples of md- spike bursts are shown in figure 4.2. This classification includes the bursts of Philip (1969) and Markeev and Chernov given in Chapter 1. The observed range of b_o is again limited on the low side by the requirement of detectable frequency drift. Very few md- spike bursts are seen to cross an entire observing band and none are seen to extend from one band into another (with the possible exception of the bursts shown in figure 7.1, which are on the borderline between md- and fd- spike bursts.

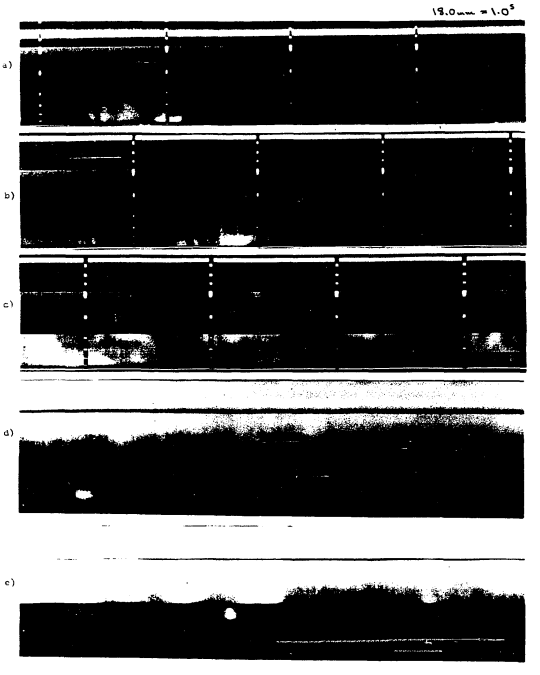

Fig. 4.1. fd-spike bursts: a) 6-20-68, 2231:09 UT. b) 6-20-68, 1920:08 UT. c) 6-20-68, 1840:30 UT. d) 7-24-67, 2332:00 UT. e) 7-24-67, 2356:24 UT.

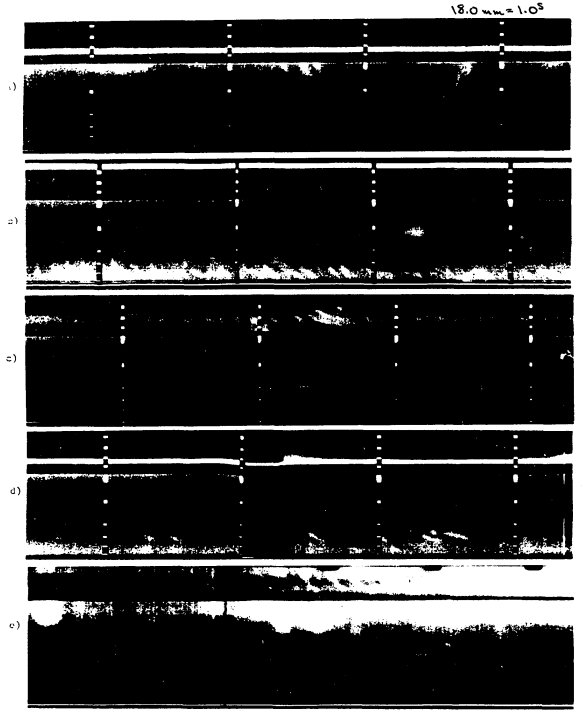

Fig. 4.2. md-spike bursts: a) 7-18-68, 0037:25 UT. b)6-20-68, 1846:48 UT. c) 6-24-68, 0305:41 UT. d) 8-17-68, 0033:20 UT. e) 7-24-67, 1432:29 UT.

Figure 4.3 gives several examples of s- spike bursts. These bursts appear to resemble the "knots" reported by Elgarøy (1961), the "blots" reported by Elgarøy and Rødberg (1964), and the "bright spots" reported by de Groot (1970). They are also included in the spike bursts reported by Philip (1969).

The above classifications are useful because of the quite distinct appearance of "typical" bursts of each classification. However, it appears very likely that there is a continuous variation of $\dot{f}$ between md- and fd- spike bursts, and a continuous variation of b_o between s- spike bursts and md- and fd- spike bursts.

The relative frequency of occurrence of fd-, md-, and s- spike bursts is indicated approximately by table 4.1. Table 4.1 contains all spike burst events recorded in the data scanning log. The events are broken down into the band in which the event occurred and the type of spike burst involved. Each event may contain one or several spike bursts. A small percentage of the events included as fd- spike burst events, may be composed of md- or s- spike bursts but were not designated as such in the log. The enhanced number of spike bursts reported on band B may be due to both the greater sensitivity (lower detectable $\Delta T/T$, see Chapter 3) of the band B system, and expanded frequency scale of band B, in comparison to bands A and C. However, there still appears to be a strong tendency for more fd- spike bursts to occur than other types, and for spike bursts to occur at higher frequencies. The events in table 4.1 occurred in the ~375 hours of high-speed data, being the most active portions of ~2000 hours of monitoring the sun.

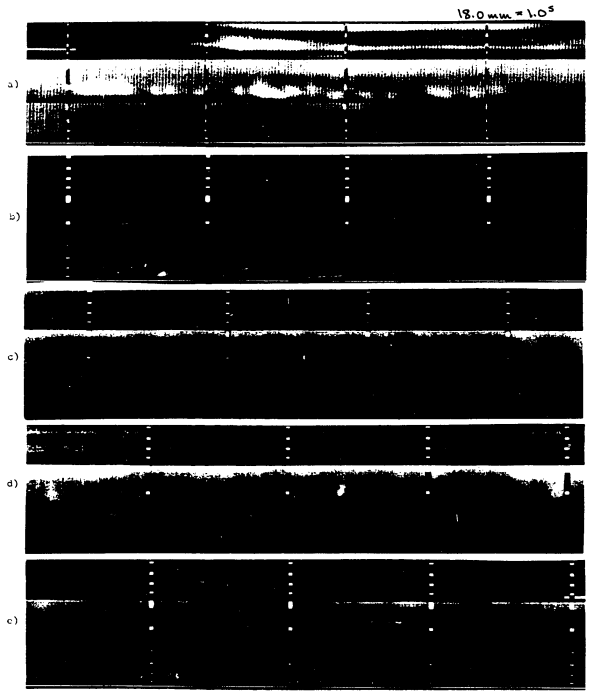

Fig. 1.3. s-spike bursts: a)7-24-67, 2201:37 UT.
b) 7-14-68, 1651:25 UT. c) 6-17-68, 0313:55 UT. d) 7-11-68, 1644:18 UT.
e) 7-17-68, 2101:43 UT.

Table 4.1

			Spike Bursts			
			fd-	md-	s-	Total
band	A	255-235 MHz	307	2	61	370
	B	190-180 MHz	760	8	27	795
	C	155-135 MHz	133	7	25	165
Total			1200	17	113	

B. Groups of Spike Bursts

Spike bursts are observed to occur either singly, in small groups of ∿2-4 bursts, in short complex groups lasting ∿2-4 seconds (termed "sprays") and in large groups lasting up to several minutes (termed "storms"). In figure 4.4, we have examples of sprays (a., b.) and storms (c.). Spike bursts also appear to occur as a semi-continuous, diffuse background, termed "spike burst background" (figure 4.4.d).

Spike bursts have a tendency to occur in groups of similar bursts with somewhat regular recurrence (de Groot, 1966, 1970) which is apparent in several examples in figures 4.1 - 4.4. A most dramatic example of this tendency is shown in the quasi-periodic spike bursts (figures 4.4.e, 4.4.f) reported by Philip (1968) (see Chapter 1). Prints of the quasi-periodic spike bursts and the parallel drifting structure observed in conjunction with them are presented in Chapter 6.

CHAPTER 5. SPIKE BURST-TYPE III BURST ASSOCIATION

We shall now examine observations made with the HTR Radiospectrograph which give evidence of a close association between spike bursts and type III bursts. Three classes of associations will be presented. These observations support the plasma hypothesis (type III burst mechanism) interpretation of spike bursts and suggest a morphological continuity between spike bursts and type III bursts. The possibility of generating spike bursts by the same mechanism thought to produce type III bursts is discussed in section B.

A. Observations

In figure 5.1. we have several examples of type III bursts as they appear in the HTR Radiospectrograph records. Examples include an isolated type III burst (figure 5.1.a.); a small group of type III bursts, which we will denote IIIg (<10 bursts; figure 5.1.b.); and a large group of type III bursts, which we will denote IIIG (>10 bursts; figure 5.1.c.).

Figure 5.2. shows several events, reported by Philip (1969), in which the HTR Radiospectrograph showed spike bursts occuring within a sharply defined time interval which matched the period that would have shown type III activity had the starting frequency of the type III bursts been high enough to register on band A.

Additional HTR Radiospectrograph observations of such events are shown in figure 5.3. Figure 5.4 shows what may be a similar event in the HTR multichannel observations reported by de Groot (1966). Figure 5.5. shows what appears to be a further example of a similar event in the HTR 60-channel radiospectrograph observations reported by deGroot (1970).

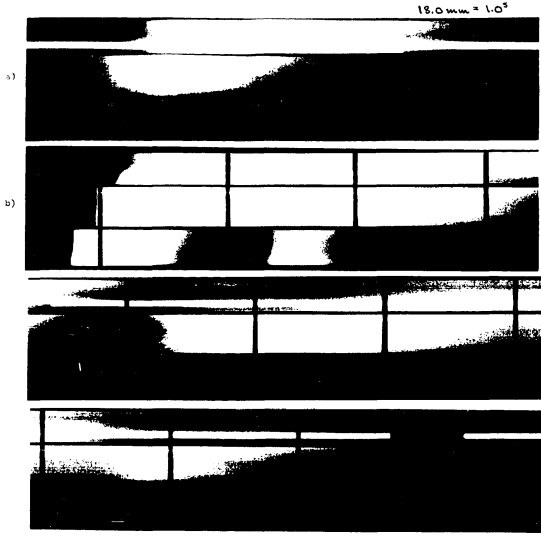

Fig. 5.1(a-b) Type III bursts: a) 8-2-67, 0240:51 UT.
b) 8-12-68, 2049:00 UT.

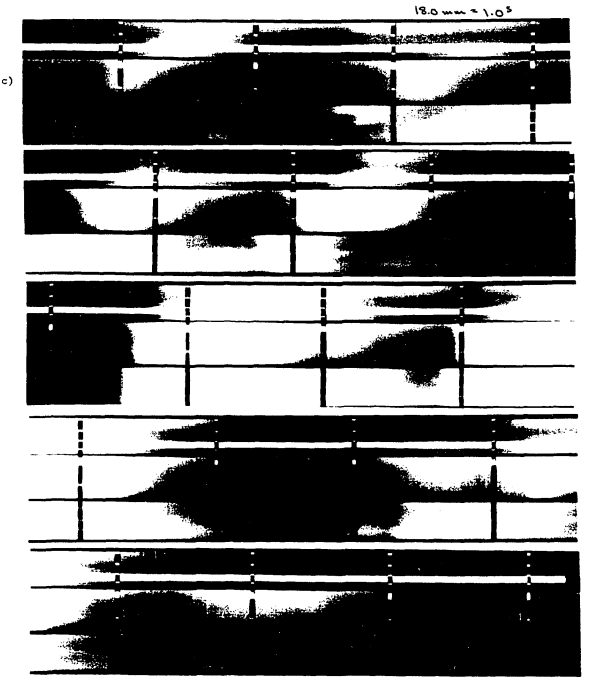

Fig. 5.1c. Type III bursts: c) 8-13-68, 1826:50 UT.

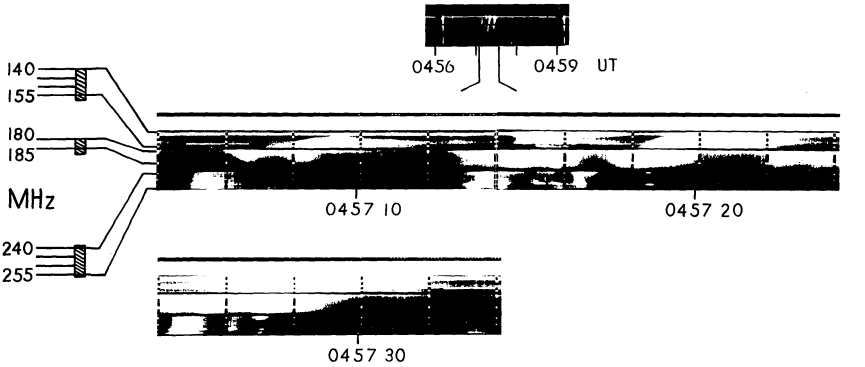

FIG. 5.2.A. SPIKE BURST - TYPE III BURST ASSOCIATION

7 JUNE 1968

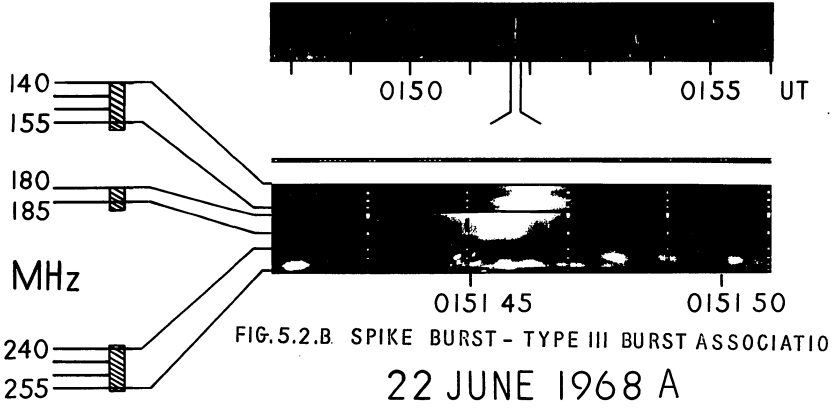

FIG. 5.2.B SPIKE BURST - TYPE III BURST ASSOCIATION

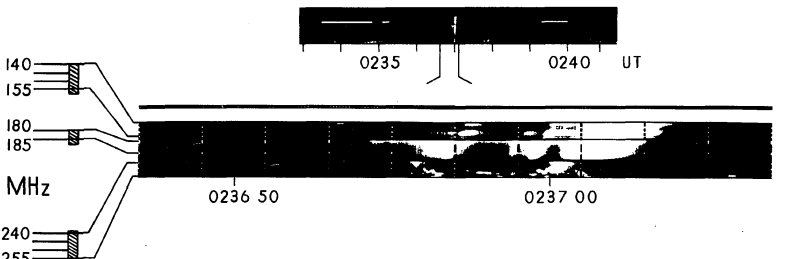

FIG. 5.2.c. SPIKE BURST - TYPE III BURST ASSOCIATION

22 JUNE 1968 B

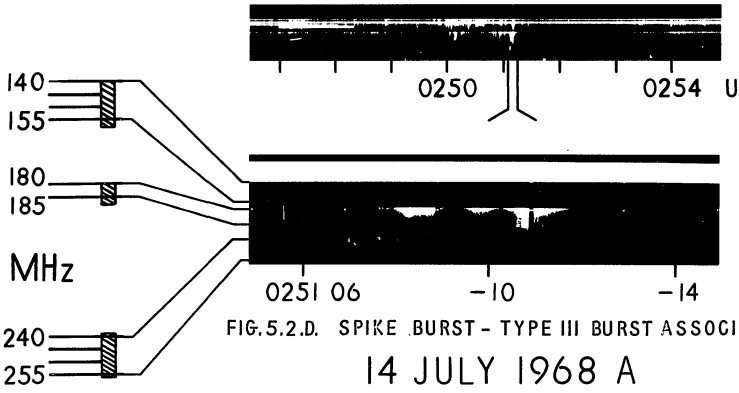

FIG. 5.2.D. SPIKE BURST - TYPE III BURST ASSOCIATION

14 JULY 1968 A

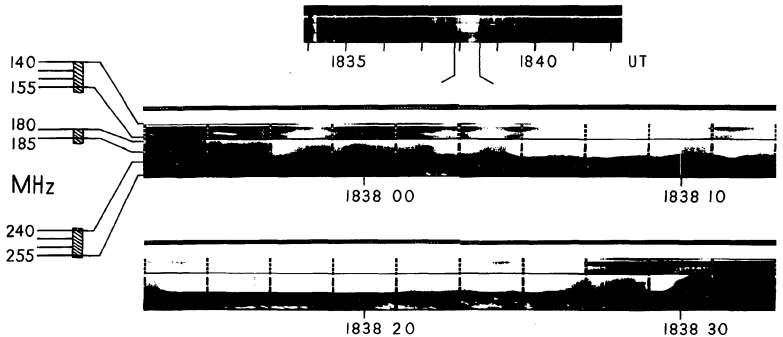

FIG. 5.2.E. SPIKE BURST - TYPE III BURST ASSOCIATION

14 JULY 1968 B

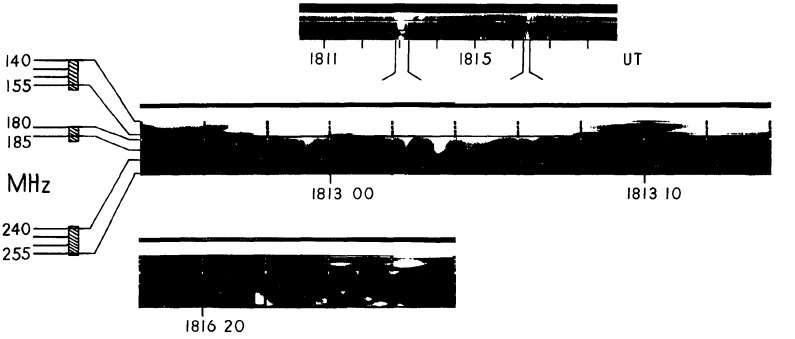

FIG. 5.2.F. SPIKE BURST - TYPE III BURST ASSOCIATION

16 JULY 1968

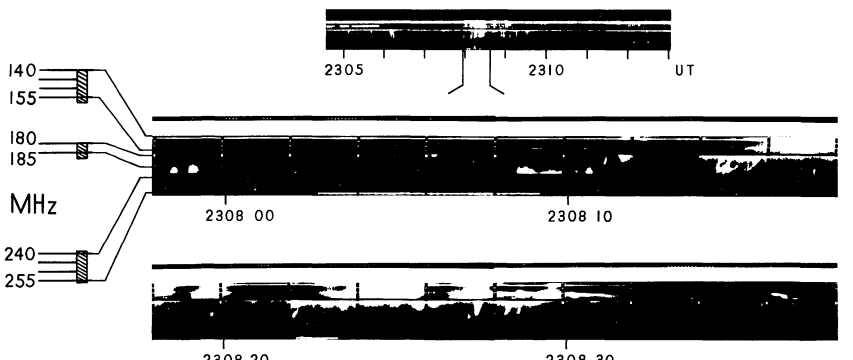

FIG. 5.2.G. SPIKE BURST - TYPE III BURST ASSOCIATION

17 JULY 1968

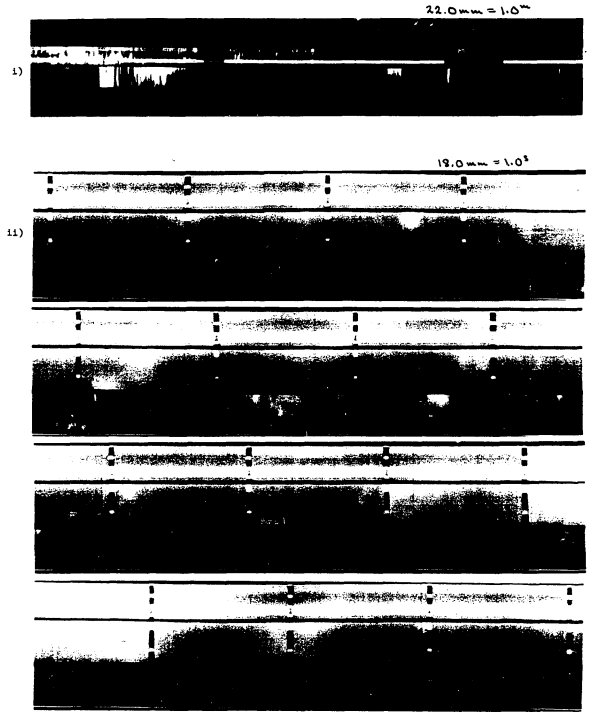

Fig. 5.3a. Spike burst-type III burst association, 9 July 1968: i) 0316-0322 UT. ii) 0318:11 UT.

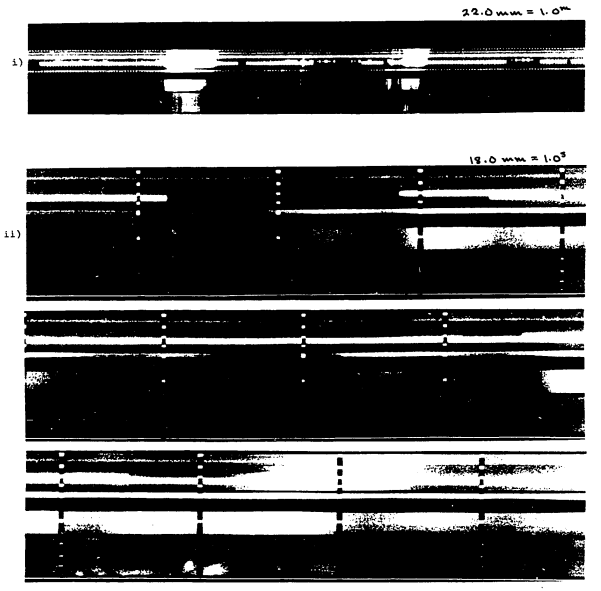

Fig. 5.3b. Spike burst- type III burst association,
18 July 1968 i) 2341-2350 UT. ii) 2347:50 UT.

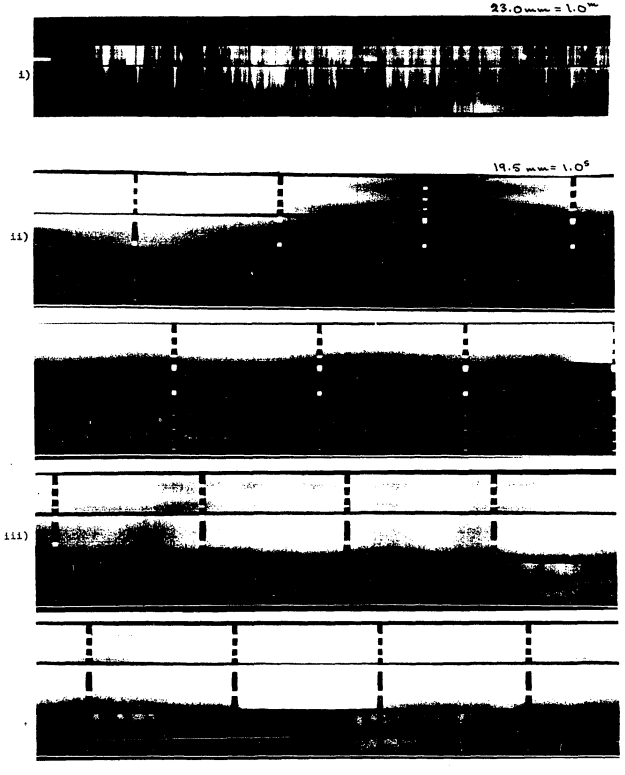

Fig. 5.3c Spike burst-type III burst association, 26 September 1968: i) 0026-0032 UT.(LS film) ii) 0026:47 UT. iii) 0028:18 UT.

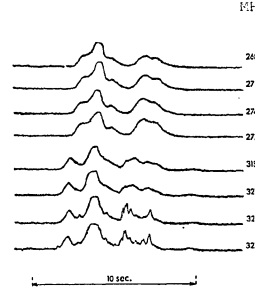

Fig. 5.4. Possible spike burst-type III association. (from deGroot, 1966).

Fig. 5.5. deGroot's "bright spots" and type III bursts, 12-30-68, 1424 UT. (from deGroot, 1970).

The above burst associations appear to involve only s-, and md- spike bursts and to constitute a distinct class of spike burst-type III burst association. These observations suggest that

1) the spike bursts in question were initiated by type III burst exciters, and that
2) the spike bursts originated near the plasma frequency level (since the exciter was passing through the plasma frequency level at the time the spike bursts were emitted).

Thus these observations support a plasma hypothesis (charged particle stream, plasma wave, em-wave) interpretation of s-, and md- spike bursts. Possible exceptions to the trend of the above associations, in which s-, and md- spike bursts occur aligned with type III bursts in the frequency - time plane, at frequencies above those occupied by the type III bursts, are two events reported by Elgarøy and Rødberg (1964) in which several small bursts, resembling our s-, and md- spike bursts, occurred during and after the passage of type III bursts through their observing band. Another exception is the unusual event shown in figure 5.6., in which reverse drift fd-spike bursts appear in band A instead of s-, and md- spike bursts. The event in figure 5.6., given a plasma hypothesis interpretation of spike bursts, suggests the exciters of the type III bursts and spike bursts originated in the corona, between the 240 and 190 MHz plasma frequency levels.

The plasma hypothesis interpretation of fd- spike bursts is supported by observations of a second class of spike burst - type III burst association. Spike bursts occasionally occur interspersed

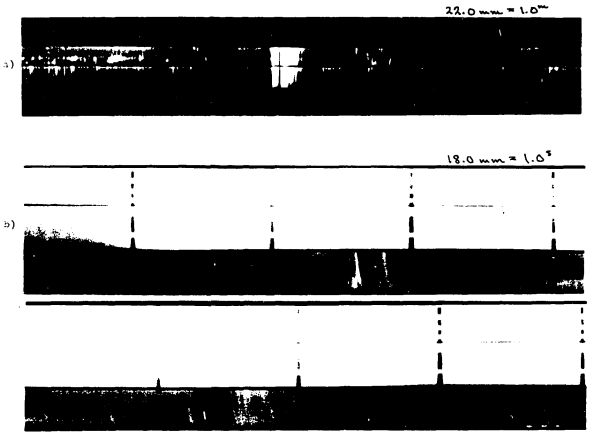

Fig. 5.6. Positive drift fd-spike bursts during type III event 9 July 1968, 0250 UT. a) 0248-0254 UT. (LS film) b) 0250:20 UT.

among the type III bursts of a IIIg or IIIG event (figure 5.7.). T. de Groot (1966) acknowledges the occurrence of such events (figure 5.8.). The occasional appearance of a volley of fd- spike bursts after a single type III burst may be a simpler form of this association (figure 5.9.).

In the same fashion in which we find the above fd- spike bursts interspersed in a IIIg(G) event, we find short-duration type III bursts occurring during IIIg(G) events. Since Elgarøy and Rødberg (1964) reported type III burst durations ranging down to 0.1 second at 200 MHz, it is reasonable to ask whether spike bursts are the short-duration extension of the observed distribution of type III burst durations. It was thus decided to examine the short-duration type III bursts observed with the HTR Radiospectrograph. Figure 5.10. shows many of the shorter-duration type III bursts observed, including some comparisons with simultaneous spectra of the type III events recorded by the Harvard Radio Astronomy Station, Ft. Davis, Texas (courtesy A. Maxwell). Apparent in figure 5.10. is the fortunate distribution of the observing bands of the HTR Radiospectragraph. Previous HTR studies have been largely limited to one band of about 20 MHz frequency range. A type III burst of the kind shown in figure 5.1. is recognizable, on only one band, largely by its long duration and large bandwidth (type I bursts have bandwidths of a few MHz at these frequencies). The use of three spaced bands allows the characteristic negative drift, large frequency range, and increase of duration with decreasing frequency to be observed. Some of the short-duration type III bursts in figure 5.10., if observed only on band B, for example, might not be classified as type III bursts.

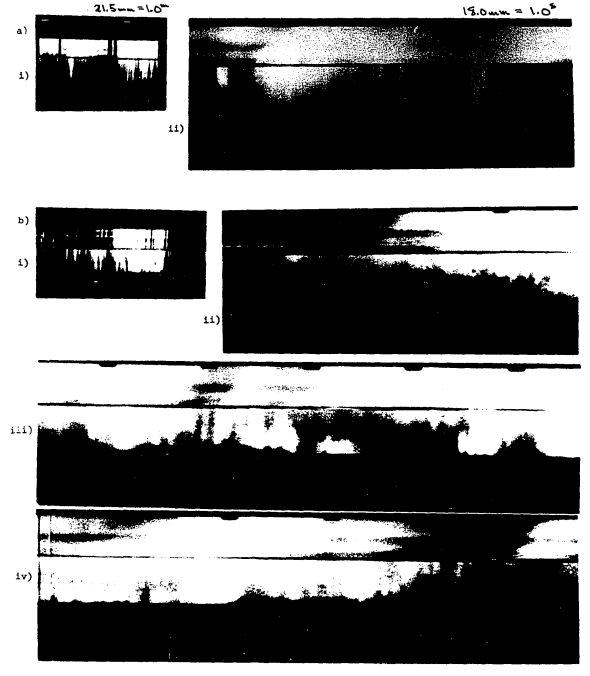

Fig. 5.7. Spike bursts occuring during type III burst events: a-i) 7-26-67, 0748-0750 UT. (LS film). a-ii) 0749:14 UT. b-i) 7-9-67, 1649-1651 UT. (LS film). b-ii) 1649:27 UT. b-iii) 1649:35 UT. b-iv) 1650:02 UT.

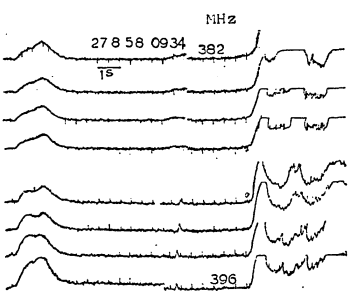

Fig. 5.8. Spike bursts concurrent with type III bursts (from deGroot, 1966).

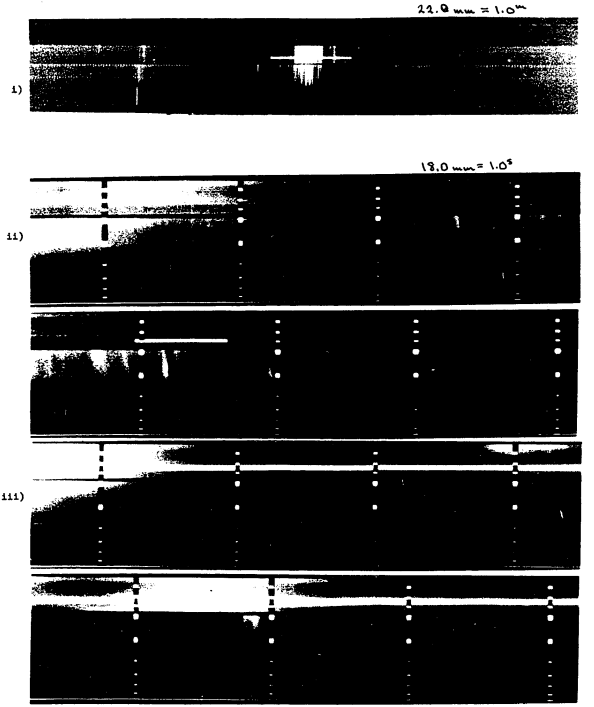

Fig. 5.9a. fd-spike bursts following type III bursts.
17 October 1968. i) 2151-2157 UT. (LS film)
ii) 2152:49 UT. iii) 2155:01 UT.

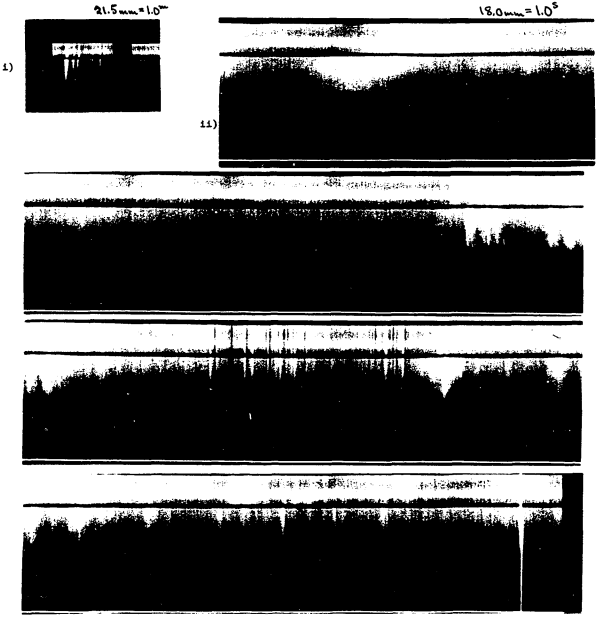

Fig. 5.9b. fd-spike bursts following type III bursts, 27 July 1967. i) 2036-2037 UT. (LS film). ii) 2036:35 UT.

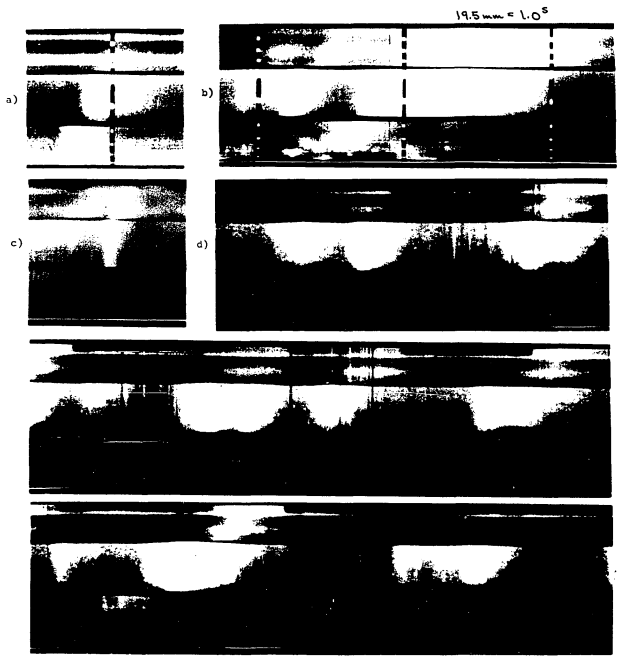

Fig. 5.10(a-d). Short- duration type III bursts: a) 6-21-68, 1659:35 UT. b) 6-22-68, 0236:59 UT. c) 6-20-67, 1540:12 UT. d) 7-9-67, 1338:18 UT.

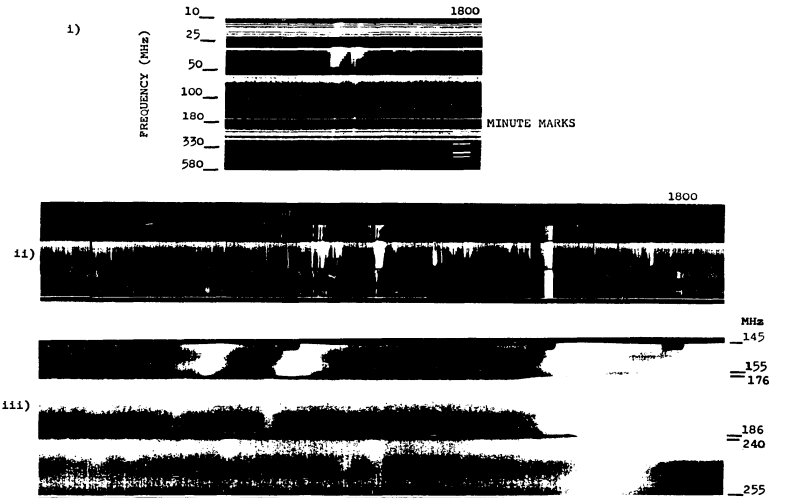

Fig. 5.10e. Short-duration type III bursts, 25 June 1967. i) wide band dynamic spectrum, 1754- 1800 UT. (courtesy A. Maxwell). ii) 1754-1800 UT. (L3 film). iii) 1757:00 UT. (width of sprocket hole represents 0.25 seconds along time axis)

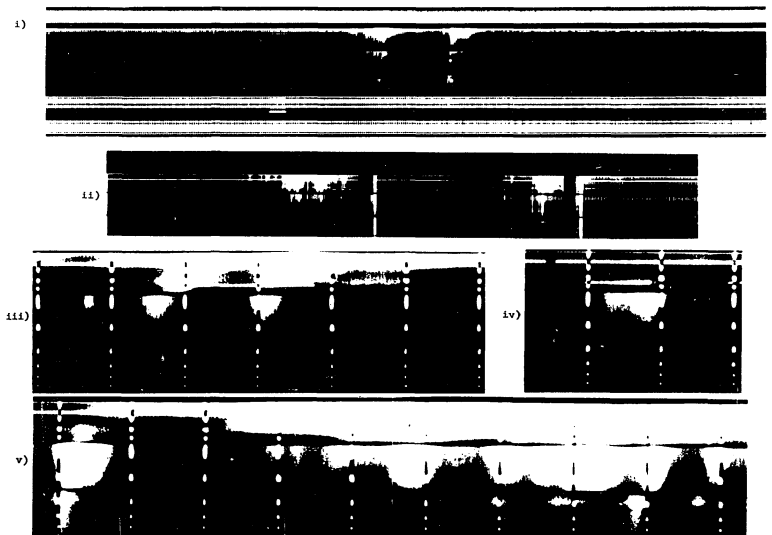

Fig. 5.10f. Short-duration type III bursts, 25 August 1967. i) wide band dynamic spectrum, 1953-2016 UT. (courtesy A. Maxwell); see format, fig. 5.10e. ii) 2001-2007 UT.(LS film). iii) 2003:31 UT. (interval between frequency calibrations is 1.0 second). iv) 2005:23 UT. v) 2005:43 UT.

The band B portions of some of the bursts in figure 5.10. would normally be classified as fd- spike bursts. We thus have the possibility that fd- spike bursts are actually short-duration type III bursts of limited frequency range. As a limited test of this hypothesis, all bursts (not classified as type III bursts) which had been catalogued as appearing on more than one band were examined. Since fd- spike bursts of $\geq$ 20 MHz frequency range occur in the HTR Radiospectrograph records, they might be expected to appear across the 20 MHz gap between bands B and C. If fd- spike bursts and short duration type III bursts are to be distinguished by their dynamic spectra, spike bursts must show a different behavior in the large frequency range limit than that shown by short duration type III bursts. The survey of the above bursts revealed that very few bursts appear to extend from band B to C (or the reverse) and that, with the exception of the two unusual events shown in figures 7.1. and 7.2., all bursts appearing on both bands exhibit the same behavior as shown by the short duration type III bursts (negative drift, increase in duration).

Uncovered in this survey were two storms of (sometimes large b_o) fd-spike bursts which occurred during periods corresponding quite well with type III burst activity on meter- or dekameter- wavelengths reported in the I.A.U. Quarterly Bulletin on Solar Activity. Figures 5.11.a. and 5.11.b. compare these events with the Ft. Davis spectra (courtesy A. Maxwell) recorded simultaneously. While the type III burst activity is quite well developed in the 27 July 1967 event (figure 5.11.a), the 27 June 1968 event contains only very faint activity. We tentatively designate these events as a third class of

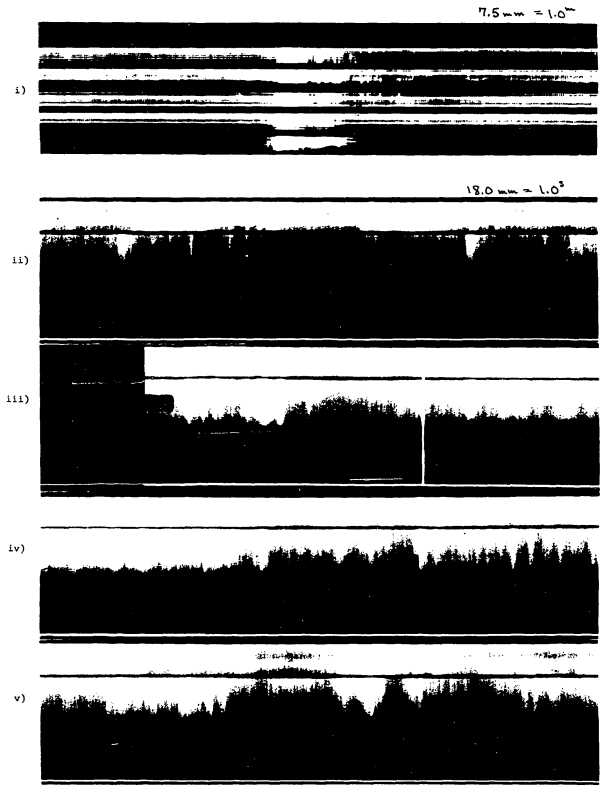

Fig. 5.11a. Large-frequency-range fd-spike bursts during type III burst event, 27 July 1967. i) Wide band dynamic spectrum, 2004-2022 UT. (courtesy A. Maxwell); see format, fig. 5.10e. ii) 2012:58 UT. iii) 2015:28 UT. iv) 2015:54 UT. v) 2015:29 UT.

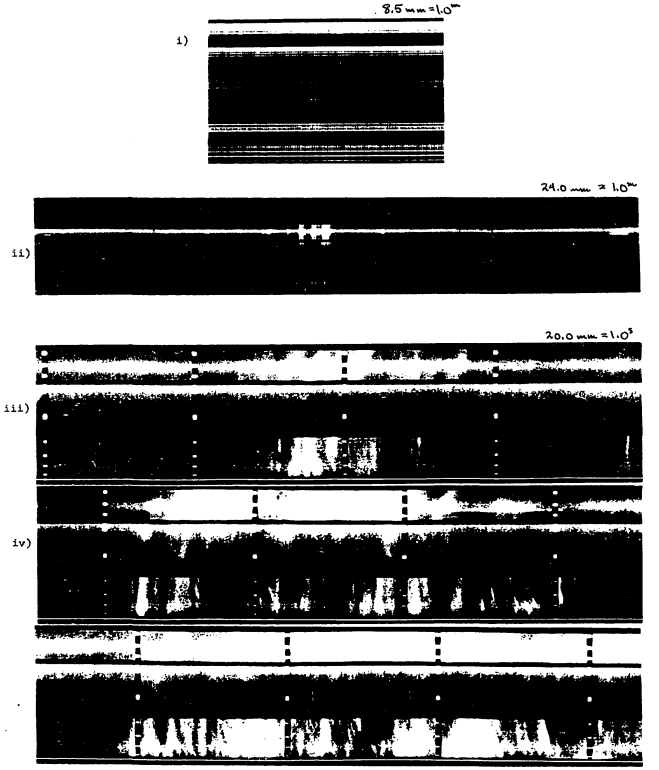

Fig. 5.11b. Short-duration type III bu sts, 27 June 1968.
i) wide-band dynamic spectrum, 0024-0031 UT.
(courtesy A. Maxwell); see format, fig. 5.10e.
ii) 0024-0031 UT.(LS film). iii) 0026:48 UT.
iv) 0026:58 UT.

spike burst - type III burst association

B. Plasma Hypothesis Interpretation of Spike Bursts

We see that spike bursts are occasionally observed as fine structure in type III burst events; that type III bursts exist with durations approaching 0.1 second, the upper limit for spike burst durations; and that spike bursts exist with >50 MHz frequency range and, predominantly, the negative drift and increasing duration characteristic of type III bursts. As shown in figure 2.2, type III bursts with frequency ranges (b_o) as small as 30 MHz are observed. Markeev and Chernov (1971) report observing md- spike bursts with b_o values up to 30 MHz. In the present study fd- spike bursts with b_o > 15 MHz were occasionally observed; but spike bursts bridging the ∿ 20 MHz gap between bands B and C were very rarely observed.

Elgarøy and Rødberg (1964) report a range of type III burst $\dot{f}$ values of -20 MHz/sec to -150 MHz/sec. Drifting spike bursts exhibit $|\dot{f}|$ values ranging from ∿ 10 MHz/sec to >300 MHz/sec.

Both type III bursts and spike bursts tend to occur in sequences of regularly spaced similar bursts, occasionally exhibiting remarkable periodicity.

We thus have an apparent morphological continuity between type III bursts and spike bursts and it is reasonable to ask whether both types of bursts could be produced by the same mechanism. Short-duration type III bursts and large b_o spike bursts are much rarer than normal type III bursts and spike bursts respectively. We conclude that spike bursts cannot simply be the short-duration wing of the distribution of

type III bursts. A model attempting to produce spike bursts and type III bursts from the same mechanism must explain the tendency to produce either spike bursts or type III bursts, with the production of very few intermediate bursts.

In the following, we shall attempt to extend the plasma hypothesis interpretation of type III bursts to produce a model for spike bursts. We assume the observed em-waves are due to scattering of plasma waves excited by the passage of an exciter consisting of a stream of electrons with average streaming speed $\sim \frac{1}{3}$ c. We assume an ambient electron density, N_e, monotonically decreasing with height above the photosphere, with ∇N_e comparable to average values for the corona (at a given N_e, values of ∇N_e vary little between active regions and the quiet corona). The plasma waves excited at a given level in the corona are assumed to fall in a narrow bandwidth of frequencies near the local electron plasma frequency, f_o. Since the magnetic field is generally believed small ($\sim$ 1 - 10 gauss) in the lower corona, oscillation at the upper-hybrid frequency is consistent with this assumption. Em-waves produced by oscillations at the lower-hybrid frequency, if significantly different from f_o, would have considerable difficulty escaping from the corona, since they would be produced beneath the plasma ("critical") frequency level.

We will adopt the interpretation of type III burst duration proposed by Hughes and Harkness (1963). The observed duration, d_f, and band width, b_f, of spike bursts will be shown to require exciters much smaller than are normal for type III bursts. The requirement of producing relatively few intermediate bursts is met if exciters smaller

than a certain critical size decay rapidly, producing bursts of short lifetime (d_o) and small frequency-range (b_o), while exciters larger than that critical size decay relatively slowly, producing bursts of long d_o, which consequently drift over a large b_o. Such a mechanism is discussed in Zheleznyakov and Zaitsev's (1970a) analysis of quasilinear stream relaxation.

In chapter 2 we discussed the interpretation of type III burst durations as due to:

1) the passage of an exciter, through the region emitting a given frequency, in much less time than the total burst duration; then

2) collisional decay of the excited plasma waves in the time

$$t_D \sim \nu_{coll}^{-1} \sim \frac{T^{3/2}}{42\, N_e} \sim \frac{1.92 \times 10^3\, T^{3/2}(10^6 {}^\circ K)}{f^2\ (MHz)} \text{ sec.},$$

where N_e is the electron density of the ambient plasma (electrons/cm^3), and T is the kinetic temperature of the ambient electrons in degrees Kelvin. We thus have $d_f \sim t_D$. Figure 5.12., after Elgarøy and Rødberg (1964) and Hughes and Harkness (1963), shows the temperatures necessary to explain type III burst durations observed by several authors. Optical studies of the undisturbed corona give temperatures of $\sim 1\text{-}2 \times 10^6 {}^\circ K$; the active region corona appears to be $\sim 2 - 3 \times 10^6 {}^\circ K$, with isolated portions reaching temperatures of $\sim 4 - 6 \times 10^6 {}^\circ K$. We have extended the graph to include

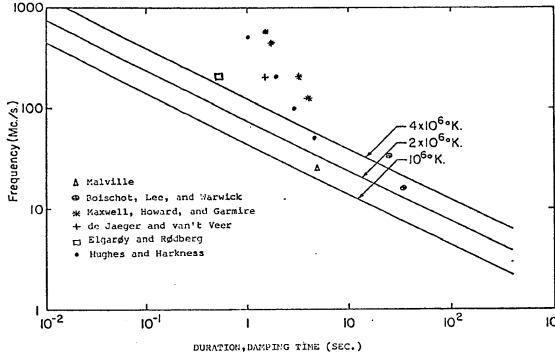

Fig. 5.12. Duration of type III bursts as a function of frequency, after Elgarøy and Rødberg, 1964, and Hughes and Harkness, 1963. The lines give collisional damping times as a function of plasma frequency for various temperatures.

durations characteristic of spike bursts. It appears that spike burst durations may be explained by the above analysis more easily than type III bursts, ie., without requiring such extreme temperatures.

Hughes and Harkness (1963) chose to assume a temperature of $\sim 1 \times 10^6$°K, and that the plasma waves collisionally decayed in the appropriate ν_{coll}^{-1} ($\sim$0.1 second) and that the balance of the type III burst duration was due to the passage of a spatially dispersed exciter through the region emitting the frequency in question. That is, they assumed

1) the plasma waves decay in

$$t_D \sim \nu_{coll}^{-1} \sim \frac{T^{3/2}}{42N_e} \sim \frac{1.92 \times 10^3}{f^2\ (MHz)} \quad \text{sec.},$$

with $T = 1 \times 10^6$°K,

2) the balance of the burst duration represents excitation of the plasma waves by the passage of the exciter.

Figure 5.13., from Huges and Harkness (1963) shows average observed burst durations and calculated decay times. In figure 5.14., from Hughes and Harkness (1963) spatial extent of the exciter, calculated from the balance of the burst duration, is compared with the spatial extent of type III sources as determined by interferometer observations. The vertical extent of Hughes and Harkness' exciter represents a range of (local) plasma frequencies which agrees with the observed instantaneous bandwidth of type III bursts ($\sim$100 MHz at 100 MHz). The spatial dispersion exhibited in figure 5.14. can be interpreted as due to a distribution of electron velocities in the exciter (figure 5.15.) with $\Delta V_s / V_s \sim 1$, where V_s is the mean stream speed and ΔV_s is its dispersion (Smith, 1970a).

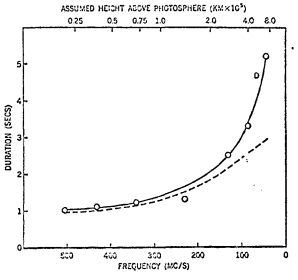

Fig. 5.13. Duration of type III bursts as a function of frequency. Solid line: average measured duration of 90 type III bursts; Dashed line: exciter pulse duration and theoretical damping time (from Hughes and Harkness, 1963).

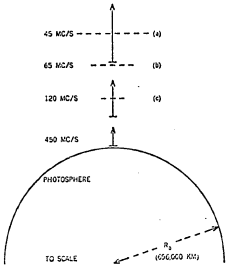

Fig. 5.14. Radial and transverse dimensions of the fast-drift burst exciter are shown by the solid and dashed lines, respectively (from Hughes and Harkness, 1963).

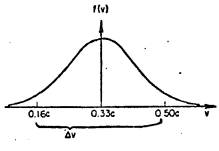

Fig. 5.15. Average velocity dispersion inferred from fig. 5.14 (from Smith, 1970).

Elgarøy and Rødberg (1964) also chose to attribute some of the observed type III burst duration and bandwidth to what they called "source size", which may be identified with Hughes and Harkness' "exciter dispersion".

We shall represent Hughes and Harkness' approach schematically by figure 5.16. At time t_o, the exciter is at height ρ_o above the photosphere, with vertical extent $\Delta\rho_o$, traveling upward through the corona at an average speed V_s, with a speed dispersion ΔV_s, (ie., speed ranges from $V_s - \frac{1}{2}\Delta V_s$ to $V_s + \frac{1}{2}\Delta V_s$).

The time t_o, and extent $\Delta\rho_o$, may be appropriate to either the original formation of the stream or the moment when em-waves produced by the stream can escape the solar atmosphere. Sturrock, 1964, hypothesized that type III burst exciters originate at the position of a flare in the chromosphere and their emission only becomes "visible" when the exciters emerge into the corona (see also Malville, 1967). However, the optical flare observed in the chromosphere may be due to particles accelerated at higher altitudes (see eg., Sakurai, 1971) and many bursts may be due to release of energetic particles from storage regions in the corona (see eg., Lin, 1970; Simnett and Holt, 1971).

Returning to the model of figure 5.16. as the exciter rises through the corona, its vertical extent increases as shown by the vertical bars at times t_o, t_1, t_2. The duration at frequency f_1 is $t_E + t_D$, where t_D is the decay time of the plasma waves produced, and t_E is the excitation time, or the time required for passage of the exciter, $t_2 - t_1$. We have for the duration at f_1

$$d_f(f_1) = (t_2 - t_1) + t_D(f_1) = \frac{\rho_1 - \rho_o}{V_s - \frac{1}{2}\Delta V_s} - \frac{[\rho_1 - (\rho_o + \Delta\rho_o)]}{V_s + \frac{1}{2}\Delta V_s} + t_D,$$

$$V_s - \frac{1}{2}\Delta V_s \qquad V_s + \frac{1}{2}\Delta V_s$$

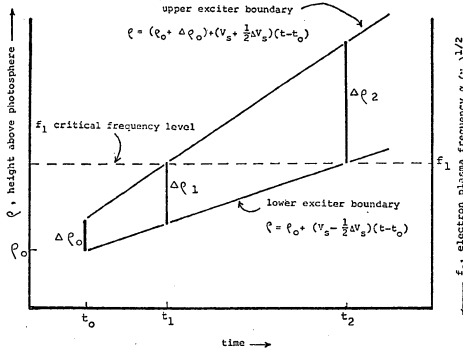

Fig. 5.16. Position and vertical extent of exciter with vertical speed V_s, total speed dispersion ΔV_s.

which reduces to

$$d_f = \frac{\Delta V_s(t_2-t_o) + \Delta\rho_o}{V_s + \frac{1}{2}\Delta V_s} + t_D,$$

$$\text{or} \quad d_f - t_D = \frac{\Delta V_s(t_2-t_o) + \Delta\rho_o}{V_s + \frac{1}{2}\Delta\rho_o} . \qquad (1)$$

The latter form is of interest in discussing spike bursts since, with $d_f - t_D \sim 0$, we are interested in reducing the value of the right-hand side of equation 1. For instantaneous bandwidth, b_t, we must consider both the range of local plasma frequency represented by the vertical extent of the exciter, $\Delta\rho$, and the vertical extent of the decaying region trailing the exciter, $\sim V_s t_D$. Namely, we have

$$\begin{aligned} b_t(t) &= (\Delta\rho + V_s t_D)\frac{df}{d\rho} \\ &= \Delta\rho \frac{df}{d\rho} + t_D \frac{d\rho}{dt} \cdot \frac{df}{d\rho} \\ &= \Delta\rho \frac{df}{d\rho} + \dot{f} t_D \\ &= (\rho_{max} - \rho_{min}) \frac{df}{d\rho} + \dot{f} t_D \\ &= \left\{ [\Delta\rho_o + (V_s + \tfrac{1}{2}\Delta V_s)(t-t_o)] - [(V_s - \tfrac{1}{2}\Delta V_s)(t-t_o)] \right\} \frac{df}{d\rho} + \dot{f} t_D \\ &= [\Delta V_s (t-t_o) + \Delta\rho_o] \frac{df}{d\rho} + \dot{f} t_D \end{aligned}$$

or

$$b_t - \dot{f} t_D = [\Delta V_s (t-t_o) + \Delta\rho_o] \frac{df}{d\rho} \qquad (2)$$

For mid-spike bursts we have $b_t \sim 1\text{-}3$ MHz, $\dot{f} \sim 40$ MHz/sec. Thus, for $t_D \sim 0.05$ second, we have $b_t - \dot{f} t_D \sim 0$, and we are interested in reducing the value of the right-hand side of equation (2).

Assuming spike bursts are produced by such a type III burst model, we wish to find what restrictions are placed on the exciters of spike

bursts. Admittedly, the above model is only a rough approximation for type III burst exciters. V_s and ΔV_s will change in the course of the exciter's traveling to maybe >50 R_o ($R_o \equiv$ solar radius), and other effects may contribute to the dispersion of the exciter. However, in applying equations 1 and 2 to spike bursts, we are only interested in a limited portion of the corona, perhaps only $\sim 0.05 R_o$ (which corresponds to a frequency range of ~30 MHz in the active region corona).

We shall assume the following values, d_f <0.1 second, t_D = 0.05 second (200 MHz, 10^6°K), b_f ~1-3 MHz. From equation 1 we have

$$\frac{\Delta V_s\ (t_2 - t_o) + \Delta\rho_o}{V_s + \frac{1}{2}\Delta V_s} < 0.05 \text{ second.}$$

In that spike bursts occur with both higher and lower drift rates than are average for type III bursts, we shall not seek the essential difference between spike bursts and type III bursts in V_s. We take $V_s \sim \frac{c}{3}$, appropriate for type III bursts, and V_s as an upper limit for ΔV_s, ie.

$$\Delta V_s\ (t_2 - t_o) + \Delta\rho_o < 8 \times 10^3 \text{km.}$$

In equation 2, we set

$$[\Delta V_s\ (t_2 - t_o) + \Delta\rho_o] \frac{df}{d\rho} < 1 \text{ MHz.}$$

For $df/d\rho$, we have values, appropriate to the 200 MHz level of the corona, ranging from 1.6 MHz/10^3km for the quiet corona, to 0.8 MHz/10^3 km for a coronal streamer of 10 times the density of the quiet corona (de Groot, 1966). Taking $df/d\rho$ = 1MHz/10^3 km, we obtain

$$\Delta V_s\ (t - t_o) + \Delta\rho_o < 10^3 \text{ km,}$$

somewhat more restrictive than the implications of equation 1. We thus have two approximate upper limits for the vertical (and, very likely,

horizontal) extent of the necessary spike burst exciter.

We obtain an independent estimate, of an upper limit to the spike burst exciter size, if we assume the horizontal extent to be less than the distance traversed by light in the time d_f. That is, we wish the delay time in receiving em-waves from the entire surface emitting at frequency f to be much less than d_f, the observed total duration at f. Taking $d_f = 0.1$ second, we have an upper limit of 3×10^4 km for the horizontal extent of the spike burst exciter.

In the above estimates we obtain spike burst exciter dimensions much less than the $\sim 2 \times 10^5$ km extent of Hughes and Harkness' average type III burst exciter at the 200 MHz plasma frequency level. For spike burst exciters of $10^3 - 10^4$ km extent, we have $\sim 10^{-2} - 10^{-1}$ times the dimensions, $\sim 10^{-4} - 10^{-2}$ times the cross section, and $\sim 10^{-6} - 10^{-3}$ times the volume, of a typical type III burst exciter.

For optically thick emission sources for spike bursts and type III bursts, of about the same size as the exciter, and similar exciter densities, these values compare favorably with the burst parameters given by de Groot (1966). From these parameters we have for typical spike bursts, flux times duration (ergs/Hz at frequency f) of $\sim 10^{-2}$ times, and integrated flux (ergs) of $\sim 10^{-4}$ times, typical type III burst values.

To obtain an estimate of $\Delta V_s / V_s$, we set

$$\Delta V_s \; d_s + \Delta \rho_o \sim 10^3 - 10^4 \text{ km},$$

where d_s is the lifetime of the exciter. For spike bursts we generally have lifetimes, d_o, <0.2 second. Since $d_o = d_s + t_D$, we have $d_s \sim 0.1$ second. This value of d_s corresponds to a frequency range

$$b_o \sim d_s V_s \frac{df}{d\rho} \sim 10 \text{ MHz},$$

which is typical for spike bursts.

Setting $\Delta\rho_o = 0$, we obtain

$$\Delta V_s < 10^4 - 10^5 \text{ km/sec}$$

or

$$\frac{\Delta V_s}{V_s} < 0.1 - 1 ,$$

where the limits of the range given correspond to exciter dimensions of 10^3 and 10^4 km, respectively.

We thus require exciters with much smaller dimensions ($\lesssim 10^{-1}$ - 10^{-2} times the dimensions) and with somewhat smaller speed dispersion ($\lesssim 0.1 - 1$ times the values of $\Delta V_s/V_s$) than are typical for type III bursts to explain the observed parameters d_f, b_f. Values of f are comparable for spike bursts and type III bursts. Integrated flux values suggest similar stream densities, N_s, for spike burst and type III burst exciters. Since we have scaled-down a model for type III burst exciters, we allow a continuous variation of burst parameters from spike bursts through type III bursts. For example, short-duration type III bursts may be produced from the above spike burst exciters by increasing d_s, the stream lifetime (hence, the spatial extent and d_f, b_f). Indeed, our next requirement is a mechanism which tends to restrict d_s for very short duration (d_f) bursts but not for long duration bursts.

Support for the existence of such a mechanism is given by the observed distribution of frequency range for type III bursts (Malville, 1962) which extends down to ~30 MHz, the upper limit of observed spike burst frequency ranges (b_o).

We recall (Chapter 2) that with type III bursts, one has difficulty explaining the large values observed for b_o, d_s. Quasilinear analysis of the two-stream instability indicates that the generation of plasma waves would be terminated in a very short time by plateau formation. Various nonlinear plasma effects have been proposed to inhibit the rapid growth of wave amplitudes to the extent that the instability would quench itself through plateau formation (Sturrock, 1964; Kaplan and Tsytovich, 1968; Tsytovich, 1970; Smith, 1970a, 1970b; Melrose, 1970a, 1970b).

We may ask if spike bursts might be produced by exciters in which these nonlinear effects have not been established. From Kaplan and Tsytovich (1968), Tsytovich (1970), we have the time of plateau formation at the 200 MHz level

$$\tau_p \sim \frac{N_e}{N_s \omega_{oe}} \sim \frac{1}{3N_s} \quad ,$$

where N_s is the density of the stream (electrons/cm^3), N_e is the electron density of the ambient plasma, and ω_{oe} is the plasma frequency of the ambient plasma. At the 200 MHz level we have $N_e \sim 5 \times 10^8$ electrons/ cm^3, $\omega_{oe} = 2\pi f_o = 4\pi \times 10^8$ radians/second. From Zheleznyakov and Zaitsev (1970b), we have $N_s \sim 1$-10 electrons/cm^3 for typical type III burst exciters at the 100 MHz level. The Hughes and Harkness type III burst exciter doubles in volume in passing from the 200 MHz level to the 100 MHz level, thus N_s is of the same order for the 200 MHz level. We thus obtain $\tau_p \sim 0.1$ - 0.01 second, in agreement with d_s values characteristic of spike bursts. Much shorter plateau formation times have been estimated from the value $N_s \sim 10^5$ electrons/cm^3 (Ginzburg and Zheleznyakov, 1958) which is based on a conservative estimate of the

efficiency with which plasma waves are produced and transformed into em-waves and is essentially an upper limit on the value of N_s necessary to produce a typical type III burst.

The values τ_p = .3 - .03 second correspond (at $V_s = 10^5$ km/sec) to $b_o \sim$30 MHz - 3 MHz, approximately the observed range of b_o for spike bursts. However, by attributing the range of b_o to variations of N_s in the above equation for τ_p, we have no continuous variation of burst parameters from normal spike bursts through large-b_o spike bursts, short-duration type III bursts to typical type III bursts. One increases b_o only by decreasing N_s, thus decreasing the net energy of the exciter (since spatial extent is limited) and by increasing the spacing between the stream particles to values greater than a Debye length (1 Debye length separation at the 200 MHz level corresponds to $N_s \sim$30 electrons/cm^3 for T = 10^{6}°K, $\sim$10 electrons/cm^3 for T = 2 x 10^{6}°K), thus greatly reducing the efficiency with which the stream produces plasma waves. For particle separation greater than a Debye length, the two-stream instability, which is a collective or coherent process, breaks down and is replaced by noncoherent Čerenkov generation of plasma waves, in which the particles act separately.

The growth rate, γ, for plasma waves produced by the two-stream instability (the reciprocal of the time necessary for the amplitude to increase by a factor of e) is given

$$\gamma \sim \frac{N_s}{N_e} \omega_{oe} \left(\frac{V_s}{\Delta V_s} \right)^2$$

(Kaplan and Tsytovich, 1968; Tsytovich, 1970). The higher a value γ has, the more that is required of any given nonlinear mechanism if the stream is to be stabilized. In that our derived spike burst

exciters may have $V_s/\Delta V_s$ somewhat greater than typical type III burst exciters, we note that such spike burst exciters would be more difficult to stabilize. However, as plateau formation proceeds, $\Delta V_s \rightarrow V_s$, and γ reduces to values we have no reason to believe are any greater than encountered in a type III burst exciter. Thus, any nonlinear mechanism capable of stabilizing a type III burst exciter would be able to stabilize a spike burst exciter. However, much of the exciter's energy may have been converted into plasma waves before γ has decreased sufficiently.

It thus appears reasonable that spike bursts could be produced by exciters which are subject to plateau formation. However, the variables N_s and $V_s/\Delta V_s$ do not seem to supply a means of limiting d_s for very short duration bursts but not for long duration bursts.

The spatial extent of the exciter may provide a critical value, $\Delta\rho_c$, such that for $\Delta\rho < \Delta\rho_c$, the exciter decays rapidly, and for $\Delta\rho > \Delta\rho_c$, the exciter decays at a much slower rate. Indeed, this appears to be the case in the analysis of quasilinear stream relaxation reported by Zheleznyakov and Zaitsev (1970a). This analysis indicates that stream relaxation (decay) is a much more protracted process than previously believed; that nonlinear effects are unnecessary to explain the lifetimes of typical type III burst exciters; and that the nonlinear effects discussed by Kaplan and Tsytovich (1968) and Smith (1970a) are inadequate to stabilize a type III burst exciter against stream decay. Quasilinear stream relaxation is shown to include an initial stage, of duration

$$\tau_i \sim \frac{N_e}{N_s}\left(\frac{\Delta V_s}{V_s}\right)^2 \frac{1}{\omega_{oe}} ,$$

during which a considerable portion of the stream energy is converted into plasma waves, and a quasistationary state, which is established in a time of the order of ν_{coll}^{-1} (τ_D above). Such is the case for a stream instantaneously "switched on". However, under conditions pertinent to the generation of type III bursts, one has a slow increase (slow compared to the characteristic times above) in the concentration of stream particles at a given point in the corona, from zero to some maximum value N_s, followed by a gradual fall-off from that peak. The phase of intense generation of plasma waves is absent. The state of the two-stream instability remains consistently close to the quasistationary state because of the slow variation of stream parameters in time and space, and because of the mild nonuniformity of the corona as the stream advances. The first stage of development of the two-stream instability would be realized, by the type III burst exciter, only if the exciter was formed in less time than required to establish the quasistationary state, ν_{coll}^{-1} (which is much less than 0.05 second in the chromosphere).

On the other hand, our spike burst exciter, with its much smaller dimensions, presents an increase in stream density at a given point in the corona, in a time interval of the order of τ_i and passes any given point in the corona in a time interval $< \nu_{coll}^{-1}$. Effectively, the stream is instantaneously "switched-on", at any given point in the corona, and passes through that point in less time than is required to establish the quasistationary state.

We thus have a mechanism which restricts d_s for very short duration bursts (very small exciters) but not for long duration bursts (large exciters).

In the above comparison between spike bursts and type III bursts, we have neglected the difference in polarization between them. Spike bursts are ∿100% circularly polarized; type III bursts are unpolarized or weakly linearly polarized when observed with the same bandwidth (de Groot, 1966). Akabane and Cohen (1961) showed that, because of strong Faraday rotation in the corona, the observed degree of polarization of type III bursts depends heavily on the bandwidth of the receiving system. Chin, et al. (1971), observing at 25 MHz with a 100 Hz bandwidth, report ∿65% linear (or weakly elliptical) polarization (with axial ratios of up to 0.8 observed). Our most encouraging results, however, come from Rao (1965) who reports a strong tendency for type III bursts of shorter duration, observed between 40 and 60 MHz, to have stronger circular polarization. Circular polarization up to 70% was observed in very short duration type III bursts. Perhaps it is significant that Rao is observing sources of smaller spatial extent and higher ambient magnetic fields than Chin, et al. Spike bursts, at ∿200 MHz, originate in still smaller sources at higher ambient magnetic fields. Yip (1970c) shows that circular polarization in type III bursts may be due to the magnetic field in the region in which the Čerenkov plasma waves are produced and transformed into em-waves.

It should be noted that the Fung and Yip (1966a, 1966b) cyclotron emission model for noise storms (type I bursts plus continuum) is

capable of producing bursts of $\sim$ 0.05 second duration, and thus capable of producing spike bursts. The essential similarity between this noise storm model and type IV burst models by these authors (Yip, 1967; Fung, 1969) is supported by

1) the observation of spike bursts during both noise storms and type IV bursts,
2) the occasional development of a type IV burst into a noise storm, and
3) the identical appearance of noise storms and stationary type IV bursts in Kai's (1970) 80 MHz radioheliograph observations.

Fung and Yip (1966a, 1966b) attribute type I bursts to streams of mildly relativistic electrons traveling through a region where $f_o/f_H \sim 1$, where f_o is the electron plasma frequency and f_H is the electron cyclotron frequency. Fokker (1969) suggests that type III bursts originate above the level at which f_o/f_H has some critical value. If this critical value is $\sim$1, it is conceivable that an electron stream originating in the chromosphere could generate spike bursts (by Fung and Yip's, 1966a, 1966b model) while passing upwards through the $f_o/f_H \sim 1$ level, then proceed to produce a type III burst while continuing upwards through the corona. This would produce associated spike bursts and type III bursts resembling the events shown in figures 5.2. through 5.5. Yip (1970a) concludes, however, that a weakly relativistic electron stream in the corona would be more prone to the production of coherent Čerenkov plasma waves than the production of the low harmonic cyclotron emission required by the Fung and Yip (1966a, 1966b) noise storm model.

CHAPTER 6. PARALLEL DRIFTING BANDS

In figure 6.1, we have examples of complex events involving narrow, parallel, drifting bands (PDB) of emission reported by Philip (1968). Another example, from the observations of the HTR Radiospectrograph, is given in figure 6.2. Previous examples of such activity were reported by Boischot, Haddock and Maxwell (1960) (figure 6.3) and Elgarøy (1959, 1961) (figure 6.4).

By consideration of the dynamic spectra alone, the above events divide naturally into two categories:

1) "Parallel constant-drift bands", or
   PCDB: 1430 UT 18 August 1959
   2131 UT 24 October 1967
   2355 UT 3 June 1968
   1656 UT 7 June 1968
   1718 UT 7 June 1968

2) "Parallel variable-drift bands", or
   PVDB: 1400 UT 4 November 1957
   1430 UT 18 August 1959
   0049 UT 9 June 1968
   1907 UT 9 June 1968

In the above observations, PCDB and PVDB occur together only in the 18 August 1959 event. Of the five PCDB events observed, spike bursts were observed during four events, quasi-periodic spike bursts during three events. Of the four PCDB events observed with the HTR Radiospectrograph, all were preceded by spike bursts, three by quasiperiodic spike bursts. Of the four PVDB events above, none contained spike bursts. In the 4 November 1957 event, however, time resolution was insufficient to observe spike bursts. Neither of the two PVDB events observed with the HTR Radiospectrograph contained spike bursts. Thus, although the sample of events is small, the designations PCDB and PVDB appear to

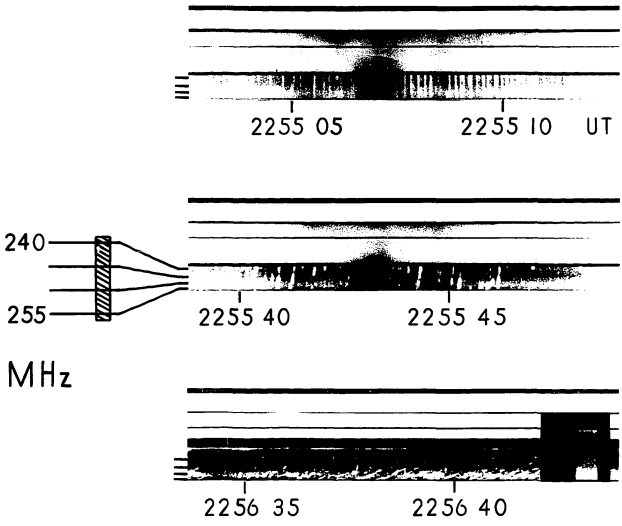

3 JUNE 1968
FIG. 6.I.A. PDB EVENT

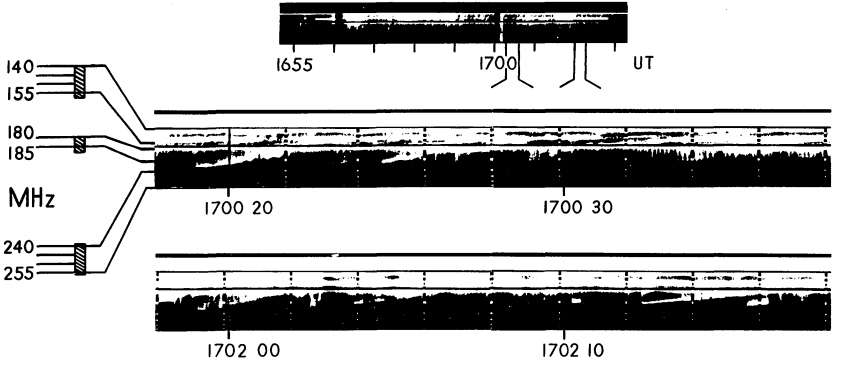

FIG. 6.1.B. PDB EVENT 7 JUNE 1968 A

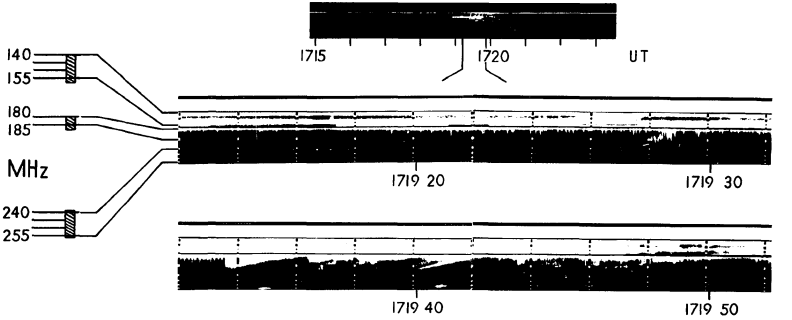

FIG. 6.I.C. PDB EVENT 7 JUNE 1968 B

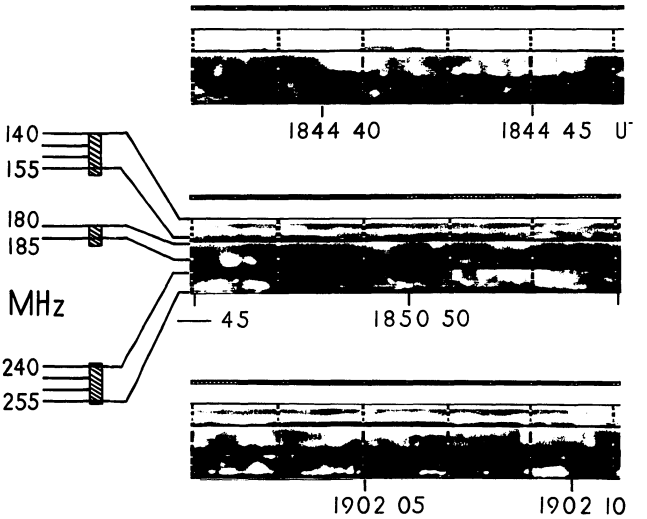

9 JUNE 1968

FIG. 6.I.D. PDB EVENT

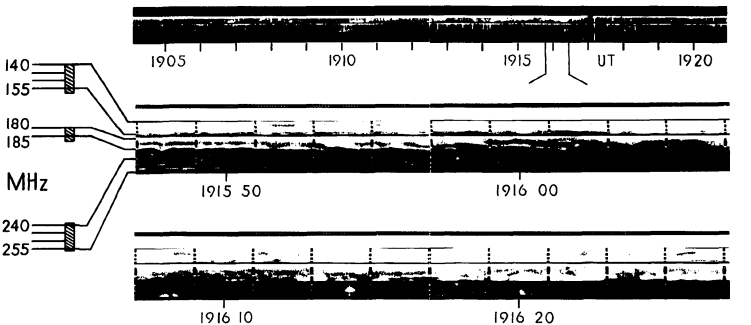

FIG. 6.I.E. PDB EVENT 9 JUNE 1968 CONT.

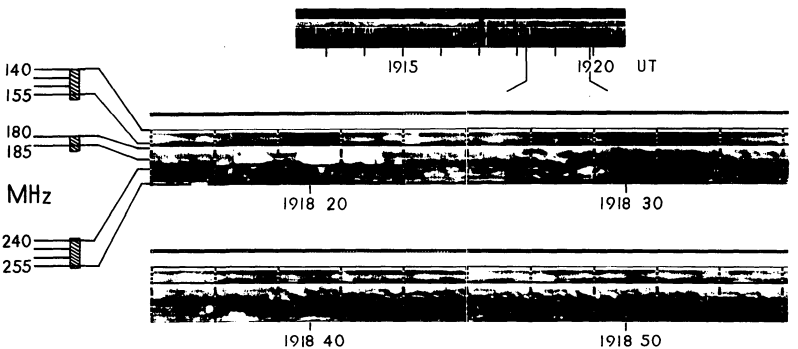

FIG. 6.I.F. PDB EVENT 9 JUNE 1968 CONT.

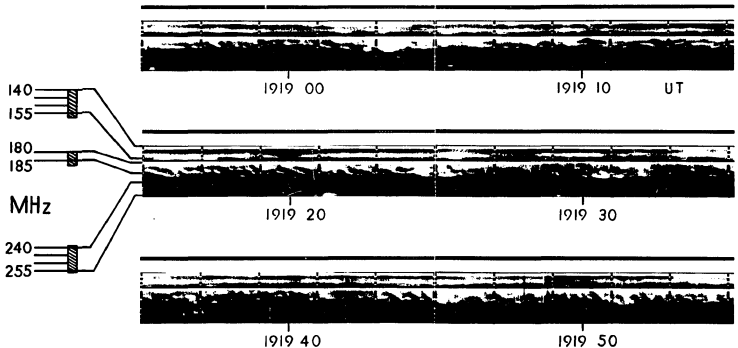

FIG. 6.I.G. PDB EVENT 9 JUNE 1968 CONT.

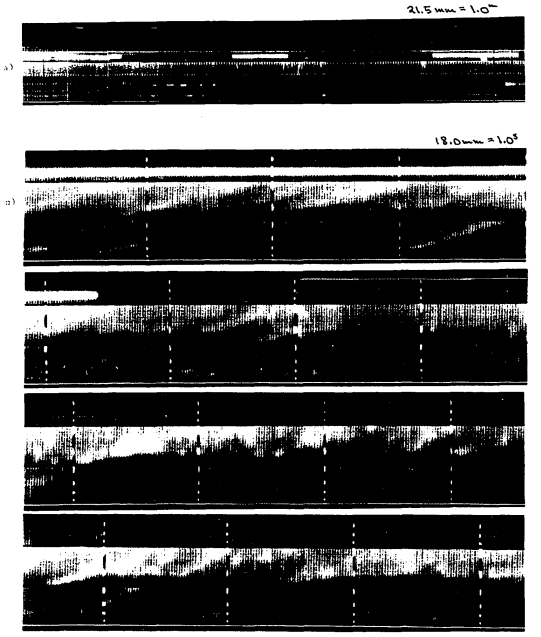

Fig. 6.2. [illegible] event 24 October 1967: a) 2131-2177 UT.
b) 2133:42 UT.

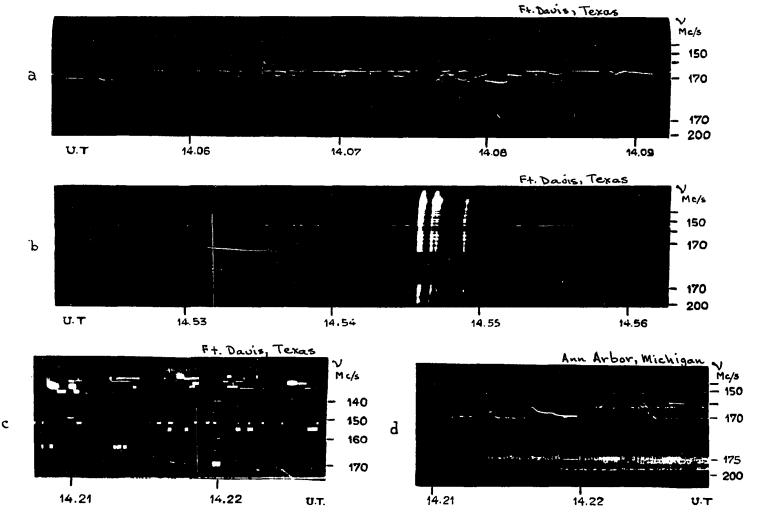

Fig. 6.3. PDB event 4 November 1957 (from Bøischot, et al.,1960).

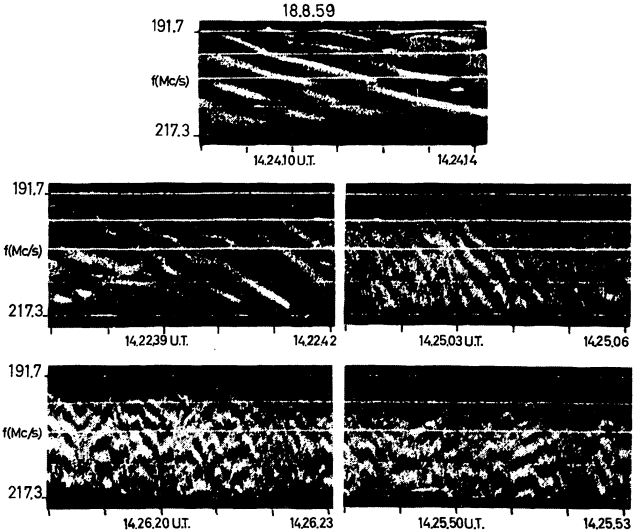

Fig. 6.4. PDB event 18 August 1959 (from Elgarøy, 1961).

represent distinct types of activity or distinct forms of the same type of activity.

The distinction between PCDB and PVDB events is supported by examination of the history of solar activity preceding each event. In figure 6.5, we have histories for all the above PcDB events. PVDB event histories are presented in figure 6.6. Information for figures 6.5 and 6.6 was obtained from ESSA Solar-Geophysical Data, with the exceptions of the 4 November 1957 event, for which Boischot, et al., (1959) was used, and the 18 August 1959 event, for which the Ling-Temco-Vought Solar Activity Catalogue, Vol. 4, Table VIII, was used. Of the seven PDB events in these two figures, four are seen to be concurrent with Dkm-λ continuum emission (I, IV, or "cont.") and four concurrent with m-λ continuum emission. We notice that PCDB events tend to follow small flares (importance 1N, 1F) represented at meter wavelengths by little more than a type III burst. PVDB events, on the other hand, are invariably part of a major radio event initiated (with one exception) by a major flare (importance 2,3). The major radio event not preceded by a major flare was the "great outburst of 4 November 1957" (Nera, 1958; Bioschot, Fokker, and Simon, 1959; Boischot, Haddock, and Maxwell, 1960). It is not unreasonable to assume the great outburst of 4 November 1957 was due to a major flare on the far side of the sun. McMath regions 4188 and 4189, responsible for one 3+ flare, two 2+ flares, and four 2 flares during the period 17-23 October 1957, were on the far side of the sun at the time (IGY Solar Activity Report Series Number 12). In the IGY Solar Activity Report Series Number 14,

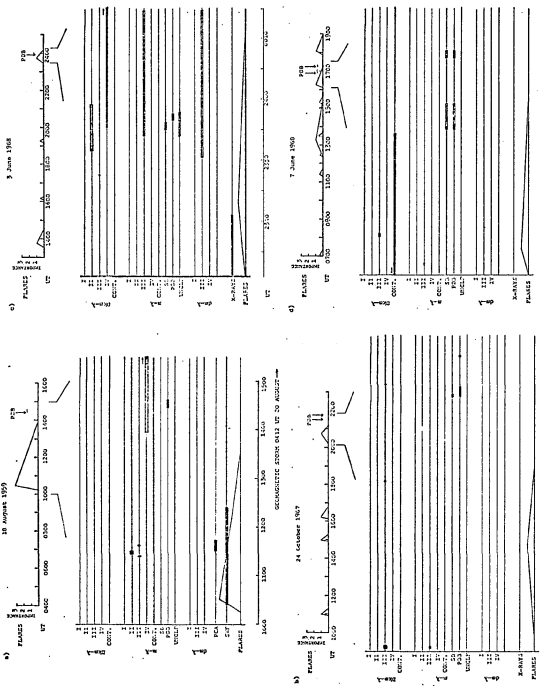

Fig. 6.5. Histories of PCDB events. a) 18 August 1959. b) 24 October 1967. c) 3 June 1968. d) 7 June 1968 A,B.

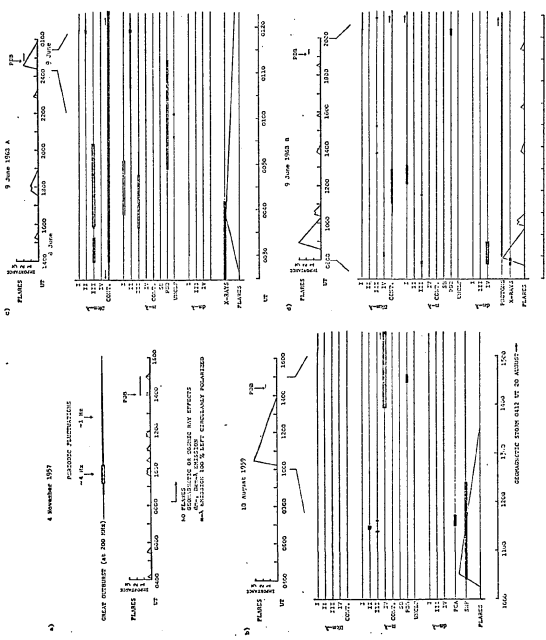

Fig. 6.6. Histories of PVDB events. a) 4 November 1957. b) 18 August 1959. c) 9 June 1963 A. d) 9 June 1963 B.

we see that the daily flare index was $\leq$ 10 for the period 1 - 10 November, and often > 20 during the period 12-29 October (the rotational period of the sunspot zones is about 27 days).

Thus, we have a tendency among PCDB events to occur following importance 1 flares with associated type III bursts, to include spike bursts and quasiperiodic spike bursts, to exhibit negative frequency drift. PVDB events tend to occur following importance 2 or 3 flares, often by several hours, as part of a major radio event. In that PCDB and PVDB events do resemble each other and appear to both occur during the 18 August 1959 event, they appear to be distinct forms of the same type of activity. Any model for this phenomenon must explain both forms and their tendencies to occur as described above.

Since the frequency separation, Δf, of the drifting bands is $\sim$ 5 MHz ($\sim$200 MHz/$\sqrt{1836}$, that is, approximately the proton plasma frequency to be found at the 200 MHz electron plasma frequency level in the corona), Elgarøy (1961) suggested that PDB are due to modulation of existing electron emission by harmonics of the proton plasma frequency or absorption of continuum emission at these harmonics. This interpretation is supported by preliminary investigations of the frequency dependence of Δf exhibited in the events in figure 6.1 (Philip, private communication, 1969) and in observations over a 2 to 1 frequency range (Elgarøy, private communication, 1969). Another possibility considered by Elgarøy, (1961) is that the continuum emission is synchrotron emission from relativistic electrons in a magnetic field of some gauss. This field strength corresponds to an electron cyclotron frequency of $\sim$ 5 MHz.

One may then assume that interaction between relativistic and non-relativistic electrons results in continuum emission with absorption at intervals of $\sim$ 5 MHz.

From the discussion of cyclotron and synchrotron emission in Wild, Smerd, and Weiss (1963), we see that as the energy of the emitting particles increases, the harmonics of the cyclotron frequency merge to form a continuum (figure 6.7). Conceivably, the intermediate form of emission, the so called "gyrosynchrotron emission", could produce a series of resolvable harmonics which could exhibit drift as the magnetic field or energy of the particles changed.

Although it conflicts with the observation of identical bursts with two different radiospectrographs (Boischot, et al., 1960; figure 6.3 above), it is interesting to consider a moiré pattern interpretation of PDB events. As shown in figure 3.6, swept-frequency radio spectrographs are particularly prone to the production of moiré patterns from periodic signals or interference. The only reported PDB observations have been made with swept-frequency equipment. To produce, for example, the PDB events in figure 6.4, we require bursts of $\sim$ .0013 second duration, a recurrence rate of $\sim$ 300 MHz, and frequency range $\geq$ 18 MHz.

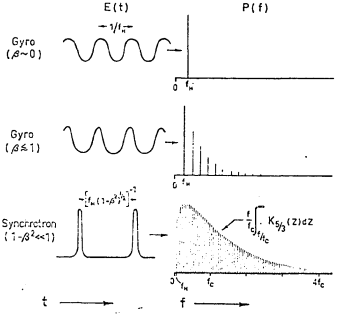

Fig. 6.7. Illustrating the origin of synchrotron radiation. E(t) represents the electric field at a stationary observer in the orbital plane of an electron gyrating at velocity βc. The emission spectrum P(f) is the Fourier transform of E(t). (from Wild, et al.,1963).

CHAPTER 7. UNUSUAL FINE STRUCTURE

A. Unusual Spike Bursts

In figure 7.1 we have an unusual event which consists of a quasi-periodic sequence of extremely short-duration ($d_f \approx 0.02$ second) md- or fd- spike bursts ($f \approx 100$ MHz/second). The frequency range of the bursts, b_o, is $\gtrsim 50$ MHz. In contrast to the large b_o spike bursts of figures 5.11.a and 5.11.b, the bursts in figure 7.1 have positive drift. Comparison of figure 7.1.a with the examples of ionospheric scintillation in figure 3.7 and with figure 3.8 from Wild and Roberts' (1956) dynamic spectra of ionospheric scintillation suggests that the large scale event in figure 7.1.a is due to ionospheric and/or solar scintillation. Note that the background continuum between the "ridges" in figure 7.1.a is of lower intensity than the continuum preceding and following the event. The event was observed $\sim$1800 local time. It thus appears likely that the very fine bursts in figure 7.1.b are fine structure in ionospheric scintillation.

In figure 7.2 we have examples of an extremely rare type of burst, characterized by an extremely short rise time ($\sim$0.01 second). We will refer to such bursts as srt-spike bursts (for "short rise time"). Observations of srt-spike bursts appear to be limited to the bursts shown in figure 7.2, which occurred during an extensive type III burst event observed 0026 UT 26 September 1968, following an importance 2B flare (IAU Quarterly Bulletin on Solar Activity). Of particular interest is the large b_o burst in figure 7.2.b. This burst has $f \sim 300$ MHz/sec and $b_o \gtrsim 50$ MHz. Given a plasma hypothesis interpretation,

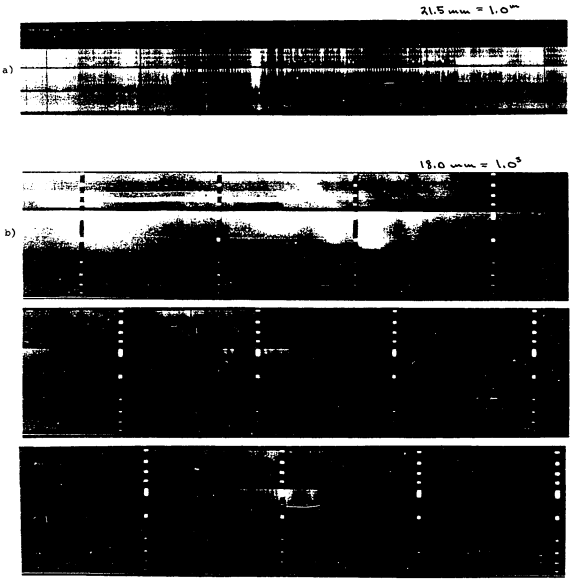

Fig. 7.1. Unusual spike bursts: a) 7-14-68, 1416-1422 UT. (LS film). b) 7-14-68, 1419:03 UT.

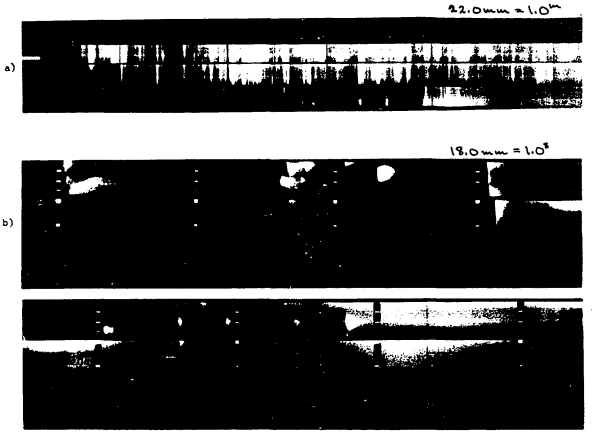

Fig. 7.2. srt-spike bursts: a) 9-26-68, 0026-0032 UT. (LS film). b) 9-26-68, 0028:02 UT.

this burst could indicate the passage of a very small exciter through regions of varying T, hence, varying decay time, t_D, for the plasma waves excited.

In figure 7.3, we have a burst with duration somewhat long for a type I burst, and bandwidth much larger than that of a normal type I burst. Centered in the burst is a feature resembling a fd- spike burst. No other bursts of this nature were noticed.

B. Unusual Chains of Spike Bursts and Type I Bursts

A few patterns were observed occasionally in chains of type I bursts or spike bursts. The most unusual of these is shown in figure 7.4. We shall refer to events of this nature as sis-chains, consisting of a long-duration burst preceded and followed by fast-drifting bursts of shorter duration. The long-duration burst may range in scale from a type I(s) burst to a s- spike burst; the short-duration burst may be type I (fd, r) bursts or fd- spike bursts. While only one long-duration burst is found in sis-chains, anywhere from one to several short-duration bursts may be present. The short-duration bursts may be divided into preceding and following groups, or they may all precede or follow the long-duration burst. The short-duration bursts in any given sis-chain generally have about the same drift rate. The total duration of sis-chains ranges from $\sim$0.5 to $\sim$4 seconds. Quite often, sis-chains appear to be only partially observed, running off the low-frequency edge of band B. This edge of band B represents the highest gain in the entire observing range (figure 3.4), and the lowest value of $\Delta T/T$ (due to the nonlinearity of the frequency scale). It is possible, therefore, that some of the sis-chains recorded may be partial observations of a

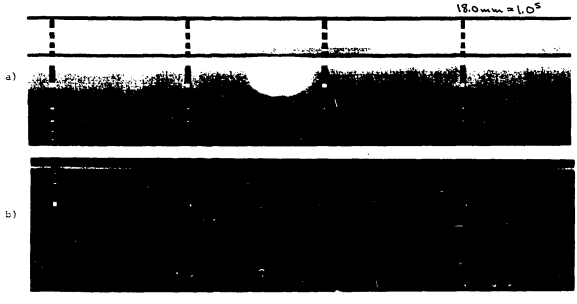

Fig. 7.3. a) Unusual burst. 7-11-68, 1743:47 UT.
b) Same burst exposed to show spike
& rat-like feature in center.

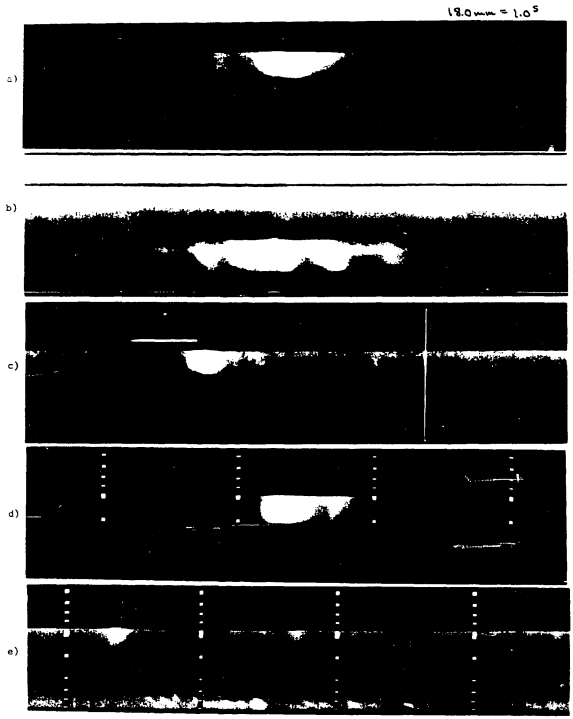

Fig. 7.4. sis-ch ins: a) 6-25-67, 1348:11 UT. b) 7-24-67, 1936:10 UT. c) 8-25-67, 2109:50 UT. d) 9-27-68, 2359:42 UT. e) 8-16-68, 2325:41 UT.

pattern such as ridges with fine structure, high dispersion, or ribbed interference shown in figure 3.8, from Wild and Roberts' (1956) study of dynamic spectra of (ionospheric) radio star scintillation. It is interesting that the fine structure in band C at 041916-18 UT in figure 7.1.b, which is apparently fine structure in ionospheric scintillation ridges, resembles sls-chains and the above patterns in figure 3.8.

Some chains, which we shall call $\ddot{f}$-chains, exhibit a systematic change of $\dot{f}$ from one burst to the next in the course of the chain (figure 7.5). Assuming a plasma hypothesis interpretation of the bursts in the chain, we see from Chapter 2 that a change in $\dot{f}$ may be produced by a change in v_s, $|\nabla Ne|$, or the angles $\angle \vec{V}_s$, ∇Ne or $\angle \vec{V}_s$, $\hat{r}$, where $\vec{V}_s$ is the velocity of the exciter, ∇Ne is the gradient of ambient electron density, and $\hat{r}$ is a unit vector directed toward the observer.

The resemblance between $\ddot{f}$-chains and whistlers suggest that dispersion may be responsible for the change of $\dot{f}$ in $\ddot{f}$-chains. Indeed, many phenomena observed in the quasi-dipole magnetic field and dispersive medium surrounding the earth (and Jupiter) should be sought in the quasi-dipole magnetic field in solar active regions above bipolar sunspot groups (see, for example, Chiu, 1970; Fokker, 1969).

Several chains exhibit a sharp cut-off on the high-frequency edge of the chain (figure 7.6.b). The bursts, which individually vary in b_o, appear to be lined up along either a constant-frequency boundary or a slowly drifting boundary on the high-frequency edge of the chain. We shall refer to such chains as hco-chains (for "high cut-off"). While some hco-chains with constant-frequency boundaries might be attributable to decrease of gain with frequency (e.g., band B), the existence of

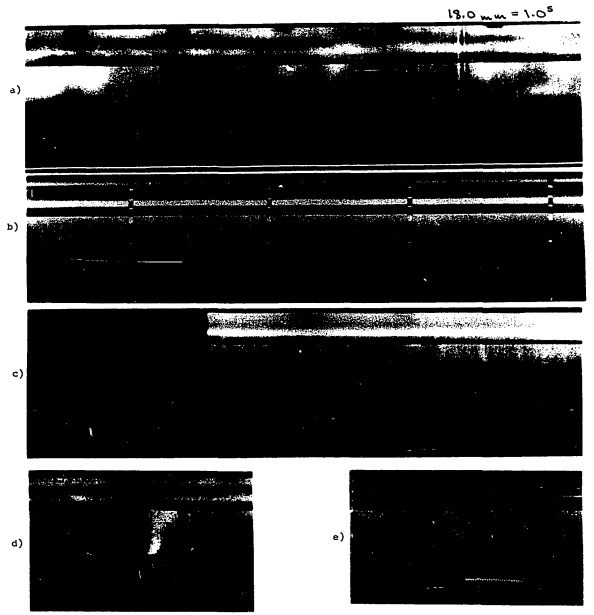

Fig. 7.5. F-chains: a)7-23-67, 0048:32 UT. B) 7-17-68, 1856:27 UT. c) 7-25-67, 1802:41 UT. d)7-24-67, 2116:55 UT. e) 5-23-68, 0349:11 UT.

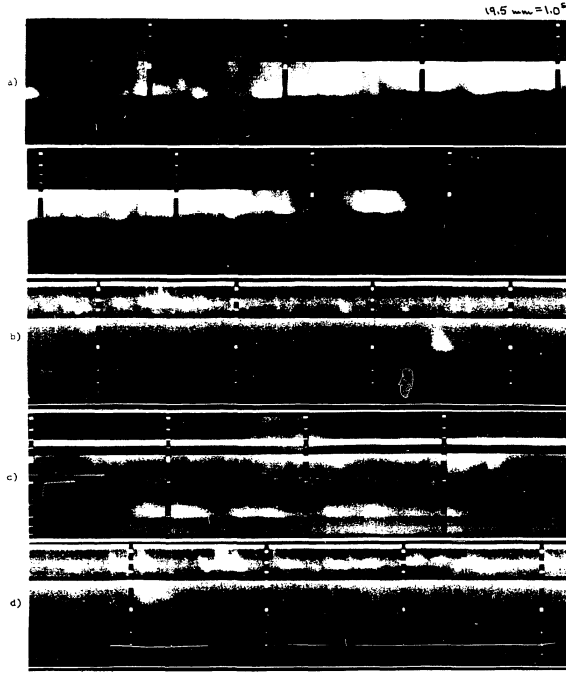

Fig. 7.6.(a-d). hco-chains: a) 8-16-68, 0230:24 UT. b) 8-16-68, 1635:24 UT. c) 6-23-68, 1956:32 UT. d) 8-16-68, 1635:32 UT.

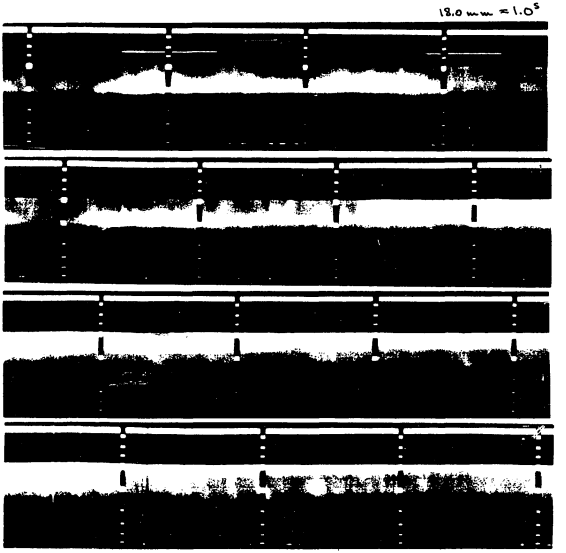

Fig. 7.6e. hco-chains: 10-19-68, 0052:45 UT.

drifting boundaries precludes an instrumental interpretation of all hco-chains. Indeed, such a chain is shown in Elgarøy and Ugland's (1970) examples of short chains, and it appears that the high cut off feature in some chains has been recently pointed out by Markeev and Chernov (1971). Hco-chains in which the bursts could conceivably originate at the boundary are consistent with the type I burst models of Takakura (1963) and Trakhtengerts (1966), in which type I bursts are produced by particle streams originating at the front of a MHD wave packet, in which case all bursts would start at the local plasma frequency corresponding to the position of the wave front and then decay with a range of decay times, hence, a range of b_o values. Such hco-chains are also consistent, for the same reasons, with the analyses of Wild and Tlamicha (1964) and Hanasz (1966), which suggest that chains of type I bursts are produced by MHD waves (or shock waves) propagating through the corona. However, in figure 7.6.b and 7.6.d, we see bursts which terminate on the cut off boundary instead of originating on the boundary.

The chains in figure 7.6.b and 7.6.d may belong to another peculiar type of activity in which fd- spike bursts are seen to start or terminate in type I(s) bursts or s- spike bursts (figure 7.7).

In figure 7.8, we have several events which may be man-made carriers, chains of unresolved bursts, or a new type of burst. While operating the HTR radiospectrograph, such bursts would appear occasionally on the (amplitude-modulated) monitor oscilloscope, with the same frequency profile as type I bursts, much weaker and wider than a carrier, having no detectable modulation, and often lasting several seconds. Such

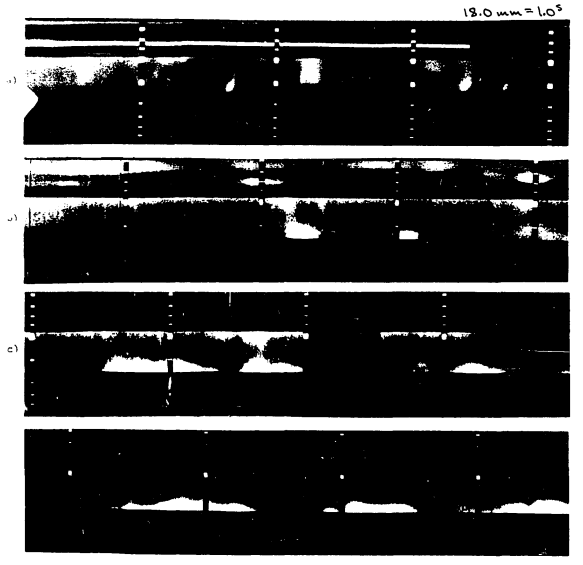

Fig. 7.7. Combination of drifting spike bursts and
S-spike burst (a), type I(s) bursts (b and c).
a)10-11-63, 0020:51 UT. b) 8-17-63, 1803:51 UT.
c)8-17-63, 0422:55 UT.

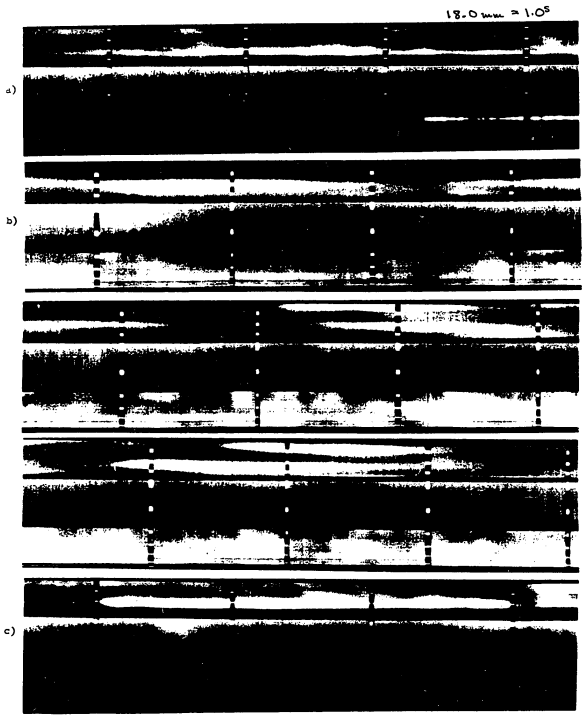

Fig.7.8. Persistent bursts (PB). a)7-13-68, 0359:15 UT. b) 6-22-68, 0429:54 UT. c) 7-12-68, 0051:11 UT.

bursts were termed "persistent bursts", or PBs. In the film record, PBs are more diffuse than carriers, have wider band widths than carriers, occasionally exhibit very slow drift, and do not appear during periods of low activity (however, almost all HS observations were made while the sun showed some activity, and the time resolution of the LS film is insufficient to reliably identify PBs). A possible interpretation in terms of man-made rf emission, would be as sporadic scattering of carriers off meteor trails (McNarry, 1962; Thompson, 1961b). Thompson reports meteor scatter bursts of average duration 10 seconds, maximum dur duration 4 minutes, at 60 MHz. The duration of the signals is inversely proportional to the square of the frequency. At 200 MHz, we would expect average duration ~ 1 second, maximum duration ~20 seconds; at 120 MHz, ~2 seconds average, maximum ~40 seconds. Most PBs have been observed in band C (~149 MHz); durations up to 30 seconds have been observed. Carriers are frequently observed on band C, which includes frequencies allocated for the following uses (ITT Reference Data for Radio Engineers, 5th ed., 1968): land mobile (approximate range 150 - 156 MHz), maritime mobile (156 - 158 MHz), aeronautical mobile (144, 148, 157 MHz), amature (144 - 148), government (including Armed Forces, 138 - 144, 150 - 151, 157 MHz), space (earth-space, space, satellites; 136 - 138, 148, 150, 154 MHz). However, no identifications between PBs and carriers have been made.

Quite similar to PBs were several chains observed with rope-like, parallel structure, called ps-chains (figure 7.9). PBs may be ps-chains in which the often very fine separation of the successive bursts which

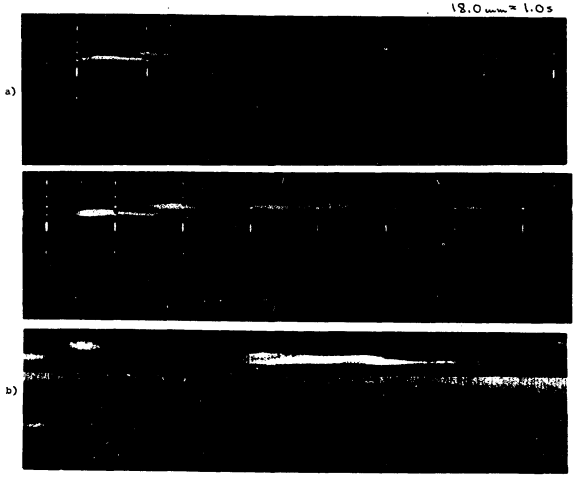

Fig. 7.9. Rope-like Parallel Structure (PS): a) 8-1-67, 2130:21 UT. b) 8-2-68, 0256:10 UT.

form the turns of the rope, so to speak, is not visible. On the other hand, parallel structure may be imposed on a PB by passage through a medium with selective absorption in sharp, slowly drifting bands.

CHAPTER 8. SUMMARY

A review of the literature on solar radio spike (or "flash") bursts indicates there is variety in the dynamic spectra of the bursts being discussed. We have adopted a definition consistent with this literature; namely, we accept as spike bursts all meter wavelength bursts with duration at one frequency, d_f, $\leq$ 0.1 second. Spectral observations with $\leq$ 0.01 second time-resolution reveal spike burst dynamic spectra of three types:

1) fast drift (fd-) spike bursts, with $\dot{f} \geq$ 100 MHz/sec;

2) medium drift (md-) spike bursts, with $\dot{f} <$100 MHz/sec; and

3) simple (s-) spike bursts, with no apparent drift.

Drifting spike bursts exhibited both positive and negative drift. Drift rates as high as $\geq$ 300 MHz/sec have been observed for fd-spike bursts; as low as $\sim$10MHz/sec for md-spike bursts. Spike bursts occur more frequently on $\sim$ 250 MHz than on $\sim$ 140 MHz; fd-spike bursts occur more frequently than md-, or s- spike bursts. There is a strong tendency for spike bursts to occur in regular sequences of similar bursts. This effect is most pronounced in rare, extensive sequences of quasi-periodic fd-spike bursts.

High-time-resolution observations of type III burst reveal occasional fine-structure in the forms:

1) md-, s-spike bursts occuring at frequencies above the starting frequency of a type III burst, aligned with the type III burst in the frequency time plane;

2) fd-spike bursts occuring during or following a group of type III bursts, at frequencies occupied by the type III bursts; and

3) storms of large-frequency-range spike bursts occuring at or above the starting frequency of a group of type III bursts.

Type III bursts are observed with durations approaching the range of spike burst durations; that is, type III bursts are observed with durations of $\geq$ 0.1 second at 190 and 250 MHz. Large-frequency-range fd-spike bursts are observed to predominantly exhibit the negative drift and increasing duration which are characteristic of type III bursts. The existence of such a morphological continuity between spike bursts and type III bursts suggests that both burst types may be due to the same emission mechansim. Type III bursts are commonly attributed to plasma frequency oscillations generated by the two-stream instability upon the passage of a short stream of electrons, called the "exciter", through the corona. This mechanism can produce bursts with values of d_f and instantaneous bandwidth, b_+, characteristic of spike bursts provided exciter dimensions do not exceed $\sim 10^3 - 10^4$ km and the kinetic temperature of the ambient electrons is $\sim 10^{6}$°K. Exciters of density, $N_S \sim$ 1-10 electrons/cm^3, as recently suggested for type III bursts, would undergo quasilinear plateau formation in times comparable to the observed lifetimes of spike bursts. It appears that exciters of dimensions $<<10^5$ km may be more prone to plateau formation than normal type III burst exciters ($\sim 10^5$ km). This effect may explain the morphological continuity between spike bursts and type III bursts. Given a distribution of dimensions for exciters of comparable density, the smaller exciters would tend to produce spike bursts, the larger exciters would tend to produce type III bursts.

Among the unusual fine structure observed were complex patterns

of parallel drifting bands of emission. These events appear to divide into patterns with constant drift, which tend to associate with spike bursts and small flares; and patterns with variable drift, which tend to occur during major radio events following large flares, and which are not associated with spike bursts.

Chains of spike bursts and type I bursts exhibited a few distinct patterns, most notable among them being chains with a sharp high-frequency cut-off.

On one occasion unusual spike bursts were observed with extremely short rise-times of $\leq$ 0.01 second and variable decay times ranging from $\sim$ 0.01 second to $\sim$ 0.1 second.

Repeated evidence of ionospheric scintillation of solar continuum sources appeared in the records, normally on a time scale of > 1 second. Some chains of type I bursts or spike bursts appear to be the effect of scintillation in the ionosphere or corona. The morphology and interpretation of dynamic spectra of meter wavelength ionospheric scintillation should be studied in order to assist the interpretation of solar spectral observations made at elevation angles of $< \sim 20°$. Coronal scintillation should be studied as a possible source of fine structure at meter wavelengths.

The most desirable single improvement in the HTR Radiospectrograph is wider bands of continuous frequency coverage. The width of the observing bands is presently limited by the bandwidths of the mixer stages of the receiver. Observing over a total frequency range > 20 MHz requires the use of more than one receiving band and either time-sharing between bands for recording data or far more elaborate techniques for recording data. Time-sharing results in either significant reduction

in time-resolution or an increase in receiver noise level.

The widths of the present observing bands are comparable to the frequency-ranges of spike bursts. An increase in the width of observing bands would aid the study of the distribution of spike burst frequency-ranges; would allow a better comparison of large-frequency-range spike bursts and short-duration type III bursts; would aid the study of meso-scale structure, such as associations between different burst types; and would provide observations of a greater amount of activity in any given observing period.

TABLE OF SYMBOLS

A	Receiver band, 235-255 MHz
B	Receiver band, 180-190 MHz
B	Indicating burst parameter measured with respect to background (Chapter 1, 2)
b	Bandwidth (Fig. 1.1)
b_o	Frequency range (Fig. 1.1)
b_T	Instantaneous bandwidth (Fig. 1.1)
C	Receiver band, 135-155 MHz
d	Duration (Fig. 1.1)
d_o	Lifetime (Fig. 1.1)
d_f	Duration at one frequency (Fig. 1.1)
d_s	Lifetime of burst exciter
Dkm-λ	Dekameter wavelength
dm-λ	Decimeter wavelength
em	Electromagnetic
f	Frequency, Hz
f_o	Electron plasma frequency
f_H	Electron cyclotron frequency
$\dot{f}$	Frequency drift (Fig. 1.1)
$\ddot{f}$	Indicating burst chain with systematic change of burst f values
fd-	Fast-drift spike burst (Chapter 4)
HP	Half-power
HS	High speed camera
HTR	High-time-resolution

TABLE OF SYMBOLS (Continued)

hco-	High-frequency cut-off
i.f.	Intermediate frequency
l.o.	Local oscillator
LS	Low speed camera
m-λ	Meter wavelength
md-	Medium-drift spike burst (Chapter 4)
N_e	Ambient coronal electron density, electrons/cm^3
N_s	Electron density of burst exciter, electrons/cm^3
PB	Persistant burst (Chapter 7)
PCDB	Parallel constant-drift bands (Chapter 6)
PDB	Parallel drifting bands (Chapter 6)
ps-	Parallel structure (Chapter 7)
PVDB	Parallel variable-drift bands (Chapter 6)
s-	Simple spike burst (Chapter 4)
sls-	Indicating burst chain with sequence short-duration bursts, long-duration burst, short-duration bursts
srt-	Short-rise-time spike burst (Chapter 7)
t	Time, sec.
t_D	Decay time
T	Electron kinetic temperature (Chapters 2, 5)
T	Antenna temperature (Chapter 3)
V_s	Average streaming speed of a burst exciter
V_T	Electron thermal velocity
ΔT	Minimum detectable noise fluctuation (Chapter 3)
ΔV_s	Speed dispersion of burst exciter (Fig. 5.15)

TABLE OF SYMBOLS (Continued)

$\Delta\rho$	Instantaneous vertical spatial extent of burst exciter
γ	Temporal growth rate for plasma oscillations
λ	Wavelength
ν_{coll}	Electron-ion collision frequency, Hz
ρ	Height above photosphere
τ_p	Plateau formation time
ω_{oe}	Electron plasma frequency, radians/sec.
I	Burst type (Fig. I.2, § 2.B.2.); see § 2.B.2 for types I(s), I(d), I(r), I(f)
II	Burst type (Fig. I.2)
III	Burst type (Fig. I.2., § 2.A)
IIIg	Group of < 10 type III bursts
IIIG	Group of > 10 type III bursts
IV	Burst type (Fig. I.2)
V	Burst type (Fig. I.2)

BIBLIOGRAPHY

Aarons, Ed., Solar System Radio Astronomy, Plenum Press, New York, 1965.

Akabane, K., and M. H. Cohen, Polarization measurements of type III bursts and Faraday rotation in the corona, Astrophys. J., 133, 258, 1961.

Alexander, J. K., H. H. Malitson, R. G. Stone, Type III radio bursts in the outer corona, Solar Phys., 8, 388, 1969.

Anderson, K. A., and R. P. Lin, Observations on the propagation of solar-flare electrons in interplanetary space, Phys. Rev. Letters, 16, 1121, 1966.

Bohm, D., and E. P. Gross, Theory of plasma oscillations. B. excitation and damping of oscillations, Physical Review, 75, 1864, 1949.

Boischot, A., A. D. Fokker, and P. Simon, The 1957 November 4 event, I. A. U. Symposium No. 9, Ed. by R. N. Bracewell, 1959.

Boischot, A., F. T. Haddock, and A. Maxwell, Spectrum of 1957 November 4 solar outburst, Ann.' d' Astroph., 23, 478, 1960.

Boischot, A., J. de la Noë, and B. Møller-Pedersen, Relation between metric and decametric noise storm activity, Astron & Astrophys., 4, 159, 1970.

Chin, Y. C., B. B. Lusignan, and P. C. Fung, Polarization measurements of solar type III radio bursts at 25.3 MHz, Sol. Phys., 16, 135, 1971.

Chiu, Y. T., Theory of solar radio pulsation, Solar Phys., 13, 420, 1970.

Daigne, G., Structure and movement of solar noise storms, Nature, 220, 567, 1968.

de Groot, T., Contribution from the Utrecht Observatory: Fine structure on a type IV burst, Inf. Bull. Solar Radio Obs., No. 15, 4-5, 1963.

de Groot, T., Contribution from the Utrecht Observatory: 'Spike' - bursts, Inf. Bull. Solar Radio Obs., No. 9, 4-5, 1962.

de Groot, T., Dynamic Spectra and polarization of small bursts in solar radio emission, B. A. N., 15, 229, 1960.

de Groot, T., Solar spectra between 160 and 320 MHz, Sol. Phys., 14, 176, 1970.

de Groot, T., Weak solar radio bursts, Recherches Utrecht XVIII-1, 1966.

de Groot, T., and J. Van Nieuwkoop, Some preliminary results of multi-channel radiospectrography, Solar Physics 4, 332, 1968.

Dröge, F., Beobachtungen solarer radiobursts mit hoher zeitauflösung, Zeit. Astrophys., 66, 200, 1967.

Dröge, F. and P. Reimann, Contribution from the Radiosternwarte Kiel: some solar radio-events in the period from May to August 1961, Inf. Bull. Solar Radio Obs., No. 8, 6-7, 1961.

Eckhoff, H. Kr., On some properties of solar storm bursts in the 200 Mc/s region, Rept. No. 18, Inst. of Theor. Astrophys., Blindern - Oslo, Univ. of Oslo, 1966.

Elgarøy, Ø., Contribution from the Oslo Solar Observatory: Bursts of very short lifetime, Inf. Bull. Solar Radio Obs., No. 9, 3-4, 1962.

Elgarøy, Ø., High-resolution spectrometry of enhanced solar radio emissions, Astrophys. Norv., 7, 123, 1961.

Elgarøy, Ø., Narrow-band studies of solar bursts 201, Solar System Radio Astronomy, Plenum Press, New York, Ed. by J. Aarons, 1965.

Elgarøy, Ø., On the wavelength dependence of the bandwidth and the duration of type I solar radio bursts, Astrophys. Letters, 1, 13, 1967.

Elgarøy, Ø. and H. K. Eckhoff, On the active region corona and the interpretation of type I bursts, Astrophys. Norv., 10, 127, 1966.

Elgarøy, Ø. and Ø. Hauge, On the features of storm bursts in the 200 Mc/s range, Astrophys. Norv., 6, 85, 1958.

Elgarøy, Ø., in Jensen, E., Research in solar physics during 1965, Sci. Rept. No. 11, Contract AF61 (052)-743, Inst. of Theor. Astrophys., p. 9-10, p. 20, 1966.

Elgarøy, Ø. and H. Rødberg, On some properties of solar radio bursts of spectral type III, Astrophys. Norv., 8, 271, 1964.

Elgarøy, Ø. in Rosseland, S., Researches in the field of solar radio noise and sunspots, Ann. Rept. for 1962. Contract AF61 (052)-186, Inst. Theor. Astrophys., 5, 1963.

Elgarøy, Ø. in Rosseland, S., Researches in Solar Physics during 1964, Sci. Rept. No. 1, Contract AF61(052)-743, Inst. Theor. Astrophys., 10, 1965.

Elgarøy, Ø. and O. Ugland, Characteristic Properties of small chains of type I solar radio bursts, Astron. & Astrophys., 5, 372, 1970.

Ellis, G. R. A. and P. M. McCulloch, Frequency splitting of solar radio bursts, Aust. J. Phys., 20, 583, 1967.

Ellis, G. R. A., Fine structure in the spectra of solar radio bursts, Aust. J. Phys., 22, 177, 1969.

Fainberg, J. and R. G. Stone, Type III solar radio burst storms observed at low frequencies I. Storm morphology, Solar Phys., 15, 222, 1970a.

Fainberg, J. and R. G. Stone, Type III solar radio burst storms observed at low frequencies II. Average exciter speed, Solar Phys., 15, 433, 1970b.

Fokker, A. D., Coronal scattering of radiation from solar radio sources, Bull. Astr. Inst. Netherlands, 18, 111, 1965.

Fokker, A. D., Spectral characteristics of medium-sized solar radio events, Solar Phys., 8, 376, 1969.

Fung, P. C. W., Origin of solar type IV meterwave storms, Can. J. Phys., 47, 179, 1969.

Fung, P. C. W. and W. K. Yip, Cyclotron radiation from electron streams as the origin of solar type I noise storms, Aust. J. Phys., 19, 759, 1966a.

Fung, P. C. W., and W. K. Yip, Theoretical dynamic spectra of solar type I storm bursts, Planet. Space Sci., 14, 1139, 1966b.

Ginzburg, V. L., and V. V. Zheleznyakov, On the possible mechanisms of sporadic solar radio emission (radiation in an isotropic plasma), Sov. Astron. - AJ, 2, 653, 1958.

Ginzburg, V. L., and V. V. Zheleznyakov, Noncoherent Mechanisms of sporadic solar radio emissions in the case of a magnetoactive coronal plasma, Soviet Astron. - AJ, 5, 1, 1961.

Gnezdilov, A. A., Determination of the two-dimensional structure of the noise storm of May 20, 1966 from data of eclipse observations at four stations, Sov. Astron. - AJ, 14, 59, 1970.

Hanasz, J., Chains of type I solar radio bursts, Aust. J. Phys., 19, 635, 1966.

Hartz, T. R., Type III solar radio noise bursts at Hectometer wavelengths, Planet. Space Sci., 17, 267, 1969.

Hughes, M. P. and R. L. Harkness, Spectral observations of solar radio bursts. IV., Astrophys. J., 138, 239, 1963.

Jaeger, J. C. and K. C. Westfold, Transients in an ionized medium with applications to bursts of solar noise, Aust. J. of Sci. Res., 2, 322, 1949.

Kai, K., The structure, polarization, and spatial relationship of solar radio sources of spectral types I and III, Solar Phys., 11, 456, 1970.

Kaplan, S. A. and V. N. Tsytovich, Radio emission from beams of fast particles under cosmic conditions, Sov. Phys. - Astron., 11, 956, 1968.

Kraus, J. D., Radio Astronomy, McGraw-Hill Book, New York, 1966.

Kundu, M. R., Solar Radio Astronomy, Interscience, New York, 1965,

Kundu, M. R. and C. L. Spenser, Spectral characteristics of solar continuum radiation in the 500 - 1000 Mc/s range. Astrophys. J., 137, 572, 1963.

Le Squeren-Malinge, Étude des orages radioélectriques solaires sur 169 MHz a l'aide de l'interféromètre en croix de la station de Nancay, Ann. d'Astrophys., 26, 97, 1963

Lin, R. P., Correlations of solar-flare electron events with radio and X-ray emission from the sun, Can. J. Phys., 46, S 757, 1968.

Lin, R. P., The emission and propagation of 40kev solar flare electrons, Sol. Phys., 13, 453, 1970.

Malville, J. M., Characteristics of type III radio bursts, Astroph. J., 136, 266, 1962.

Malville, J. M., The starting frequencies of type III bursts, Sol. Phys., 2, 484, 1967.

Malville, J. M., H. D. Aller, and C. J. Jenson, Spike bursts during the type IV event of February 5, 1965, Astrophys. J., 147, 711, 1967.

Markeev, A. K. and G. P. Chernov, Observations of solar radio-bursts with high spectral resolution, Soviet Astron. - AJ, 14, 835, 1971.

Martyn, D. F., Origin of radio emissions from the disturbed sun, Nature, 159, 26, 1947.

Maxwell, A., W. E. Howard, G. Garmire, Some statistics of solar radio bursts at sunspot maximum, J. Geophys. Research, 65, 3581, 1960.

Maxwell, A., G. Swarup, and A. R. Thompson, The radio spectrum of solar activity, Proc. I. R. E., 46, 142, 1958.

McNarry, L. R., Forward scatter of radio signals via meteor trails and short-lived solar radio bursts, Nature, 193, 1271, 1962.

Melrose, D. B., On the theory of type II and type III solar radio bursts. I., Austral. J. Phys., 23, 871, 1970a.

Melrose, D. B., On the theory of type II and type III solar radio bursts. II., Austral. J. Phys., 23, 885, 1970b.

Mollwo, L., Interpretation of type I - and IV mB-bursts and noise storms by mode coupling in the warm plasma, Sol. Phys., 12, 125, 1970.

Néra, A remarkable solar radio event, Nature, 181, 542, 1958.

Payne-Scott, R., D. E. Yabsley, and J. G. Bolton, Relative times of arrival of burst of solar noise on different radio frequencies, Nature, 160, 256, 1947.

Philip, K. W., Fine structure in meter wavelength solar radio bursts, Astron. J., 73, S197, 1968b.

Philip, K. W., High time - resolution observations of fine structure concurrent with type III bursts, Bull. Amer. Astron. Soc., 1, 359, 1969.

Philip, K. W., Studies of solar radio emissions at VHF - high time resolution spectrometry, Research Proposal to N. S. F., G68-15, 1968a.

Rabben, H. H., Spektralbeobachtungen des solaren radiophänomens vom 25. und 26. August 1959, Zeit. für Astrophys., 55, 73, 1962.

Rao, U. V. G., The polarization structure of type III solar radio bursts, Austral. J. Phys., 18, 283, 1965.

Roberts, J. A., Evidence of echoes in the solar corona from a new type of radio burst, Aust. J. Phys., 11, 215, 1958.

Roberts, J. A., Solar radio bursts of spectral type IV, Aust. J. Phys., 12, 327, 1959.

Sakurai, K., On the acceleration of relativistic electrons in solar proton flares, Publ. Astron. Soc. Pacific, 83, 23, 1971.

Simnett, G. M. and S. S. Holt, Long term storage of relativistic particles in the solar corona, Sol. Phys., 16, 208, 1971.

Slysh, V. I., Observations of type III solar radio bursts with the Venus 2 probe, Sov. Astron. - AJ., 11, No. 3, 389, 1967.

Smith, D. F., Towards a theory for type III solar radio bursts, Sol. Phys., 15, 202, 1970b.

Smith, D. F., Type III solar radio bursts, Adv. in Astron. and Astrophys., 7, 147, 1970a.

Spitzer, Lyman, Physics of Fully Ionized Gases, Interscience Publishers Inc., New York, 1956.

Stewart, R. T., The polarization of "Herring-Bone" features in solar radio bursts of spectral type II, Aust. J. Phys., 19, 209, 1966.

Sturrock, P. A., Type III solar radio bursts, 357-361, Physics of Solar Flares, edited by W. N. Hess, NASA SP-50, 1964.

Takakura, T., Origin of solar radio type I bursts, Publ. Astron. Soc. Japan, 15, 462, 1963.

Tandberg - Hanssen, E., Solar Activity Blaisdell Publ., 1967.

Thompson, A. R., Spectral observations of solar radio bursts. I., Astrophys. J., 133, 643, 1961a.

Thompson, A. R., Sweep frequency observations of meteor scatter bursts, J. Atmos. Terr. Phys., 22, 161, 1961b.

Trakhtengerts, V. Yu., A theory for type I solar radio bursts, Sov. Astron. - AJ., 10, 281, 1966.

Rao, U. V. G., The polarization structure of type III solar radio bursts, Austral. J. Phys., 18, 283, 1965.

Roberts, J. A., Evidence of echoes in the solar corona from a new type of radio burst, Aust. J. Phys., 11, 215, 1958.

Roberts, J. A., Solar radio bursts of spectral type IV, Aust. J. Phys., 12, 327, 1959.

Sakurai, K., On the acceleration of relativistic electrons in solar proton flares, Publ. Astron. Soc. Pacific, 83, 23, 1971.

Simnett, G. M. and S. S. Holt, Long term storage of relativistic particles in the solar corona, Sol. Phys., 16, 208, 1971.

Slysh, V. I., Observations of type III solar radio bursts with the Venus 2 probe, Sov. Astron. - AJ., 11, No. 3, 389, 1967.

Smith, D. F., Towards a theory for type III solar radio bursts, Sol. Phys., 15, 202, 1970b.

Smith, D. F., Type III solar radio bursts, Adv. in Astron. and Astrophys., 7, 147, 1970a.

Spitzer, Lyman, Physics of Fully Ionized Gases, Interscience Publishers Inc., New York, 1956.

Stewart, R. T., The polarization of "Herring-Bone" features in solar radio bursts of spectral type II, Aust. J. Phys., 19, 209, 1966.

Sturrock, P. A., Type III solar radio bursts, 357-361, Physics of Solar Flares, edited by W. N. Hess, NASA SP-50, 1964.

Takakura, T., Origin of solar radio type I bursts, Publ. Astron. Soc. Japan, 15, 462, 1963.

Tandberg - Hanssen, E., Solar Activity Blaisdell Publ., 1967.

Thompson, A. R., Spectral observations of solar radio bursts. I., Astrophys. J., 133, 643, 1961a.

Thompson, A. R., Sweep frequency observations of meteor scatter bursts, J. Atmos. Terr. Phys., 22, 161, 1961b.

Trakhtengerts, V. Yu., A theory for type I solar radio bursts, Sov. Astron. - AJ., 10, 281, 1966.

Tsytovich, V. N., Nonlinear Effects in Plasma, Plenum Press, New York - London, 1970.

Twiss, R. Q., Radiation transfer and the possibility of negative absorption in radio astronomy, Aust. J. Phys., 11, 565, 1958.

Twiss, R. Q., and J. A. Roberts, Electromagnetic radiation from electrons rotating in an ionized medium under the action of a uniform magnetic field, Aust. J. Phys., 11, 424, 1958.

Vitkevich, V. V. and M. V. Gorelova, Dynamic spectra and principal characteristics of short-lived bursts of solar radio emission, Sov. Astron. - AJ., 4, 595, 1961.

Vitkevich, V. V. and M. V. Gorelova and T. A. Lozinskaya, The spectrum of peaks in solar radio emissions, Sov. Astron. - AJ., 3, 626, 1960.

Vitkevich, V. V. and Z. I. Kameneva, Bursts of solar radio emission, Sov. Astron. - AJ., 2, 343, 1958.

Warwick, J. W., Sweep-frequency measurements of solar bursts, Solar System Radio Astronomy, Ed. by J. Aarons, Plenum Press, New York, 1965.

Warwick, J. W. and G. A. Dulk, Spectrum and polarization of solar radio bursts on a 10 millisecond time scale, Astrophys. J., 158, 2123, 1969.

Wild, J. P., Observations of the spectrum of high-intensity solar radiation at metre wavelengths, Aust. J. Sci. Research, 3A, 399, 1950.

Wild, J. P., Observations of the spectrum of high-intensity solar radiation at metre wavelengths IV. Enhanced radiation, Aust. J. Sci. Res., A 4, 36, 1951.

Wild, J. P., Radio evidence of instabilities and shock waves in the solar corona, Plasma Instabilities in Astrophysics, Ed. by Wentzel & Tidman, 119, 1969.

Wild, J. P. and L. L. McCready, Observations of the spectrum of high-intensity solar radiation at metre wavelengths, I. The apparatus and spectral types of solar bursts observed, Aust. J. Sci. Res., A 3, 387, 1950.